BACKCALCULATION AND SENSITIVITY OF NON-DESTRUCTIVE TESTS TO TEMPERATURE VARIATIONS IN FLEXIBLE PAVEMENTS

By

ANASTASIA NEZHENTSEVA, B.SC. (CIVIL ENGINEERING)

A Thesis

Submitted to the School of Graduate Studies

In Partial Fulfillment of the Requirements

for the Degree

Master of Applied Sciences M.A.Sc.

McMaster University

BACKCALCULATION AND SENSITIVITY OF NON-DESTRUCTIVE TESTS TO TEMPERATURE VARIATIONS IN FLEXIBLE PAVEMENTS

MASTER OF APPLIED SCIENCES (2009) McMaster University

(Civil Engineering) Hamilton, Ontario

TITLE: Backcalculation and Sensitivity of Non-Destructive Tests to Temperature Variations in Flexible Pavements

AUTHOR: Anastasia Nezhentseva, B.Sc. (Belgorod State Technological University)

SUPERVISOR: Professor Dieter F.E. Stolle

NUMBER OF PAGES: xx, 213

ABSTRACT

The Light Weight Deflectometer (LWD) is a smaller version of the Falling Weight Deflectometer (FWD) non-destructive test for determining the properties of the pavement-subgrade systems. Unlike the FWD, normally having up to 9 sensors measuring load-deflections histories, the LWD records the data using a central geophone located right under the loading plate. Up to two sensors can be attached to the device though. Therefore, the limited information obtained from the LWD creates some difficulties for the backcalculation.

Elastostatic method of backcalculation layer elastic moduli of pavement structures does not take into account the dynamic nature of tests. Another limitation of the elastostatic approach is that it gives only one piece of information from each load-deflection history recorded by a geophone. The number of unknowns typically exceeds two (at least pavement and subgrade elastic moduli for a two-layer approximation) for the real pavement-subgrade structure.

The dynamic impedance function for the Mindlin plate idealization supported by elastic half space is calculated and related to the impedance of an equivalent single degree of freedom (SDOF) oscillator approximation. Unlike elastostatic, dynamic backcalculation provides one with two pieces of information (real and imaginary components of the dynamic impedance) allowing one to back-calculate an additional pavement-subgrade system property. It is shown, that elastostatic backcalculation gives

the elastostatic stiffness value which, combined with the dynamic impedance of the Mindlin plate model, allows one to estimate an effective subgrade modulus E_s, and elastic modulus of pavement E_p or an equivalent asphalt thickness h_a. The presence of shallow bedrock indicated, however, the backcalculation with the simplified model can be problematic.

The back-calculation approach suggested in this study is applied to sets of in-situ and simulated data. A frequency domain analysis showed some limitations for backcalculation of pavement-subgrade properties for real LWD data.

The low frequency LWD and FWD devices (up to 50-80 Hz), as well as the higher frequency IE test (20 kHz), are compared in terms of temperature sensitivity of the respective responses. Non-isothermal computer simulations were performed and comparison was made. The results demonstrate that the LWD is more sensitive to temperature changes in the pavement layer than the FWD. Back-calculated elastic moduli of the subgrade did not show any sensitivity to temperature fluctuations. The impact echo test response showed high sensitivity of the response to temperature changes in thin pavements (up to 100 mm thick).

ACKNOWLEDGEMENTS

In presenting this thesis I wish to express my deep gratitude to my research supervisor, Dr. Dieter F.E. Stolle, for his priceless guidance, tolerance, concern and encouragement throughout every stage of this study.

I would also like to express my sincere appreciation to my co-supervisor Dr. Gabriel Sedran for his valuable comments, support, research experience, suggestions and help during experimental part of the work. Without his technical advice with the preparation and actual temperature, testing my laboratory work would have been much more complicated and extended.

I gratefully acknowledge Dr. Peijun Guo for the help he offered with some field experiments and theory during the course of the experimental work.

Field testing of the pavement specimens was carried out with the LWD and IE testing equipment of John Emery Geotechnical Engineering Ltd (JEGEL) by Ms. Ramona Mirtorabi, (B.Eng) and Mr. Seth Zhang, (M.Sc. M.Eng.). Their help is acknowledged and highly appreciated.

Financial support for the current study was provided by McMaster University through the Department of Civil Engineering. This financial aid is greatly appreciated.

Finally, I wish to express my sincere thanks to my husband Nebojsa Dimitrijevic for his encouragement, support and love during my thesis write-up.

TABLE OF CONTENTS

LIST OF FIGURES

LIST OF TABLES

LIST OF SYMBOLS

A	Average value
a	Radius of the loading plate
B	Amplitude of the wave
C	Damping coefficient; Specific heat capacity
$\boldsymbol{C}$	Damping matrix
$\boldsymbol{C^*}$	Generally full damping matrix
C_p	Speed of propagation of P-wave
C_s, v_s	Speed of propagation of S-wave (shear wave velocity)
D	Flexural rigidity of the plate of uniform thickness
$d(r)$	Deflection at distance r
E	Modulus of elasticity
E_{ac}	Asphalt concrete modulus
E_{eff}	Effective subgrade modulus
E_{FWD}	FWD back-calculated resilient surface modulus
E_{LWD}	LWD back-calculated resilient surface modulus
E_p	Reference pavement modulus (4000 MPa), elastic modulus of pavement
E_s	Elastic modulus of subgrade
$E_{SM}(r)$	Surface modulus at a distance r from the centre of the loading plate
F_{peak}	Peak load of the load-deflection history
f	Test frequency
$\boldsymbol{f(s)}$	Vector, corresponding to the spatial distribution of the load constant

	in terms of time
G	Shear modulus of elasticity
G_s	Shear modulus of subgrade
G'	Adjusted shear modulus
h_a	Equivalent asphalt thickness
h_e	Equivalent thickness (in terms of subgrade material)
h_p	Pavement thickness
$Im(S(\omega))/S(0)$	Normalized imaginary component of dynamic impedance function
$J_0(mr)$	Bessel function of the first kind and order zero
$\boldsymbol{K}$	Stiffness matrix
$\boldsymbol{K^*}$	Generally full stiffness matrix
K_{aver}	Average value of stiffness
K_{peak}	Static stiffness
k^2	Shear modulus correction factor
$\boldsymbol{L}$	Vector, representing the impulse
$\boldsymbol{M}$	Mass matrix
$\boldsymbol{M^*}$	Diagonal matrix
N	Interpolation (shape) function
P_0	Peak concentrated load
P_{200}	Percent aggregate weight passing # 200 sieve
P_{ac}	Percent asphalt content by volume of mix
$P(t)$	Load vector
$P(\omega)$ and $w(\omega)$	Fourier transforms of $P(t)$ and $w(t)$
p	Momentum

$p(r)$	Function of vertical axisymmetric loading
$q(r)$	Foundation reaction
$\bar{q}(r)$	Transformed reaction
$\boldsymbol{R}$	Matrix of the time-independent mode shapes (Ritz vectors)
$Re(S(\omega))/S(0)$	Normalized real component of dynamic impedance function
r	Radial distance from the centre of loading
$r(t)$	Scalar function of time, which describes the frequency content of the loading
$S(\omega)$	Dynamic impedance
T	Pavement temperature at a depth 25 mm in the asphalt layer; Time of observation
$T(t,z)$	Temperature of the pavement at time t and depth z
Δt	Time increment used in sampling
Δt, Δx	Time and displacement increments, respectively
t_p	Middle depth asphalt concrete layer temperature
V_a	Percent air voids in mix
w_{peak}	Peak displacement
$w(r)$	Function (deflection) of radial coordinate
$\bar{w}(m)$	Transformed space (displacement)
$w(t)$	Displacement of the system
$\ddot{w}(t)$, $\dot{w}(t)$	Differentiation of deflection with respect to time
$\boldsymbol{Z}$	Time-dependent generalized displacement vector of the reduced system, comparable to participation factors in modal analysis
α	Thermal diffusivity of asphalt concrete layer and base

δ	Kronecker Delta
$\eta_{70,10}{}^{6}$	Asphalt viscosity at 70 F
θ	Natural coordinate; Phase angle
λ	Thermal conductivity
ν	Poisson's ratio
ξ	Damping ratio
π_j	Independent dimensionless π group
ρ	Density of the material
ρ_p and ρ_s	Density of pavement and subgrade, respectively
σ_{app}	Maximum applied pressure
σ_0	Contact pressure
ω	Angular frequency of loading
∇^2	Laplace operator

Chapter 1 INTRODUCTION

1.1 General

Monitoring and estimation of the deterioration of the transportation infrastructure (including roads and highways) over their design service life are important activities of highway engineers. The amount of funding required for maintenance and repair depends on the state of the roads. The problem is becoming more acute as the traffic load and volume increase. Historically, the design of pavements and rehabilitation strategies has been largely empirical in nature, relying heavily on the experience gained from monitoring the performance of existing pavements. The National Cooperative Highway Research Program (NCHRP) completed its development of the mechanistic-empirical procedures, AASHTO 2002, that makes use of resilient modulus (M_r) to characterize the material stiffness of base/subbase materials and subgrade soils. The design procedure is expected to improve design reliability and yield more cost-effective pavement designs. A certain level of disagreement is usually expected between measured in-situ data and predicted response by pavement models. This thesis addresses some of the issues associated with these differences.

1.2 Non-Destructive Testing (NDT) Techniques

Non-destructive testing (NDT) techniques have become essential for estimating the integrity of pavement structures. These techniques are also used for determining the in-situ layer characteristics of pavement-subgrade systems. One must take into account that it is not easy to estimate real pavement behavior knowing that mechanical properties of the pavement-subgrade layers are not uniform and depend on such factors as moisture content, temperature within pavement structure and state of stress (Stolle and Hein, 1989; Stolle and Peiravian, 1996).

For many years the FWD (Falling Weight Deflectometer) has been popular for evaluating pavement-subgrade integrity. In the recent past, portable devices such as LWD (Light Weight Deflectometer) have received increasing attention for the quality control of pavements. Considerable research has been done with regard to FWD data interpretation, including, for example:

- Lytton (1989), Siddharthan et al. (1991), Stolle and Jung (1992), Stolle and Sedran (1994), Stolle and Peiravian (1996), Guzina and Osburn (2002), Irwin (2002), Stolle and Guo (2005), Turkiyyah (2005), Horak and Khumalo (2006) , Horak (2008) – backcalculation for isothermal measurements;
- Chen et al. (2000), Park et al. (2002), Fernando (2003) - temperature correction on FWD backcalculated asphalt concrete (AC) modulus;

Some researchers who contributed significantly to studying LWD data are Hoffman et al. (2004), Lin et al. (2006), Steinert et al. (2006), Horak and Khumalo (2006), Fleming et al. (2007) and Horak et al. (2008).

The principle of both devices is based on measuring the response to an impact load, which basically occurs by dropping a weight onto a plate. Yet the "state-of-the-practice" algorithms, which are mostly based on elastostatic models, for interpreting FWD and LWD data do not simulate real dynamic response of a pavement to FWD or LWD loading. Furthermore, these devices have an important restriction. The interpretation of test data using current algorithms is more reliable for new pavements or pavements free of defects (like cracking, rutting, potholing etc) than for pavements that contain flaws. Not accurately taking into account flaws can lead to systematic errors in interpretation of data. At the same time, highway engineers are primarily interested in keeping track of the deterioration of strength and stiffness of pavement-subgrade systems, particularly those that are developing defects, and therefore exact determination of system parameters is not always necessary.

1.3 Falling Weight Deflectometer (FWD) Testing Technique

The falling weight deflectometer (FWD) is a well-known device used to evaluate the structural integrity of pavement-subgrade systems of pavements. A test consists of dropping a hydraulically elevated weight onto a circular plate (disc) of 30 cm diameter, supported by the pavement surface. The test usually lasts 0.06s. The impulse load, which

is measured by a load cell set on top of the loading plate, simulates a passing heavy single-tire wheel load from a truck that has a load duration of ~25-30 ms. The FWD was designed to measure the deflection history of pavement at a number of sensors (velocity transducers, deflectors) located at different offsets from the load. The location of geophones tracking pavement surface displacements is usually set at offsets corresponding to 0, 200, 300, 450, 600, 900, 1200, 1500 and 1800 mm away from the centerline (Horak, 2008). The peak displacements acquired from the sensors define a deflection basin.

The FWD device has several limitations. Reliable information about thicknesses of asphalt-subgrade layers is often not available at the FWD test sites making FWD data interpretation more difficult. Another limitation of the FWD is that backcalculated subgrade moduli are not helpful in analyzing pavement deterioration and determining the reasons that cause flaws (Tayabji and Lukanen, 1999).

1.4 Portable Light Weight Deflectometer (LWD) Testing Technique

Over the past decade, the LWD has become a popular device for testing structural integrity of single pavement layers as it has a shallower depth of influence than the FWD. Therefore, different correlations with other non-destructive testing (NDT) tools such as the FWD and plate load test (PLT) have been performed worldwide (see Kamiura et al., 2000, Livneh and Goldberg, 2001, Fleming et al., 2007, Horak et al., 2008).

The principle of the light falling weight deflectometer (LWD), a portable, scaled-down version of the falling weight deflectometer (FWD), is similar to that of the FWD simulating the loading of a single tire moving truck. At the same time, the LWD has a smaller load range and interval over which the maximum load is applied. The load pulse is 15 to 20 ms for Prima 100 LWD (Nazzal et al. 2007), and 15 to 25 ms for Dynatest 3031 LWD. Typical LWD generates a load up to 15 kN to form a deflection bowl in the pavement comparable to a moving single wheel truck with an axle load of 4000 lbs. By dropping a lighter weight on a plate compared to that of the FWD less volume of the pavement-subgrade system is being noticeably excited under the load, meaning a shallower depth of influence than encountered with the FWD. In their research study, Nazzal et al. (2007) suggested that the influence depth for the Prima 100 model LWD (developed by CarlBro, Denmark) was about 1.5 times the loading plate diameter (200 mm) and varied between 270 and 280 mm. Having tested two types of the LWD with 200 and 300 mm load plate diameters, Mooney and Miller (2009) suggested that the measurement depth of the LWD was about 0.9-1.1 times the load plate diameter. Therefore, the LWD is measuring an effective or composite modulus for all layers (average properties of the pavement-subgrade model) reaching lower pavement layers and upper subgrade. The choice of the loading plate diameter for the LWD normally ranges between 150 and 300 mm and is recommended by the LWD manufacturer depending on the value of measured composite modulus. Smaller plate size (100 mm) is suggested for pavement structures with stiff subgrade (i.e. more than 170 MPa for Prima 100 LWD)

providing higher contact pressure under the plate. For pavements with the composite modulus value less than 125 MPa, a plate size of 300 mm is suggested (Lin et al. 2006).

The LWD can easily be operated by one person. The test variables include drop height, drop weight, contact area of the load, time of loading and the number of geophones. Force and the centre deflections are measured by the LWD with a centre deflection sensor (geophone, seismic transducer). Important restriction of the LWD is that it performs partial measurements of the deflection bowl since only up to two additional geophones located at 300 mm spacing can be attached to the device (Fleming et al., 2007). Using one geophone makes use of backcalculated results for pavement-subgrade layered structures questionable. The automatically recorded data is often processed by LWDmod software that is correlated to the device and backcalculates a surface deflection modulus using the same procedure as developed for ELmod for Dynatest FWD (Hoffmann et al, 2003; Ullidtz, 1987). The principle is based on Boussinesq solution and Odemark's method (for multi-layer pavement systems) presuming a constant weight on an elastic half-space with consistent Poisson's ratio (Horak et al., 2008).

Research done in the past illustrates that there is a good agreement between the results for moduli determined with LWD and FWD devices. Nevertheless, one must be aware that this relationship depends on pavement structure and kind of material (Horak et al. 2008). Fleming et al. (2000) found that the surface modulus backcalculated with the FWD device (E_{FWD}) correlates well with moduli determined from the main three types of

LWD (E_{LWD}) present currently in the market; yet, the correlation coefficients were found to be sensitive to a particular LWD tool:

$$E_{FWD} = 1.031 \cdot E_{LWD} \quad (1.1)$$

where E_{FWD} (in MPa) -backcalculated resilient surface moduli, E_{LWD} (in MPa) - the LWD surface modulus. Nazzal et al. (2007) provided a similar relationship for different pavement material types:

$$E_{FWD} = 0.97 \cdot E_{LWD} \quad (1.2)$$

with coefficient of determination $R^2 = 0.94$, significance level < 99.9% and standard error = 3.31 .Rahimzadeh et al. (2004) suggested that the correlation between FWD and LWD was pavement material type and thickness dependent.

1.5 Impact Echo (IE) Testing Technique

Researchers in the past used small hammers to strike the surface of concrete structures to discover possible flaws inside them, and by the sound that the hammer caused, one could detect the presence of cracks, voids and other delaminations. The value of such a method highly depends on the experience of the practitioner with the main disadvantages being the inability to objectively analyze the results and detect surface defects, and the limited hearing abilities of a human ear to distinguish only sound frequencies up to 18 kHz (Germar, 2000). To minimize the shortcomings of this

technique ultrasonic high frequency devices started to appear at the end of the 19th century.

The impact echo (IE) is a nondestructive method that is used to detect delaminations like voids or cracks inside the concrete structures. This higher frequency method was first introduced at Cornell University by Sansalone and Carino (1986) and was applied first to determine material properties and flaws in concrete structures. IE devices were later applied for testing masonry structures (Sadri, 2003), as well as rigid Portland cement concrete (PCC) and flexible asphalt concrete (AC) pavements. In 1997, the impact echo method was standardized under ASTM Standard C1383-98a (Gibson et al., 2005).

According to Carino (2001) three main components of the IE testing equipment are:

- an impactor (a small metal ball) producing short-duration impacts depending on its weight and other factors;
- a receiver to capture the surface response;
- and a data acquisition-signal analysis system.

The impactor induces three various types of stress waves propagating in the vertical and horizontal directions in soil (see Fig.1.1):

- P-wave travelling in a vertical direction with depth;
- S-wave related to shear stress and also propagating vertically;
- R-wave spreading horizontally along the surface of the pavement.

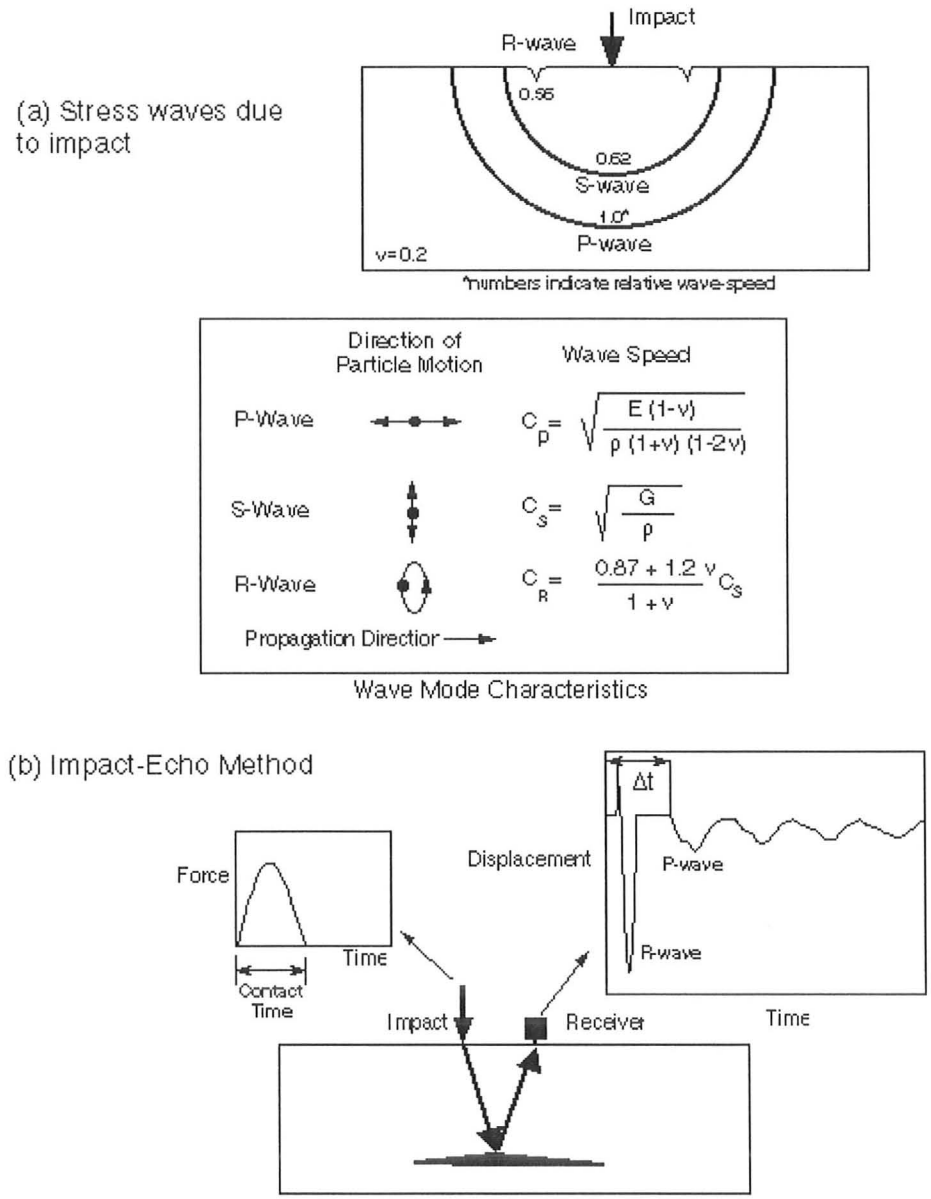

Figure1.1- Principle of the Impact Echo (IE) method (source http://ciks.cbt.nist.gov/~carino/ieprin.html)

P-wave speed, C_p, depends on the modulus of elasticity, E, Poisson's ratio, ν, and the density of the material, ρ, (Krautkrämer and Krautkrämer, 1990):

$$C_p = \sqrt{\frac{E(1-\nu)}{\rho(1+\nu)(1-2\nu)}} \tag{1.3}$$

The speed of propagation of S-wave, C_s, is slower:

$$C_s = \sqrt{\frac{G}{\rho}} = \sqrt{\frac{E}{2\rho(1+\nu)}} \tag{1.4}$$

where G - the shear modulus.

Flaws (voids, cracks and other defects) and the boundaries reflect the propagation of the waves in the pavement-subgrade structure. Propagation continues back and forth within the pavement structure and reflects at the surface of the pavement and the bottom of AC layer or internal defects (Cam et al. 2005) until the waves damp out.

Approximate velocities of different pavement materials are given in Table 1.1.

Table 1.1- Approximate velocities of different materials (Santamarina et al., 2001; Hall, 2000; Bodare, 1997)

Material	C_s (m/s)	C_p (m/s)	Density (kg/m^3)	Poisson's ratio
Concrete	1300-2800	2000-4600	2400	0.20
Asphalt*	600-2500	1100-4500	2300-2400	0.20-0.40
Pavement base	250-500	350-800	2100-2300	0.10-0.30

*Viscoelastic material

In the current research, asphalt concrete layer was assumed to have the following mechanical properties for isothermal case: E_p=4000 MPa, ν= 0.3 and ρ=2000 kg/m3.

Therefore, C_p and C_s calculated using Eqn. (1.3) and (1.4) were found to be in the order of 1640 m/s and 880 m/s, respectively.

Among the factors affecting the performance of the IE method are (see Abraham et al. 2000): the source function, response of sensors, size and shape of flaw, its depth, mechanical impedance of the pavement material and delamination (generally, in plate-type of structures a thin layer with lower acoustic impedance is easier to detect than one with a higher one) (see Lin et al. 1990), coefficient of absorption of material.

In the past 15 years, the IE method has proven to be a faster and more advantageous non-destructive testing technique than, for example, sounding which used to be a quite popular device in the past (see Cheng and Sansalone 1993). The main advantages of IE methods are speed of performance, possibility of detecting deep flaws, no significant influence of traffic noise on its measurements and the results are less affected by biased interpretation of the operator. Parvini (1997) suggested that high frequency tests (more than 1000 rad/s or 160 Hz) are more suitable for pavement layer moduli determination as dominant frequency magnitude of impact load of such NDT devices as the FWD and LWD is not sufficient to identify the characteristics of the asphalt concrete layer. These low frequency devices capture surface deflections which are more sensitive to the changes in subgrade layer modulus than in surface layer.

The application of impact echo testing, nevertheless, has limitations. According to research completed (Summary report "Nondestructive Thickness of Distressed

Concrete Pavement Using Impact-Echo" 2002), IE has proven to be an inappropriate NDT device for evaluation of thickness of aged distressed concrete pavements, showing poor accuracy. On the contrary, estimation of thickness of newly constructed pavement sections with IE testing has shown results with high precision. Furthermore, experience with viscoelastic materials such as asphalt concrete is limited.

The location of the receivers and stiffness of asphalt concrete (AC) layer affect the measurement of the primary resonant frequency making it complicated for estimation, especially in pavement systems with numerous reflection boundaries. The consequence of unstable resonant frequencies, which depend on receiver positioning, can be minimized by means of using multiple receivers. Receivers, placed farther from the fixed boundaries, can better pick up the resonant frequency. Boundary conditions, however, have no effect on the primary resonant frequency (horizontal resonance) (see Cho et al. 2005). Multiple reflections and noisiness of the traveling waves bouncing between flaws and surfaces of the pavement layers affect the frequency spectrum creating numerous peaks and making their interpretation in the frequency domain complicated (see Medina et al. 2007).

Finite element analyses carried out by Cho (2001) has shown that the resonant frequencies calculated using finite element code were in poor agreement with theoretical results found in literature on IE device. This shows that IE theory still needs improvement and further studies for the better and more precise results (Cho et al. 2005).

1.6 Objectives of the Thesis

The main objectives of the present research study are:

- study and extend application of impedance functions developed by Peiravian (1994) for dynamic backcalculation of FWD and LWD data;
- develop an understanding of what each NDT device is actually measuring;
- establish the sensitivity of the NDT equipment to asphalt-concrete layer properties affected by temperature changes;

In principle, each device operates the same with the main difference being the amount of energy used to excite the pavement-foundation system. Given this difference, an objective of the thesis is to see if this difference can be exploited to provide different information with regard to the system that is being measured.

The thesis provides an interpretation of the physics with regard to the influence of temperature and thickness of the asphalt-concrete pavement. Emphasis is on what is happening as a response problem, similar to what was done for FWD and LWD backcalculation analyses.

1.7 Outline of the Thesis

Chapter 2 describes existing backcalculation procedures based on elastostatic and elastodynamic approaches. Single degree of freedom (SDOF) parameter identification for FWD tests introduced by Peiravian (1994) in his research is also discussed. This simplification allows one to evaluate *M, C* and *K* of a SDOF equivalent based on the load-displacement histories provided from the tests either in time or frequency domain. Dynamic impedance function approach developed by Peiravian (1994) and based on a Kirchhoff plate model was compared to the more sophisticated Mindlin plate-on-elastic-foundation model, which takes into account shear deformations.

Chapter 3 introduces results of the experimental studies on the LWD carried out at McMaster University. Time-deflection data were analyzed using time domain analysis (TDA). Frequency domain analysis limitations for the real data were also discussed in this chapter.

Chapter 4 describes isothermal simulations of FWD and LWD tests. Ritz vector and Newmark algorithms were presented and results obtained from both methods were compared. Results of the LWD and FWD computer simulations were analyzed using elastostatic and elastodynamic approaches. The dimensional analysis of the elastostatic and elastodynamic problem is also covered in this chapter. A set of appropriate dimensionless π-groups is suggested for both approaches.

Chapter 5 describes the effect of temperature on elastic modulus of pavement layer as well as on overall flexible pavement response. Temperature variations in flexible

pavements were monitored near Applied Dynamics Laboratory (ADL) building at McMaster University by thermocouples set up at different depth at each location during August, 2008. Temperature profiles were collected and used as an input data for non-isothermal LWD, FWD simulations presented in this chapter and IE simulations introduced in the following chapter. Elastostatic and elastodynamic backcalculation approaches presented in Chapter 2 were used to backcalculate pavement-subgrade system parameters and to check how sensitive the elastic modulus of subgrade is to temperature changes in AC layer.

Chapter 6 contains results of isothermal and non-isothermal simulations of "fictitious" impact echo (IE) test using Newmark time-stepping algorithm. Elastodynamic approach based on time domain analysis (TDA) and developed by Peiravian (1994) was used to summarize and compare the results of computer simulations.

Chapter 7 summarizes the results and conclusions of the present research and finishes the thesis. Suggestions on future research are also provided in the finale of this chapter.

Chapter 2 BACKCALCULATION PROCEDURES

2.1 General

Pavement integrity evaluation is an important activity of the highway engineer. High popularity of NDT tests for assessment of pavement integrity has affected the growth of various backcalculation techniques and pavement-subgrade models for evaluation of the elastic layer moduli and field data analysis. Backcalculation is a numerical iteration method for finding an acceptable match between the measured deflection basin and the one predicted by a simplified model by means of adjusting the elastic moduli of the pavement layers.

The most popular backcalculation techniques for FWD data interpretation are based on analyzing the peak deflections from load-displacement history of each geophone (sensor or velocity transducer) located at specific distance from the centre of the load (up to a distance of about 1.2-1.8 m from the centerline). Various programs have been developed to determine the layer moduli, including ELMOD software system (by Dynatest) and MODULUS developed at the Texas Transportation Institute (Uzan et al., 1988, 1989). There are two simplified backcalculation approaches for two-layered pavement-subgrade models: elastostatic and elastodynamic approaches; see, for example, Peiravian (1994) and Stolle (1996). Both of them characterize the pavement structure by an equivalent asphalt thickness h_a and assume subgrade layer to be an elastic half-space, often incompressible. Considering the dynamic nature of FWD device, elastostatic

backcalculation is often considered to be a method producing incorrect approximation of elastic moduli of subgrade especially when a stiff layer is located close to the surface of the pavement; see, for example, Davies and Mamlouk (1985), Stolle et al. (1988), Stolle and Jung (1992), Peiravian (1994), Stolle (1996). Elastostatic backcalculation method is, however, very popular in pavement engineering practice as it is easy to use and computationally efficient regardless of the dynamic character of FWD testing. At the same time, according to Stolle and Peiravian (1996) given the dynamic nature of FWD loading impact, one can not expect that elastic moduli evaluated based on elastostatic model provide trustworthy results. Elastostatic approach will be further discussed in Sections 2.3 and 4.6.1.

The elastodynamic approaches developed by Magnuson et al. (1991), Uzan (1994), Parvini and Stolle (1998), on the other hand, are considered to provide a better understanding of wave reflection, refraction and dispersion phenomena. Unlike elastostatic approach, this framework often considers viscoelastic properties of AC layer.

Both elastostatic and elastodynamic approaches have drawbacks (see i.e. Stolle and Hein 1989):

- Several solutions are possible because of the non-uniqueness of backcalculation;

- In spite of their complexity, pavement-subgrade mechanical models are simplified approximations of real systems and, therefore, introduce systematic errors in the backcalculated elastic moduli results;
- Owing to the assumptions made for pavement-subgrade models, systems of equation for elastic moduli evaluation are often ill-conditioned.

Ullidtz (1987) and Stolle et al. (1988) suggested that evaluation of the subgrade moduli using backcalculation is fairly accurate considering that about 60-80 percent of the pavement-deflection basin is related to the subgrade response, although one may get poor results trying to backcalculate elastic moduli of other pavement layers.

Research on dynamic interpretation of FWD tests was also carried out more recently by Konrad and Grenier (2009). They discovered the importance of using deflection basin and deflection histories together, which allows one to take into account dynamic phenomena of the FWD. In their research, they performed dynamic analysis and backcalculation using a numerical computer code called DYNAPAV-UL (Dynamic Analysis of Pavement - Université Laval) based on the spectral element method and time domain analysis. The spectral element method is a high order finite element method. It allows one to accomplish high accuracy and steady solution algorithms with a small number of elements. Inverse Fourier transform is applied to convert the results in the time domain. DYNAPAV-UL is a very powerful numerical code for simulation of the FWD test on

flexible pavements at different load durations, temperatures of the asphalt-concrete layer and various bedrock conditions.

A simplified procedure for FWD elastodynamic data interpretation developed by Stolle and Peiravian (1994) that takes into account the dynamic nature of the FWD test, is extended and presented in Sections 2.4 and 4.6.2. According to this procedure the load and displacement histories are used to determine dynamic impedance, which depends on the properties of the pavement and foundation. The analysis methodology was applied to synthetic simulated data from finite element simulations and is further discussed in Sections 3.2.1 and 4.6.2.

Interpretation of the data using elastodynamic backcalculation approach does not always give better results for pavement-subgrade properties evaluation than using elastostatic one (Peiravian 1994, Parvini 1997).

2.2 Correlation between Backcalculated and Actual Pavement Properties

One of the main questions pavement engineers are interested in is, can they rely on the accuracy of the results obtained during backcalculation? No one can answer this question with a high level of confidence. In general, several factors can cause incorrect results as discussed by Irwin (2002):

- Assumptions in the model used for backcalculation of properties for real pavement-subgrade system not appropriate (random and systematic errors).

- Presence of defects like cracks within the radius of the testing surface.
- Non-homogeneous thicknesses and material properties of actual pavement samples.
- Blind estimation of thicknesses of the AC and subgrade layers due to trial and error technique used for setting pavement models.
- Limitation associated with very thin pavements for backcalculation.
- Temperature effects on elastic modulus of AC not taken into account.
- Stress-dependent behavior of pavement materials in majority of backcalculation techniques not taken into account.

One can also take measurements at various stations along the highway pavement to make sure that the backcalculated results match well the real field data. There is one limitation of this method though, as no one can guarantee that the subgrade properties are constant along the pavement section and, as a result, such factors as depth of the bedrock or moisture content can cause "strange" results which might be interpreted as incorrect.

Common sense, critical judgment, experience and knowledge of pavement material properties are the requirements that aid the road engineer to minimize the potential problems caused by backcalculation and to evaluate the soundness of the results of backcalculated subgrade moduli.

It is not easy to backcalculate using a non-linear pavement model with many unknowns to provide accurate estimates of the system variables. On the other hand, linear elastic models cannot take into account horizontal and vertical elastic moduli fluctuation in real pavements. For these reasons the pavement model should be simplified but still remain reasonable to match the real one (see Peiravian 1994; Irwin 2002). All pavement layers should be taken into account. The problem is that the properties of some layers are close to one another and it's difficult to discriminate the differences in material stiffness. Often, the sophisticated model assumptions are not correct and systematic errors lead to incorrect conclusions.

2.3 Elastostatic Approach- Effective Surface Modulus and Equivalent Asphalt Thickness

Stolle (2002) suggested that surface displacement sensitivity of the pavement-subgrade system is related to the elastic modulus of each layer. Contribution ratios of the subgrade reach their maximum values at large offsets from the load, while the properties of the pavement structure together with the base layer can be captured better by the sensors located close to the load. The notion 'effective or equivalent surface modulus' can be used to capture the sensitivities.

The effective surface modulus E_{SM} characterizes the influence of subgrade response in the overall response of the pavement-subgrade system. For example, Ullidtz

(1987) demonstrated that 60 to 80 % of the centerline deflection under the applied loading is due to deflection of a subgrade layer. E_{SM} at any offset from the applied load can be calculated using modified Boussinesq's equations. For example, according to Ullidtz (1987):

$$E_{SM}(r) = \sigma_0 \cdot (1-\nu^2) \cdot (\frac{a^2}{r \cdot d(r)}) \tag{2.1}$$

where E_{SM} – effective surface modulus at a distance r from the centre of the loading plate; σ_0 – contact pressure; ν – Poisson's ratio; a – radius of the loading plate; r – radial distance from the centre of loading; d – deflection at distance r. Other approximations also appear in the literature, see, e.g., Jung (1990, 1993).

Based on the Odemark equation, an equivalent asphalt thickness h_a can be calculated as follows (Stolle 1996):

$$h_a = 0.9 \cdot \sqrt[3]{\frac{E_s}{E_p}} h_e \tag{2.2}$$

where E_s - the effective subgrade modulus,

E_p - a reference pavement modulus (4000 MPa), and

h_e - the equivalent thickness (in terms of subgrade material).

Typically, the top layers distribute the load on the lower layers forming a cone of approximately 45°. The distribution of load on pavement-subgrade layers is shown in Fig. 2.1. The surface moduli E_{SM} calculated at offset r from the centre of applied load characterizes compressed subgrade material below depth at a distance r_3 from the load. The effective surface modulus decreases with radius, but at some offset reaches its constant minimum value characteristic to the effective modulus of a subgrade. This radial distance is found to correspond approximately to the value of the equivalent thickness h_e (i.e. Stolle 1996).

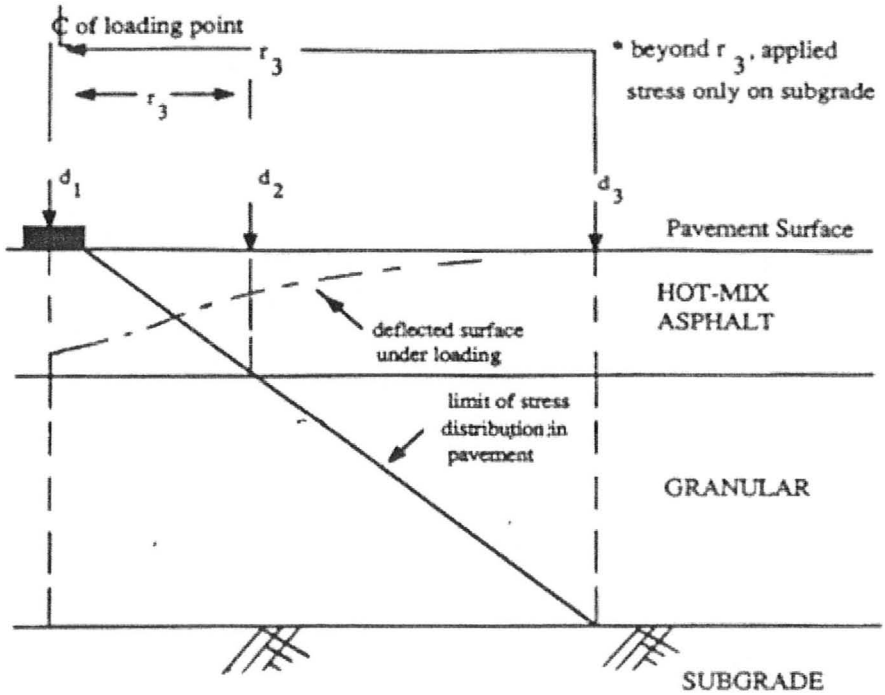

Figure 2.1 – Illustration of load distribution/deflection response in a layered pavement (source: Anderson 1987)

It should, however, be noted that although the backcalculated system parameters are fairly easy and quick to determine using the procedure described above, the individual pavement layer moduli cannot be correctly estimated using simplified backcalculation approaches as the system parameters do not represent real material properties but representative weighted average values (Stolle 1996).

2.4 Elastodynamic Approach

As it was mentioned previously, LWD has a significant limitation compared to the FWD device. Even though up to two sensors can be connected to the LWD device, typically, only one central sensor under the load plate is used to measure the deflections. This creates additional problems for pavement engineers interested in estimating pavement-subgrade properties from backcalculation analysis. Normally, there are a minimum of two variables to be backcalculated - elastic modulus of subgrade and equivalent pavement thickness (or pavement modulus). Therefore, additional simple and reliable tools should be provided for backcalculation of LWD data where only one deflection basin can be used as a set of data to solve the system of equation with two unknowns.

One such tool for the FWD data backcalculation is a simplified two-layer model dynamic approach based on Kirchhoff plate theory (Peiravian, 1994). Dynamic backcalculation has a strong advantage as it provides two pieces of information from each

sensor and, hence, can help to backcalculate more parameters of pavement-subgrade system than elastostatic one. It also provides a better model of the pavement response to the FWD and LWD loading as it takes into account radiation damping and inertial effects. According to the procedure suggested by Peiravian (1994), the load and displacement histories are used to determine dynamic impedance function of an idealized pavement-subgrade system, which depends on the properties of the pavement and foundation. Given "synthetic deflection data" corresponding to impact loads, subgrade moduli and equivalent pavement thicknesses can be backcalculated and compared to the corresponding "known" system properties.

In Kirchhoff theory, a plate is assumed to be infinite axisymmetric supported by the subgrade, assumed as elastic half-space. The basic assumption is that there is no friction between the plate and the subgrade layer. Stolle and Guo (2005), however, showed that a Kirchhoff plate model simplification might not be appropriate for thick flexible pavements.

According to Peiravian (1994) for a Kirchhoff plate under a transverse downward axisymmetric loading *p(r)* a Lagrangian form of the partial differential equation is:

$$D\nabla^4 w(r) + \rho_p h_p \ddot{w}(r) + q(r) = p(r) \tag{2.3}$$

If the point simple harmonic load is assumed in the form of $p(r) = P_0 e^{i\omega t}$ with P_0 being the peak concentrated load, ω – the angular frequency of loading, δ- Kronecker Delta, and both $w(r)$ $q(r)$ vary as a function of $e^{i\omega t}$, Eqn. (2.3) yields:

$$D\nabla^4 w(r) - \omega^2 \rho_p h_p\, w(r) + q(r) = P_0 \delta(0) \tag{2.4}$$

Using Hankel transformation of order zero to include the effect of elastic halfspace reaction (Peiravian, 1994):

$$\left(Dm^4 - \omega^2 \rho_p h_p\right)\bar{w}(m) + \bar{q}(m) = \frac{P_0}{2\pi} \tag{2.5}$$

The spatial response in radial direction *w(r)* can be expressed using the wave-number domain (m):

$$\bar{w}(m) = \int_0^\infty r w(r) J_0(mr) dr \tag{2.6}$$

where $$w(r) = \int_0^\infty m \bar{w}(m) J_0(mr) dm \tag{2.7}$$

$J_0(mr)$ is a Bessel function of the first kind and order zero;

$\bar{w}(m)$ – deflection in transformed space;

According to Peiravian (1994) the relationship between transformed reaction $\bar{q}(r)$ and the transformed displacement $\bar{w}$ as:

$$\bar{q} = G_s \frac{F(m)}{k^2 m} \bar{w} \tag{2.8}$$

where $G_s = \frac{E_s}{2(1+\nu)}$ is the shear modulus of subgrade, $k^2 = \omega^2 \rho_s / G_s$, $F(m) = (2m^2 - k^2)^2 - 4m^2 \alpha\beta$, $\alpha^2 = m^2 - \kappa^2$, $\kappa^2 = (1 - 2\upsilon_s)k^2/[2(1 + \upsilon_s)]$, and $\beta^2 = m^2 - k^2$ (Peiravian, 1994). As the depth z from the plate surface $z \to \infty$, parameters α and β for a given wave

number *m* must have such values to guarantee that $e^{-\alpha z}$ and $e^{-\beta z}$ disappear. Detailed solution was developed by Båth and Berkhout (1984) based on Lamb's research (1904).

The partial differential equation approximating the vertical motion w(r) for a Mindlin plate under a transverse downward axisymmetric loading is (Dym and Shames, 1973):

$$D\nabla^4 \mathrm{w(r)} + \left(1 - \frac{\mathrm{D}\nabla^2}{\mathrm{G'h}}\right) \mathrm{q(r)} = \left(1 - \frac{\mathrm{D}\nabla^2}{\mathrm{G'h}}\right) \mathrm{p(r)} \qquad (2.9)$$

where $D = \frac{G_p h^3}{[6(1-\nu_p)]} = \frac{E_p h^3}{[12(1-\nu_p^2)]}$ - is the flexural rigidity of the plate of uniform thickness;

$G' = \gamma^2 G_p$ – is an adjusted shear modulus taking into account the discrepancy between assumed and actual shear stress and strain variations through the depth;

$\gamma^2 \approx 5/6$ - shear modulus correction factor;

$\nabla^2 = 1/r[\partial/\partial r(r\partial/\partial r)]$ Laplace operator;

w(r)- function of radial coordinate;

q(r)- foundation reaction (contact pressure between the plate and the subgrade);

p(r)-function of vertical axisymmetric loading.

For a Mindlin plate theory Eqn. (2.9) after substituting Eqn. (2.8) into Eqn. (2.5), point load P_0, subgrade shear modulus G_s and eliminating rotational inertia and assuming harmonic response in time yields:

$$\left(D\mathrm{m}^4 - \omega^2\rho_\mathrm{p}\mathrm{h_p}\cdot a + \frac{\mathrm{F(m)G_s}}{\mathrm{k}^2\alpha}\cdot a\right)\bar{\mathrm{w}}(\mathrm{m}) = a\cdot\frac{\mathrm{P_0}}{2\pi} \tag{2.10}$$

$$a = 1 + \frac{Dm^2}{k^2 G_p h_p} \tag{2.11}$$

Or after dividing all parts of Eqn. (2.10) by coefficient a taking into account shear and calculated using Eqn. (2.11):

$$\left(\frac{D}{a}\mathrm{m}^4 - \omega^2\rho_\mathrm{p}\mathrm{h_p} + \frac{\mathrm{F(m)G_s}}{\mathrm{k}^2\alpha}\right)\bar{\mathrm{w}}(\mathrm{m}) = \frac{\mathrm{P_0}}{2\pi} \tag{2.12}$$

Kirchhoff plate theory doesn't take into account the effects of shear deformation and lets $\frac{Dm^2}{k^2 G_p h}$ go to zero (a=1) (Stolle and Guo, 2005).

To define deflections w(r) inversion of Eqn. (2.12) should be performed first to separate $\bar{\mathrm{w}}(\mathrm{m})$ on the left side. Therefore, for Mindlin plate theory the displacement under the concentrated load (i.e. at r=0) after applying the inverse Hankel transformation yields:

$$w(0) = \frac{P_0}{2\pi G_s}\int_0^\infty \frac{mdm}{(\frac{\mathrm{Dm}^4}{a} - \omega^2\rho_\mathrm{p}\mathrm{h_p})/\mathrm{G_s} + \mathrm{F(m)}/\mathrm{k}^2\alpha} \tag{2.13}$$

2.5 Equivalent SDOF Model Parameter Simplification

In the past decades, substantial research was done on developing dynamic backcalculated approaches which take into account the dynamic influence (effect of inertia) on the backcalculated subgrade modulus (Peiravian, 1994; Stolle, 1996; Parvini and Stolle,1998; Chatti et al. 2003; Chatti and Harichandran, 2004). Being a dynamic system subjected to a dynamic load of the falling weight, pavement-subgrade structure is controlled by the Newton's second law of motion. A single degree of freedom (SDOF) oscillator, shown in Fig. 2.2 is used to represent a two-layer pavement-subgrade system under a concentrated loading. The load and displacement histories are used to determine the parameters of the SDOF system, from which actual subgrade modulus and equivalent plate thicknesses are evaluated (Peiravian, 1994).

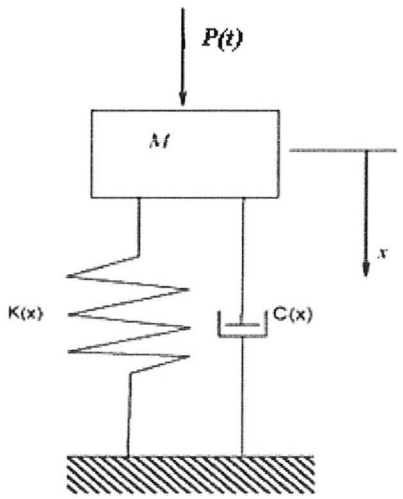

Figure 2.2- SDOF analog for the LWD Testing

(Source: http://www.mbindustries.com/images/engineering-SDOF.jpg)

The equation of the SDOF system in the time domain is as follows:

$$M\ddot{w}(t) + C\dot{w}(t) + Kw(t) = P(t) \tag{2.14}$$

where *M, C* and *K* are the mass, damping and stiffness matrices, respectively; *P(t)*- the load vector; *w(t)*- displacement of the system, with the dots referring to differentiation with respect to time. Eqn. (2.14) can be transformed into frequency domain by applying Fourier Transform (FFT) (Peiravian, 1994):

$$(-\omega^2 M + i\omega C + K)w(\omega) = P(\omega) \tag{2.15}$$

where $P(\omega)$ and $w(\omega)$ are the Fourier transforms of $P(t)$ and $w(t)$:

$$w(\omega) = \int_{-\infty}^{\infty} w(t)e^{-i\omega t}dt \tag{2.16}$$

$$w(t) = \int_{-\infty}^{\infty} w(\omega)e^{+i\omega t}d\omega \tag{2.17}$$

2.5.1 Frequency Domain Analysis

Neglecting inertial, resonance and damping effects of the dynamic loading when performing elastostatic backcalculation procedure can be a reason for considerable error in predicting the subgrade modulus (Roesset and Shao 1985, Chang et al. 1992). In the present thesis, dynamic impedance function approach suggested by Peiravian (1994) for elastodynamic backcalculation was improved by using the Mindlin plate. Based on a simple Kirchhoff plate model, the effect of shear deformation in the plate had been

neglected. Backcalculated results obtained using the simplified models are later compared to moduli that were used to produce the "synthetic deflection data" obtained from FEM and frequency analyses in Section 4.4.3 to find a better correlation for the LWD backcalculation.

The dynamic impedance of the SDOF system is a frequency-dependent characteristic of the pavement-subgrade stiffness. Dynamic impedance function is complex valued (Peiravian, 1994):

$$S(\omega) = \frac{P(\omega)}{w(\omega)} = (K - \omega^2 M) + i\omega C \tag{2.18}$$

where $(K - \omega^2 M)$ corresponds to the real component , and $i\omega C$- to the imaginary one.

For a Mindlin plate, dynamic impedance *S(ω)* relates to the properties of the pavement-subgrade model, which can be derived from Eqn. (2.13):

$$S(\omega) = \frac{2\pi G_s}{\int_0^{\infty} \frac{mdm}{(\frac{\mathrm{Dm}^4}{a} - \omega^2 \rho_p h_p)/\mathrm{G_s} + \mathrm{F(m)/k^2\alpha}}} \tag{2.19}$$

For a Kirchhoff plate, which neglects the shear deformations, dynamic impedance *S(ω)* is obtained by letting *a*=1.

The shear modulus G_s was replaced by $G_s(1 + 2\xi i)$ in Eqn. (2.19) to introduce a small amount of hysteretic damping in the system, where ξ the damping ratio, and, thus,

to prevent singularities when numerically integrating Eqn. (2.19) (Peiravian, 1994). The number of unknowns in both equations was reduced by assuming $\nu_p=\nu_s=0.5$, $\rho_p=\rho_s=2000$ kg/m^3.

To eliminate the term $2\pi G_s$ in Eqn. (2.19), dynamic impedance function was normalized with respect to the elastostatic stiffness *S(0)* (Peiravian, 1994). For a Mindlin plate:

$$\frac{S(\omega)}{S(0)} = \frac{\int_0^\infty \frac{dm}{(\frac{\mathrm{Dm}^3}{a})/\mathrm{G_s}+2}}{\int_0^\infty \frac{mdm}{(\frac{\mathrm{Dm}^4}{a}-\omega^2\rho_\mathrm{p}\mathrm{h_p})/\mathrm{G_s}+\mathrm{F(m)}/\mathrm{k}^2\alpha}} \tag{2.20}$$

where term *a* accounts for shear deformations and can be calculated using Eqn. (2.11).

As mentioned before, the dynamic impedance function *S(ω)* is a complex number. Hence, integration performed for Eqn. (2.20) provides real and imaginary parts which were plotted by Peiravian (1994) versus dimensionless parameter kh_e taking into account the influence of all variables presented in Eqn. (2.20).

The equivalent thickness h_e combines thickness of the asphalt-concrete layer h_p and the modulus ratio E_p/E_s into one variable:

$$h_e = h_p \sqrt[3]{\frac{E_p(1-\nu_s^2)}{E_s(1-\nu_p^2)}} \tag{2.21}$$

Parameter k was already mentioned in Section 2.4 in Eqn. (2.8). It is related to the angular frequency ω and shear wave velocity v_s calculated using Eqn. (1.4). Peiravian (1994) suggested that the maximum reasonable k value lies in the range up to 2 rad/m.

$$k = \frac{\omega}{v_s} = \omega \sqrt{\frac{\rho_s}{G_s}} \tag{2.22}$$

where $v_s = \sqrt{\frac{E_s}{2\rho_s(1+\nu)}} = \sqrt{\frac{G_s}{\rho_s}}$

A MATLAB code developed for the Kirchhoff plate by Peiravian (1994) and presented in Appendix B was adjusted to perform the frequency domain analysis (FDA) for the Mindlin plate.

Both Kirchhoff and Mindlin plate analyses were performed for several cases with various E_p/E_s modulus ratio, pavement thicknesses h_p and with the angular frequencies ω up to 400 rad/s, corresponding to the loading frequency of about 64 Hz. As mentioned by Peiravian (1994), most of the FWD loading is related to the loading frequency range less than 80 Hz. E_s was varied from 75 to 250 MPa, E_p- from 1000 to 6000 MPa, h_p- from 0.05 to 0.3 m. The computer simulations were performed for the material damping ratio ξ=0.5%. Plots of normalized real and imaginary components of dynamic impedance for two idealized models are shown in Fig. 2.3. As one can see, the imaginary component $(\omega C/K)$ of the normalized dynamic impedance (Fig.2.3 (a)) has an approximate linear relation with the normalized angular frequency kh_e in the frequency range of interest. Radiation damping related to inertia and wave propagation governs the imaginary

component, but not the material damping (Peiravian, 1994). The linear relationship indicates that the viscous damping of the SDOF model increases with the increase of loading frequency ω or equivalent pavement thickness h_e. For a Kirchhoff plate idealization the slope of the line is 1:1.5, while for a Mindlin plate which accounts for the shear deformations, the line lies below and has 1:2 slope. Quite a bit of scatter can be noted when $kh_e>2$ for both cases.

As for the real component of a SDOF, the relationship is parabolic in terms of ω. One can note that up to the value of $kh_e<2$ the normalized real component of dynamic impedance does not diverge a lot from 1 for the Mindlin plate, but increases quickly when $kh_e>2$. This fact shows that the mass of the SDOF system has a fairly small value indicating that inertial effect can not be properly captured by an equivalent mass M of SDOF oscillator. At high frequencies when the wavelengths become shorter and, thus, most of the energy is not reaching the subgrade layer, the response is mainly dominated by the pavement properties (Peiravian, 1994).

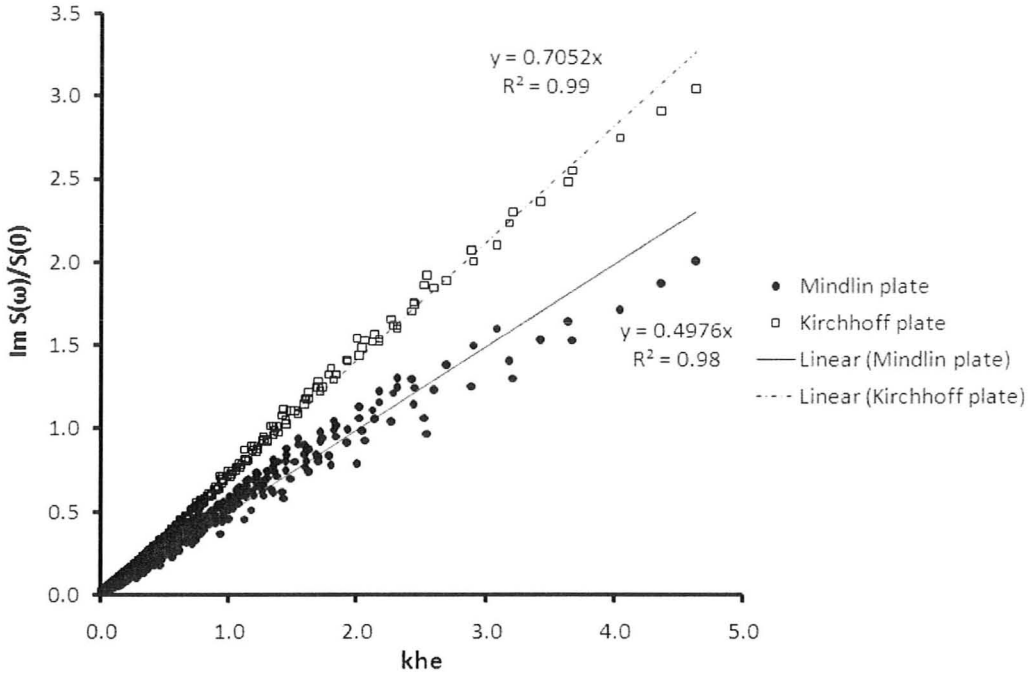

a)

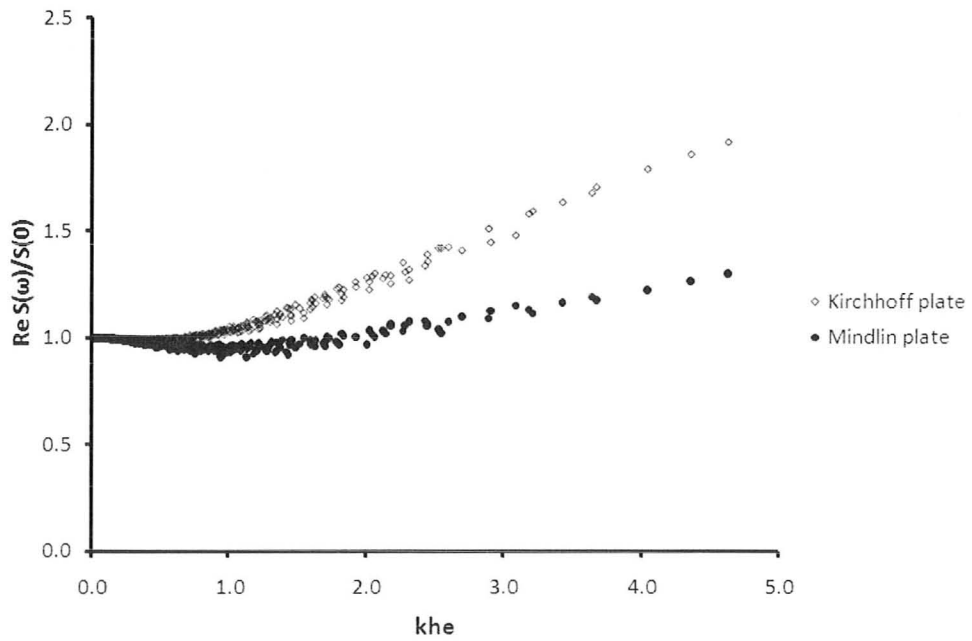

b)

Figure 2.3 - Graphs of imaginary (a) and real (b) components of normalized dynamic impedance of idealized Kirchhoff and Mindlin plate models for 0.5% damping ratio.

2.5.2 Time Domain Analysis

Movement of the testing device during operation often causes a truncation of the load-deflection histories of the LWD and FWD (Chatti et al. 2004). These problems might lead to considerable errors when recorded data is converted into frequency domain for backcalculation (Uzan 1994). In this regard, time domain analysis (TDA) can be a better than FDA as the erroneous regions of the FWD or LWD response can be neglected. Simplified SDOF oscillator approximation developed by Peiravian (1994) was used in the current thesis to perform TDA of the in-situ and simulated test data.

The load-displacement data obtained in the field for FWD and LWD can be fitted in the Eqn. (2.14) of a SDOF oscillator using a high order time-marching scheme presented by Peiravian (1994). Based on the central difference equations for given *w(t)* and *P(t)* sampled at *n* time points, the values $\dot{w}_i(t)$and $\ddot{w}_i(t)$ can be calculated using the formulae:

$$\dot{w}_i = \frac{-w_{i+2} + 8w_{i+1} - 8w_{i-1} + w_{i-2}}{12\Delta t} \tag{2.23}$$

$$\ddot{w}_i = \frac{-w_{i+2} + 16w_{i+1} - 30\, w_i + 16w_{i-1} - w_{i-2}}{12\Delta t^2} \tag{2.24}$$

where Δt- the time increment used in sampling; $t_i = \mathrm{i}\Delta t$; w_i - deflection at time *i.* The equation of motion can be written separately for each of the sampling points and converted to the matrix form. The procedure of solving the matrices and calculating *M, C*

and *K* values is described in detail by Peiravian (1994). The equations can be also found in Appendix B.

Uzan (1994) and Chatti et al. (2003) compared results from backcalculation in time and frequency domains and showed that the approach in the time domain is more appropriate for the FWD data analysis. On the other hand, Peiravian (1994) showed that time domain analysis (TDA) although being a fast and probably more precise method of evaluation of *M, C* and *K* characteristics of a SDOF oscillator, cannot provide a pavement engineer with a tool of detecting special in-situ conditions. For example, any uncommon plots of the normalized real and imaginary components of dynamic impedance in the frequency domain analysis (FDA), such as non-linearity or negative values of imaginary part, can indicate the presence of nearby bedrock (Peiravian, 1994). Therefore, frequency domain analysis (FDA) can provide a pavement engineer with additional information often hidden if only time domain analysis (TDA) is performed. FDA is a very powerful instrument when analyzing the real data. It should be used to verify the appropriateness of SDOF model as it can help identify strange in-situ conditions like stiffness variations within subgrade (i.e. sudden jump) or presence of nearby bedrock. Most elastostatic techniques are unable to provide one with such information and thus can lead to false analysis of in-situ time-deflection data.

2.6 Forward-Calculation Procedure

Even though backcalculation has shown to be accurate in terms of finding a good match for theoretical and in-situ deflections by a set of backcalculated elastic moduli of subgrade layers, it is currently considered among pavement engineers to be more of an art than a scientific approach. A major weakness of this approach is its high dependency on input model assumptions such as elasticity, homogeneity and isotropy of pavement layers, which are far from being close to reality, particularly in old damaged pavements with defects. In the recent years, a new approach called "forward-calculation" has become very popular for estimating elastic moduli of pavement layers from the field time-deflection data. This label is somewhat a misnomer as "forward-calculation" often has a different meaning specified as finding system response quantities (displacements) from the given input system parameters (i.e. geometry, material properties, loading etc.)

The first description of this approach was developed and published more than 25 years ago by Wiseman and Greenstein (1983). The idea of forward-calculation is to calculate the set of autonomous elastic moduli values and then compare the results with those obtained from backcalculation. The principle of the forward-calculation is that regardless of dissimilarities with backcalculation, estimated elastic moduli parameters calculated from the same deflection bowl should be similar to those obtained from backcalculation. The main difference of forward-calculation from backcalculation approach is that elastic moduli of pavement layers are calculated by applying closed-form

equations from the in-situ load-deflection histories compared to iterations in backcalculation. Therefore, given the deflection history and the thicknesses of the pavement-subgrade layers, a unique solution is assumed to exist that is calculated straightforwardly for each of these parameters. Particular part of the FWD deflection basin is involved in calculations of both effective surface and subgrade moduli. Thus, subgrade modulus is calculated from the deflections measured by the central (first) and utmost (last) geophones, whereas the effective surface modulus predictions are mostly dependent on the deflections measured by the intermediate sensors. The bounded surface course and the subgrade moduli are calculated straightforwardly while the middle layers/base course are estimated not directly based on the changeable relationship ratio between base course and subgrade modulus. This method has application for both flexible and rigid pavements. According to Stubstad et al. (2007) the results calculated using this method seemed to be more realistic and shown to be more consistent on a layer-by-layer basis compared to the backcalculation ones.

The primary advantages of the method are:

- Simplicity of the method for understanding and performing analysis;
- Being independent of the moduli of other pavement layers within the system, calculated subgrade and bound surface course moduli provide a single solution for every deflection bowl;
- Scatter of the data is noticeably less than in backcalculation.

Among others, the main shortcoming of forward-calculation is that it is limited to analysis of simple two- or three-layered pavement structures (Stubstad et al. 2007) and, as a result, backcalculation method is preferred by a skilled analyst. Forward-calculation is aimed to check and confirm backcalculated results, but not to replace backcalculation. It also provides one with the estimations and approximations of the elastic moduli and therefore implements systematic errors. Forward-calculation does not account for dynamic nature of the FWD and LWD loading.

In the present research study the focus was made on backcalculation technique although as being studied more thoroughly in the past and having a wider application among pavement engineers. A variation of this technique was developed by Stolle and Jung (1992).

Chapter 3 CASE STUDIES of LWD DATA

3.1 General

Lightweight deflectometer (LWD) tests were carried out by JEGEL on four pavement 60x60 cm samples, namely A to D, located close to each other in September 2007 outside the Applied Dynamics Laboratory (ADL) building at McMaster University. The asphalt-concrete thicknesses were measured to be 50, 100, 150 and 200 mm respectively. The location of the bedrock near ADL building is supposed to be at significant distance below the surface. All tests were performed with Dynatest 3031 LWD according to standard LWD testing procedures with the diameter of the loading plate of 150 mm and shown in Fig. 3.1. For each station 10 drops were made, with full load and displacement histories recorded. The recorded peak load value was approximately 7.8 kN. Characteristic load and displacements histories are presented in Fig.3.2.

Figure3.1- Dynatest 3031 LWD testing of pavement samples near ADL building, McMaster University (in this photo: Dr. Peijun Guo, McMaster University, and Seth Zhang, John Emery Geotechnical Engineering Limited)

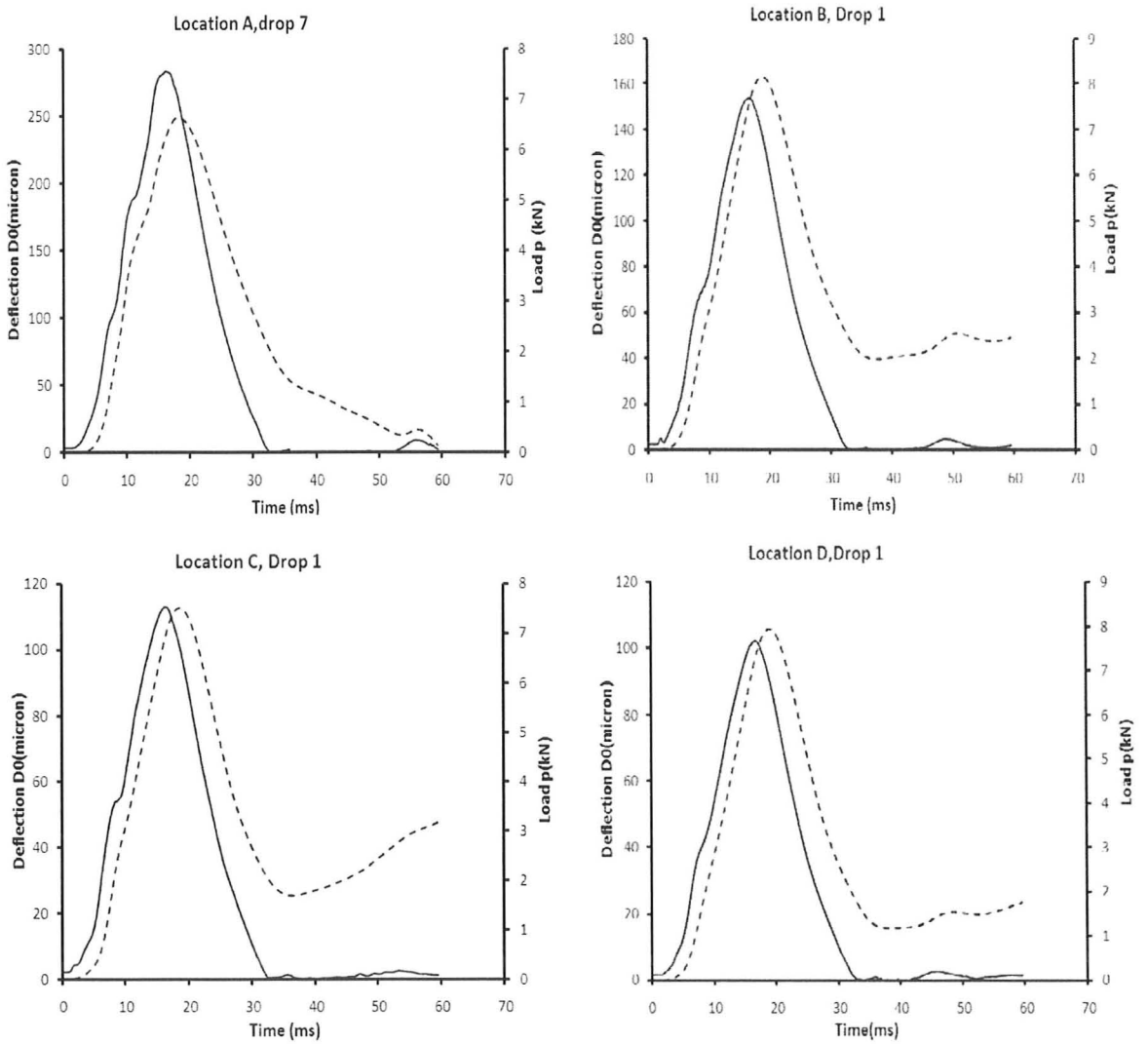

Figure3.2- Load-deflection histories of LWD test carried out on samples A-D (a-d) near ADL (--- *D0*, — Load, kN)

3.2 Analysis of LWD Data Collected at McMaster University

As one can observe from Fig. 3.2, the peak values of load and deflection are shifted indicating the inertial effects characteristic of dynamic nature of LWD tests. Some significant aspects of wave propagation can be noticed, namely:

- There is a time lag of about 2-3 ms between the peak load and displacement measured by the central geophone. This time leg is due to inertial effects (radiation damping) typical of FWD and LWD tests and tends to increase with the increase of an offset (Grenier et al. 2009);
- Some post-peak free deflection oscillations can be observed, which indicate the free vibrations of the pavement-subgrade system.

Guzina et al. (2002) made similar observations. As can be seen from the load-deflection histories, the load histories have similar shape for all samples with the peak of 7.8 kN occurring 16.5-16.75 ms after the beginning of the test. Deflection peaks occur approximately 18.25-18.5 ms after the beginning of each testing. As one can see from Fig. 3.2 time-deflection histories are not perfectly symmetrical, with the displacement not returning to zero, which would cause some problems when performing time and frequency domain analyses. This might be due to how the LWD device was held during the test, hand movements of the operator or seating problems. To avoid difficulties, the time-deflection data points after approximately 25 ms were eliminated from the analyses performed in Sections 3.2.1 and 3.2.2.

Material damping was as assumed to have a small effect on backcalculated elastic modulus of subgrade E_s and equivalent asphalt thickness h_a and, therefore, was not taken into account. This assumption is important as one determines damping C that reflects radiation damping (Peiravian, 1994).

3.2.1 Frequency and Time Domain Analyses

Frequency analysis was performed on the data collected near ADL using the SDOF analog and frequency domain approach developed by Peiravian (1994) which was discussed in Section 2.5.1. According to (Peiravian, 1994) the imaginary component is related to ω as:

$$\frac{C\omega}{K} = \alpha k h_e \tag{3.1}$$

where α is the slope, that was found to be for a Kirchhoff plate α=0.73136 (Peiravian, 1994), in this study α=0.7052 (Fig.2.3), for the Mindlin plate- α=0.4976 (Fig.2.3); $k = \omega\sqrt{\frac{\rho_s}{G_s}}$. After replacement k in Eqn. (3.1), one gets:

$$h_e = \frac{C}{\alpha K}\sqrt{\frac{G_s}{\rho_s}} \tag{3.2}$$

Odemark method of equivalent thickness states that a two-layer pavement-subgrade system can be represented as the equivalent single layer system with the maximum surface displacement w under the peak point load. Combining it with the Newmark's equation for displacement under a circular flexible plate (Jung and Phang, 1975; Stolle, 1990), one has:

$$K = \frac{P}{w} = 6G_s\sqrt{\left(0.81{h_e}^2 + a^2\right)} \tag{3.3}$$

where a- the radius of the circular loading plate (in this research 0.075 and 0.15 m for the LWD and FWD respectively), h_e can be calculated from Eqn. (2.2), $E_s = 2(1+\nu_s)G_s$, ν_s=0.5. To find the values for G_s and h_e one must solve the system of Eqns. (3.2) and (3.3) given C, K:

$$\frac{29.16G_s^3}{\rho_s}\left(\frac{C}{\alpha K}\right)^2 + 36a^2G_s^2 - K^2 = 0 \tag{3.4}$$

For the LWD backcalculation based on the Mindlin plate theory assumption and the density of subgrade ρ_s=2000 kg/m^3 Eqn. (3.4) yields:

$$0.059G_s^3\left(\frac{C}{K}\right)^2 + 0.2025G_s^2 - K^2 = 0 \tag{3.5}$$

Equivalent asphalt thickness h_a can calculated from h_e assuming an average value for the elastic modulus of pavement layer E_p=4000 MPa:

$$h_a = h_e\sqrt[3]{\frac{E_s}{E_p}} \tag{3.6}$$

Fast Fourier transform (FFT) technique was applied to the full recorded load and displacement histories using MATLAB code developed by Peiravian (1994) and adjusted for the LWD in-situ data. The code can be found in Appendix B. This was done to see the effect of the seating problems and hand movements of the LWD operator on the results of the test. Normalized dynamic impedances were calculated and plotted versus angular frequency ω or ω^2 for two pavement locations A and B (Fig. 3.3).

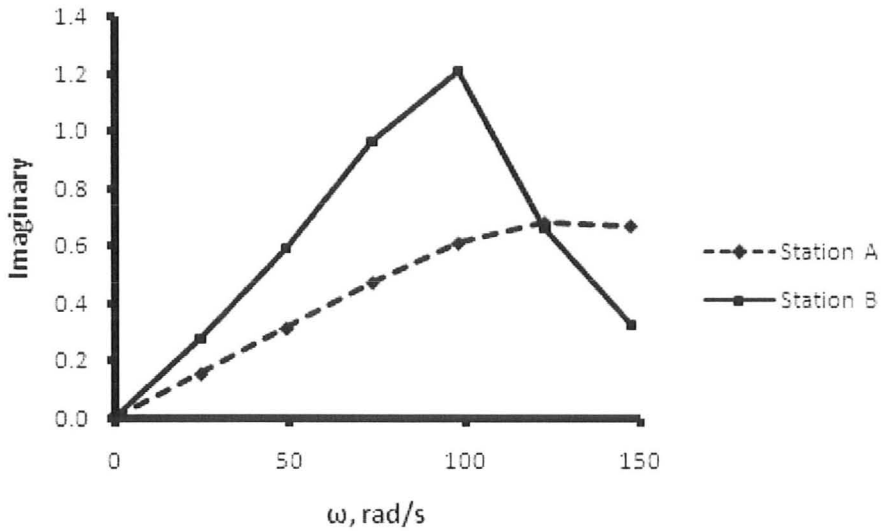

a)

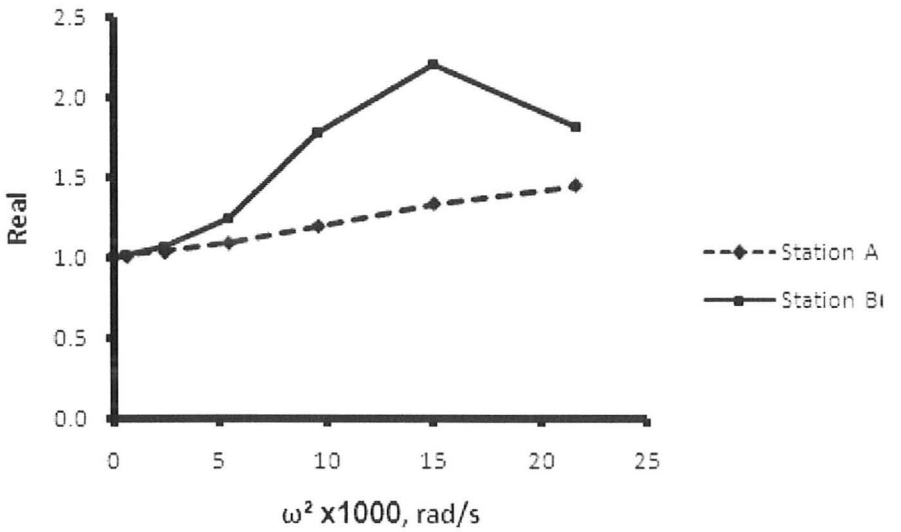

b)

Figure 3.3- Normalized dynamic impedance for full time-deflection histories, Stations A and B (imaginary (a); real (b))

Plots of the real and imaginary components of dynamic impedance for stations C and D showed similar patterns to location B and, as a result, have been omitted here. As one can see, almost linear relation was observed for imaginary component of dynamic

impedance for station A (50 mm thick), while it sharply dropped down for thicker pavement samples B to D (100-200 mm). Real component for station B also showed unusual behavior to the theoretical patterns discussed in Section 2.5.1.

The results suggest that the frequency domain analysis offers a powerful tool for assessment any unusual field or testing conditions but question the applicability of the SDOF model idealization, discussed in Section 2.5, for the backcalculation of the pavement-subgrade properties using FDA.

One of the problems which may cause systematic errors and anomalies in the impedance functions behavior is the finite size of the load plate (0.15 m) located close to the boundaries of the testing samples (0.3 m from the centerline). Close boundaries don't allow wave dissipation creating multiple reflections of travelling waves and causing noise. Possible solution to this problem is testing bigger samples representative to the real pavements and placing geophones farther from the load plate rather than using only the central sensor to record load-deflection histories. In their recent research, Ryden and Mooney (2009) suggested the minimum distance between the centre line of the LWD and geophone no less than a surface wave wavelength. They recommended the distance of at least 1 m for the load plate 0.3 m in diameter used in their research. Moreover, a peak contact stress level under the LWD plate subjected to 7.8 kN load is 441.4 kPa while the average stress under the pavement sample is 21.7 kPa, being approximately 20 time less. Using a larger load plate can minimize layer compression by distributing the load over

larger areas and, thus, noticeably reducing the stress under the plate. Owing to atypical patterns of the dynamic impedance functions, FDA was not included in the present study as potentially erroneous and causing systematic errors to the backcalculation parameters.

Time domain analysis was performed to calculate the parameters M, C and K of the equivalent SDOF systems for all stations using MATLAB code presented in Appendix B. Mass parameter M of the SDOF analog had a negative value when taking the full load-deflection histories (Fig. 3.2) indicating on possible problems with the LWD test mentioned above. This supports the statement mentioned in Section 3.1 that one should use only part of the time-deflection histories for the time domain analysis. Removing last part of the time-deflection from TDA reduced the effect of any possible problems occurring after the drop of the weight on the loading plate. This problem was eliminated after reducing the data points up to 22-25 ms for the thin pavements A and B and up to 30-33 ms for the thicker samples C and D.

Backcalculation of G_s, E_s, h_e and h_a parameters of the pavement-subgrade system was carried out for Kirchhoff and Mindlin plate approximations using Eqns. (3.2), (3.4), (3.6) and summarized in the Table 3.1 for three typical LWD drops on each of the four stations.

Table 3.1- Results of Time Domain Analysis (TDA) of asphalt samples located near ADL

Station (Drop#)	M (kg)	C 10^3 (kg/s)	K (MN/m)	Kirchhoff plate			Mindlin plate			h_p measured (mm)
				E_s (MPa)	h_e (mm)	h_a (mm)	E_s (MPa)	h_e (mm)	h_a (mm)	
A(7)	1.29	64.58	26.45	51.7	321	75	37.2	386	81	50
A(5)	1.67	62.00	27.19	55.0	310	74	39.6	372	80	50
A(9)	2.19	59.86	27.20	56.2	302	73	40.5	363	79	50
B (1)	1.59	131.25	41.68	59.9	446	110	42.8	534	118	100
B (2)	1.18	129.73	43.73	64.3	436	110	45.9	522	118	100
B (6)	3.69	120.33	43.81	67.7	414	106	48.4	496	114	100
C (1)	2.39	188.55	58.83	74.7	507	135	53.3	607	144	150
C (4)	0.8	177.08	60.82	81.4	481	131	58.0	576	140	150
C (5)	0.48	174.27	60.01	80.8	478	130	57.6	572	139	150
D (1)	1.48	210.15	64.19	78.2	530	143	55.7	634	153	200
D (4)	4.93	197.00	65.69	84.1	503	139	60.0	602	149	200
D (5)	2.05	192.40	64.08	82.6	500	137	58.9	598	147	200

The average value of backcalculated subgrade modulus E_s was found to be 69.7 and 49.8 MPa for the Kirchhoff and Mindlin plate, respectively, being almost 1.4 times higher for the Kirchhoff plate. Comparing the results obtained from Kirchhoff and Mindlin plate time domain analyses, one can observe that the effective subgrade modulus E_s is not uniform along the site. Thus, for both cases E_s for the pavement sample D (200 mm thick) is approximately 1.6 times higher than E_s at location A (50 mm). Another

important observation when comparing backcalculated results for both plate approximations is that E_s increases as h_a increases.

This fact brings some reasonable questions: Is the higher backcalculated value of E_s related to the higher thickness of pavement h_a ? And, if yes, then what does one measure with the LWD- the pavement or the subgrade stiffness? As previously discussed in Section 1.4, the diameter of the loading plate affects the influence depth of the LWD device and should be assumed based on the stiffness of the subgrade layer. According to Nazzal et al. (2007), the influence depth of the LWD was approximately 225 mm which is 1.5 times the diameter of the plate used for the case studies near ADL. Measuring the combined modulus of all layers, LWD was most likely unable to pick up the response of the subgrade layer which affected the results of backcalculation. The higher plate size of 300 mm suggested by Lin et al. (2006) for E_s less than 125 MPa can possibly partially solve this problem. Systematic errors implemented by backcalculation may also be a reason why results were not consistent. It may very well be that the finite size of the test pads had a much larger influence on the results than had originally been expected.

As one can see from Table 3.1, for pavement samples C and D with real asphalt thicknesses (h_a) 150 and 200 mm the backcalculated results were smaller in value. For stations A and B 50 and 100 mm thick, the results of backcalculation, on the contrary, overestimated the real pavement thickness values. The best accuracy was achieved for the location B 100 mm thick. The results might have been affected by the assumed average

value of pavement modulus E_p=4000 MPa, which in fact may have been higher. This would have had an impact on the value of h_a.

Chapter 4 ISOTHERMAL SIMULATIONS of FWD and LWD TESTS

4.1 General

This section presents the techniques used to provide the simulated data (load and deflection histories) generated by the elastodynamic axisymmetric finite element for the LWD and FWD tests, as well as the dimensional analysis of the data. Isothermal analysis in which the properties of asphalt concrete and subgrade elastic moduli are assumed constant during the day and are not related to temperature fluctuations was performed for flexible pavements.

As discussed in Sections 2.3 and 2.4, backcalculation of elastic moduli of pavement-subgrade layers using deflection and load histories of FWD and LWD devices is challenging. Elastostatic and elastodynamic dimensional analyses were performed on simulated data to develop relations that can be used to estimate the subgrade modulus and effective layer stiffness from LWD or FWD results using only histories directly under the load.

First, the dimensionless groups for steady state static behavior were identified in Section 4.4.2. Moreover, elastodynamic dimensional analysis is presented in Section 4.4.4 to improve the relations proposed by Peiravian (1994) for backcalculation. The objective of the analysis was to identify the frequency response functions (for LWD and FWD tests) as a function of the dimensionless group. The normalized real and imaginary

components were plotted against the dimensionless group that provided the best correlation.

Before simulating and analyzing results, a brief review of the finite element analysis techniques is presented.

4.2 Newmark Time-Stepping Algorithm

Numerical techniques for solving dynamic problems may be classified according to explicit or implicit integration schemes. The explicit method is conditionally stable regarding the size of the time step. The main limitation of this method is that very small time increments may be necessary to obtain a reasonable, numerically stable prediction. Implicit methods are unconditionally stable and therefore larger time increments may be used to solve the problem. The limit of time step depends on the desired accuracy that one wishes to achieve.

In this study, an unconditionally stable single-step implicit Newmark method was used for finite element simulations. This method was first introduced by Newmark (1959) half a century ago and later extended and improved by Wilson (1962) and others. A suitable time step (Δt) has a major effect on the accuracy of the wave propagation, in spite of which time-stepping scheme is assumed. Haigh et al. (2005) suggested that the maximum value for the length of a time increment should not exceed "one twentieth of

the time taken for a shear wave to travel across the smallest element of the finite element mesh".

By replacing the exact integration with approximate integration, one can control numerical stability of a time-marching scheme (Stolle, 1995). Let us consider the dynamic equilibrium for linear problems:

$$\boldsymbol{M\ddot{u} + C\dot{u} + Ku = F} \tag{4.1}$$

where $\boldsymbol{M}$, $\boldsymbol{C}$ and $\boldsymbol{K}$ - the mass, damping and stiffness matrices, respectively, and $\boldsymbol{F}$- the load vector which may be time dependent.

The SDOF equivalent of Eqn. (4.1) is a scalar equation

$$m\ddot{u} + c\dot{u} + ku = f \tag{4.2}$$

Applying Galerkin procedure, an integrated equivalent of Eqn. (4.2) is:

$$\int_{t_1}^{t_2} \delta u\,[m\ddot{u} + c\dot{u} + ku - f]dt \tag{4.3}$$

which after integration by parts Eqn. (4.3) yields:

$$\int_{t_1}^{t_2}[-\delta\dot{u}\,m\dot{u} + \delta u c\dot{u} + \delta u k u]dt = \int_{t_1}^{t_2} \delta u f dt - \delta u p\Big|_{t_1}^{t_2} \tag{4.4}$$

where δu- a weighting function using the same interpolation functions in time as a; $p = m\dot{u}$- is momentum; t_1 and t_2 - the times at the beginning and at the end of the time interval Δt, respectively.

The time variation of displacement over any interval $\Delta t = t_2 - t_1$ is

$$u = (1-\theta)a_1 + \theta a_2 = N_i a_i \tag{4.5}$$

where θ $(0 \leq \theta \leq 1)$ - is a natural coordinate, a_i - is the displacement at time t_i; N_i- interpolation (shape) function.

Using two-point integration scheme with the points symmetrical about θ=1/2, Eqn. (4.4) may be expressed in a form

$$\left[\frac{m}{\Delta t}\begin{bmatrix}-1 & 1\\ 1 & -1\end{bmatrix}+\frac{c}{2}\begin{bmatrix}-1 & 1\\ -1 & 1\end{bmatrix}+\frac{k\Delta t}{2}\begin{bmatrix}1-\beta & \beta\\ \beta & 1-\beta\end{bmatrix}\right]\begin{Bmatrix}a_1\\ a_2\end{Bmatrix}=\begin{Bmatrix}L_1\\ L_2\end{Bmatrix}+\begin{Bmatrix}p_1\\ -p_2\end{Bmatrix} \tag{4.6}$$

where $\beta=2\theta(1-\theta)$; $\boldsymbol{L}$- the vector, representing the impulse

$$\boldsymbol{L}=\Delta t\int_0^t N^T f\,d\theta \tag{4.7}$$

By selecting θ=1/2 Eqn. (4.6) becomes unconditionally stable form of Newmark's constant acceleration scheme (Stolle, 1995);

$$\left[\frac{m}{\Delta t}\begin{bmatrix}-1 & 1\\ 1 & -1\end{bmatrix}+\frac{c}{2}\begin{bmatrix}-1 & 1\\ -1 & 1\end{bmatrix}+\frac{k\Delta t}{4}\begin{bmatrix}1 & 1\\ 1 & 1\end{bmatrix}\right]\begin{Bmatrix}a_1\\ a_2\end{Bmatrix}=\begin{Bmatrix}L_1\\ L_2\end{Bmatrix}+\begin{Bmatrix}p_1\\ -p_2\end{Bmatrix} \tag{4.8}$$

where the first line is used to update displacement and the second is used to update momentum.

4.3 Ritz Vector Approach

Solving the dynamic equilibrium problems with minimal computational effort is important in structural dynamics. Dynamic analyses were completed using the finite element method, in which the matrix equations were integrated over time by using a Newmark method. Two strategies were adopted, one in which the full system of equations was considered explicitly, and a second where the number of equations was reduced by using a Ritz vector approach.

Typically, the dynamic response is determined by solving the matrix equations over an increment in time repeatedly, using a time-marching scheme. An approximation method to reduce computational effort is the Ritz approach where a solution can be characterized by time-dependent generalized coordinates described by space-dependent functions (Joo and Wilson 1989). Wilson et al. (1982) suggested to combine Ritz and finite element approximation and to use Ritz vectors representing a decreased number of estimated mode shapes.

The equation of motion for a finite element model can be presented in the form of coupled system of equations (see i.e. Bayo and Wilson, 1984):

$$\boldsymbol{M\ddot{u} + C\dot{u} + Ku = f(s)}r(t) \tag{4.9}$$

where $\boldsymbol{M}$, $\boldsymbol{C}$ and $\boldsymbol{K}$ are the mass, damping and stiffness matrices respectively; $\boldsymbol{f(s)}$ - vector, corresponding to the spatial distribution of the load constant in terms of time; $r(t)$- scalar function of time, which describes the frequency content of the loading.

The solution of Eqn. (4.9) can be obtained by direct integration and using Newmark time-stepping algorithm described in Section 4.2.

In dynamic analysis, the displacement vector can be expressed:

$$\boldsymbol{u = RZ} \tag{4.10}$$

where $\boldsymbol{R}$- is the matrix of the time-independent mode shapes (Ritz vectors);

$\boldsymbol{Z}$- time-dependent generalized displacement vector of the reduced system, comparable to participation factors in modal analysis (Sedran, 1994).

Another approach is to reduce the number of unknowns using Ritz vectors that are obtained from multiplying both sides by $\boldsymbol{R}^T$ and putting equation (4.10) into (4.9). Therefore, reduced system yields:

$$\boldsymbol{M}^*\ddot{\boldsymbol{Z}} + \boldsymbol{C}^*\dot{\boldsymbol{Z}} + \boldsymbol{K}^*\boldsymbol{Z} = \boldsymbol{f}^* r(t) \tag{4.11}$$

where $\boldsymbol{M}^* = \boldsymbol{R}^T\boldsymbol{M}\boldsymbol{R} = \boldsymbol{I}$; $\boldsymbol{C}^* = \boldsymbol{R}^T\boldsymbol{C}\boldsymbol{R}$, $\boldsymbol{K}^* = \boldsymbol{R}^T\boldsymbol{K}\boldsymbol{R}$, - generally full matrices; $\boldsymbol{f}^* = \boldsymbol{X}^T\boldsymbol{f}$.

Time-stepping of Eqn. (4.11) is now completed using the Newmark algorithm. Appropriate accuracy for two-dimensional finite element problems can be achieved using 16 Ritz vectors with approximately 5 per cent errors which become smaller for the high frequencies (Bayo end Wilson 1984). They also found that for soil systems 15 Ritz vectors can provide accurate results as the damping in soils is usually larger than the damping of structures. Sedran (1994) suggested that using 10 Ritz vectors is enough to describe the plate-like structures. Analysis for this thesis was carried out using Newmark integration scheme and 10 Ritz vectors as small number of vectors can provide a good estimation of wave propagation.

Following Wilson, Yuan and Dickens (1982), an algorithm for generation of Ritz vectors is as follows:

1. $\boldsymbol{M}$, $\boldsymbol{K}$ and $\boldsymbol{f}$ are calculated for Eqn. (4.9)
2. Solving for the first Ritz vector $\boldsymbol{R}_1$

$\mathrm{KU}_1 = \mathrm{f}$ where U_1 is the static mode shape, that is mass-normalized to yield

$$\mathrm{R}_1 = \frac{\mathrm{U}_1}{\|\mathrm{U}_1\|_{\mathrm{M}}},$$

with $\|U_1\|_M = \sqrt{U_1^T M U_1}$

3. Subsequent Ritz vectors R_i are generated using the classical Gram-Schmidt orthonormalization algorithm for i=2, ...L

   $\boldsymbol{KU_i = MR_{i-1}}$ to solve for $\boldsymbol{U_i}$ which is mass-orthogonalized for j=1, ..., (i-1) using

$$c_j = \boldsymbol{R_j^T M U_i}$$

$$\boldsymbol{U_i^*} = \boldsymbol{U_i} - \sum_{j=1}^{(i-1)} c_j \boldsymbol{R_j}$$

$$\boldsymbol{R_i} = \frac{\boldsymbol{U_i^*}}{\|\boldsymbol{U_i^*}\|_M}$$

The first Ritz vector is related to the static deflection of the system. Subsequent Ritz vectors are taking into account inertia and are generated as consecutive corrections to preceding vectors. All vectors are orthonormalized with respect to mass matrix $\boldsymbol{M}$ (see the algorithm). If $\boldsymbol{R}$ is determined from an eigenvalue analysis, then it is possible to convert the original system of coupled equations to uncoupled ones in which one solves for participation factors rather than displacements directly.

4.4 Simulations of FWD and LWD

4.4.1 Finite Element Model

A two-dimensional elastodynamic axisymmetric finite element model was used to model the behavior of the pavement subgrade systems. The pavement-subgrade system

was modeled using structure presented in Fig. 4.1. Fig. 4.1 (a) shows the overall subdivision adopted to define the problem with the actual mesh presented in Fig. 4.1 (b). Each layer was assumed to be homogeneous and isotropic. The pavement structure was supported by a thick subgrade.

A circular uniformly distributed dynamic load of the LWD and FWD was applied on the surface of the pavement layer to simulate the tire load. The radius of the flexible plate of the LWD and FWD devices was assumed to be 0.075 and 0.15 m, respectively. The load was modeled by a half-sine distributed impact load of 7.8 and 40 kN (LWD and FWD) amplitude with a duration of 0.03s, respectively.

Simulations were performed using FORTRAN algorithms for the cases of the full and reduced (Ritz vector approach) system of equations via the Newmark time-stepping algorithm. The grid for the full system of equations was the same as that for the reduced system. For the reduced system, the bottom boundary had to be fixed (Fig.4.1), whereas for the full system silent boundaries could be placed at the bottom. The rollers allowing sliding in the vertical direction represented the left-hand side boundary. The right-hand side boundary was modeled with viscous dampers (dashpots) (Wolf 1988, Parvini 1997, Ross 2004) to provide absorption of the energy and to minimize wave reflection back to the system.

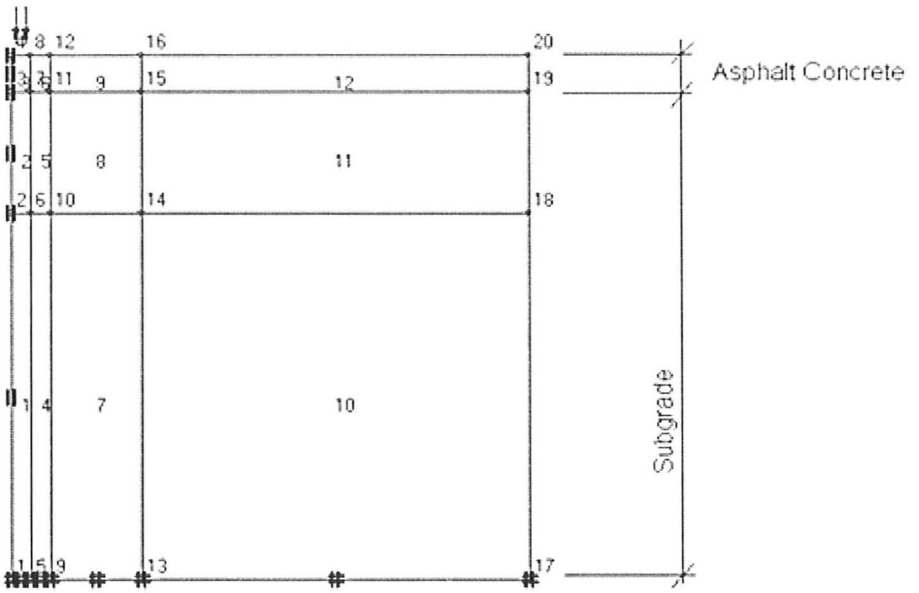

a)

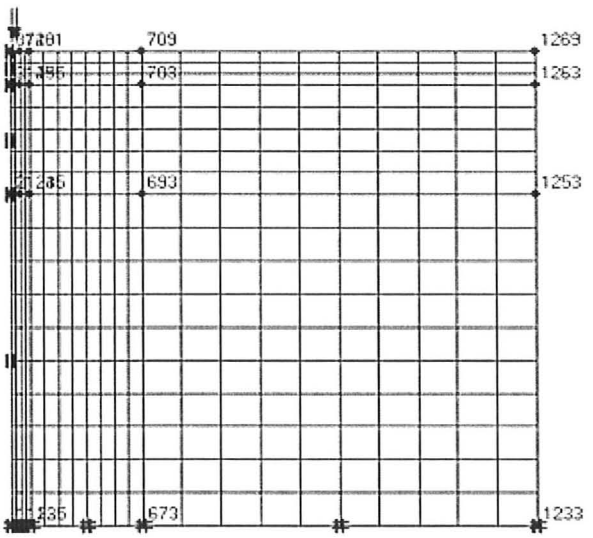

b)

Figure 4.1- Finite element model for Ritz analysis: (a) layout and (b) mesh.

The results of the simulations using full system of equations matched those obtained using reduced system of equations. Therefore, only the results of simulations

using the Ritz vector approach are presented in the thesis in Appendix A. Results of the isothermal simulations for FWD and LWD using Ritz scheme can be found in Tables A.1, A.2 of the Appendix.

The finite element model was discretized using 8-noded quadrilateral elements. Discretization of the finite element mesh was performed according to recommendations described in the literature (Lysmer and Kuhlemeyer 1969, Parvini 1997) using the following criteria:

- Under the applied distributed load, the size of the elements remained constant and relatively small compared to elsewhere - 0.0375x0.05 and 0.075x0.05 m for the LWD and FWD respectively;
- Maximum size of the elements was assumed to be less than 1/12 of the wavelength related to the peak frequency component of the loading (Lysmer and Kuhlemeyer 1969) to provide accurate results. According to Parvini (1997) the recommended element size to simulate FWD test response should be less than 0.15 m in the area near applied load.
- Increased size of elements was implemented farther from the centre line of the load to satisfy limitations of computer memory regarding the maximum number of elements (Parvini 1997).

The ranges for the depth to bedrock, material properties, magnitude of the load and other system parameters of the pavement-subgrade model are specified in Table 4.1. Poisson ratio for the pavement and subgrade was assumed according to recommendations of the Mechanistic-Empirical Pavement Design Guide (MEPDG) for asphalt concrete mixtures (Yin 2008). The damping ratio of the granular pavement materials was assumed 5% being a quite often recommended value found in literature (Richart et al 1970). Generally, the effective damping occurring because of energy spreading away from the source of excitation is significantly larger than the internal dissipation of energy within the system due to material damping. According to Sebaaly et al. (1985), material damping is not of primarily importance and can be ignored in common practice.

Table 4.1- Finite element discretization for FWD and LWD isothermal elastostatic simulations

Parameter	FWD simulations	LWD simulations
Radius R, m	4.0	4.0
Depth to bedrock, m	4.05-4.30	4.05-4.30
Radius of loading plate, m	0.15	0.075
Distributed load, kPa	565.9	441.4
AC layer thickness h, m	0.05; 0.1; 0.15; 0.2; 0.3	0.05; 0.1; 0.15; 0.2; 0.3
Modulus of elasticity of AC layer, E_p, MPa	2000; 4000; 6000	2000; 4000; 6000
Modulus of elasticity of subgrade, E_s, MPa	75; 100; 150; 200; 250	75; 100; 150; 200; 250
Poisson's ratio of AC layer and subgrade, $\nu_p=\nu_s$	0.3	0.3
Unit weight of AC layer and subgrade, $w_p=w_s$, kN/m^3	20.0	20.0

4.4.2 Dimensional Analysis: Elastostatic

Proper elastostatic dimensional analysis may help one to interpret the results of computer simulations. Though finite element simulations are elastodynamic by nature, elastostatic dimensional analysis helps identify relations corresponding to zero frequency from a frequency domain analysis described in Section 4.4.4 and provide one with additional tool for backcalculation.

The main purpose of the dimensional analysis is to find a set of normalized general parameters to characterize the phenomena of pavement-subgrade systems subject to surface loading without having to take into account the scale of the physical problem; i.e. for both FWD and LWD testing devices. The Buckingham (1914) π theorem is a foundation theorem for dimensional analysis, in which a set of dimensionless variables are produced from the original physical variables (Sedran 1999). In his π theorem Buckingham suggested that, if the primary physical relationship is given by $f(A_1, A_2, A_3 .... A_n) = 0,$ then it can be converted into another functional $\phi(\pi_1, \pi_2, \pi_3 ... \pi_{n-k}) = 0,$ where A_i are the n primitive variables, and π_j –independent dimensionless π groups for which the number of variables is less than the number of primitive variables and is equal to n-k . The physical problem presented in this thesis takes into account three original physical fundamental dimensions- length, mass and time- [L,M,T]. Therefore, the number of dimensionless π groups can be reduced up to three ($k \leq 3$) , see e.g. Sedran (1999).

Let us assume that a static load test on a pavement-subgrade system is fully defined by the set of primitive variables listed in the Table 4.2

Table 4.2 Primitive set of variables for pavement-subgrade system under static loading

	variable		units	dimensions
A_1	σ_{app}	maximum applied pressure	kPa	$ML^{-1}T^{-2}$
A_2	a	radius of loading plate	m	L
A_3	w	deflection at the center of the plate	m	L
A_4	E_p	pavement elastic modulus	kPa	$ML^{-1}T^{-2}$
A_5	E_s	subgrade elastic modulus	kPa	$ML^{-1}T^{-2}$
A_6	h_p	pavement thickness	m	L
A_7	ν_p	Poisson's ratio of pavement	-	*dimensionless*
A_8	ν_s	Poisson's ratio of subgrade	-	*dimensionless*

Other variables such as, for instance, the unit weight of pavement-subgrade layers are not taken into account. Various sets of π groups can be formed depending on what primitive parameters are taken as normalizing variables. σ_{app} and w are assumed to be the normalizing variables in the current study. Therefore, the Buckingham π theorem comes up with the set of π groups presented in Table 4.3 The dimensionless π groups are absolutely self-governing given that all the primitive variables are taken into account and are representative of the real behaviour of the simplified elastostatic prototype of pavement-subgrade system.

Table 4.3 π-Groups for pavement-subgrade system under elastostatic loads

π_1	$\frac{E_p}{\sigma_{app}}$	normalized pavement elastic modulus
π_2	$\frac{E_s}{\sigma_{app}}$	normalized subgrade elastic modulus
π_3	$\frac{a}{w}$	normalized radius of loading plate
π_4	$\frac{h_p}{w}$	normalized pavement thickness
π_5	ν_p	Poisson's ratio of pavement
π_6	ν_s	Poisson's ratio of subgrade

The results of isothermal elastostatic finite element computer simulations for FWD and LWD tests were used to generate synthetic data to establish the functional relations. Figures 4.3-4.5 show the series of the best condensation of π groups based on data from 75 simulations carried out for LWD, FWD and combined LWD and FWD tests respectively. Influence of plate radius, although included as a variable in dimensionless group, was not taken into account in simulations.

From these plots an estimated function is given by:

$$(\frac{a}{w}) = \alpha \cdot (\frac{E_s}{\sigma_{app}})^m \cdot (\frac{E_p}{\sigma_{app}})^n \cdot (\frac{h_p}{w})^p \qquad (4.12)$$

Coefficients α, m, n, and p for the LWD, FWD and combined LWD and FWD cases for isothermal computer simulations are presented in Table 4.4

Table 4.4- Coefficients, standard deviation and standard error of the estimate for functional

Parameter	LWD	FWD	LWD and FWD combined case
α	0.6417	0.7718	0.7065
m	0.3187	0.3839	0.349
n	0.2211	0.1753	0.196
p	0.4399	0.428	0.4318
standard deviation	0.55	0.26	0.5
standard error of the estimate	0.044	0.02	0.04

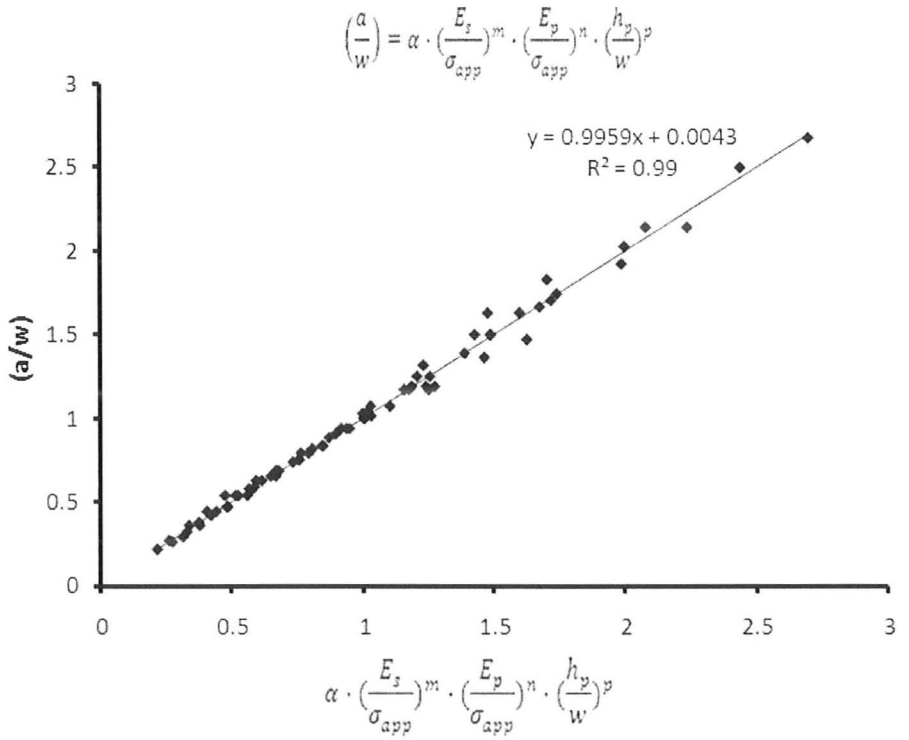

Figure 4.3- Condensation of π groups for LWD

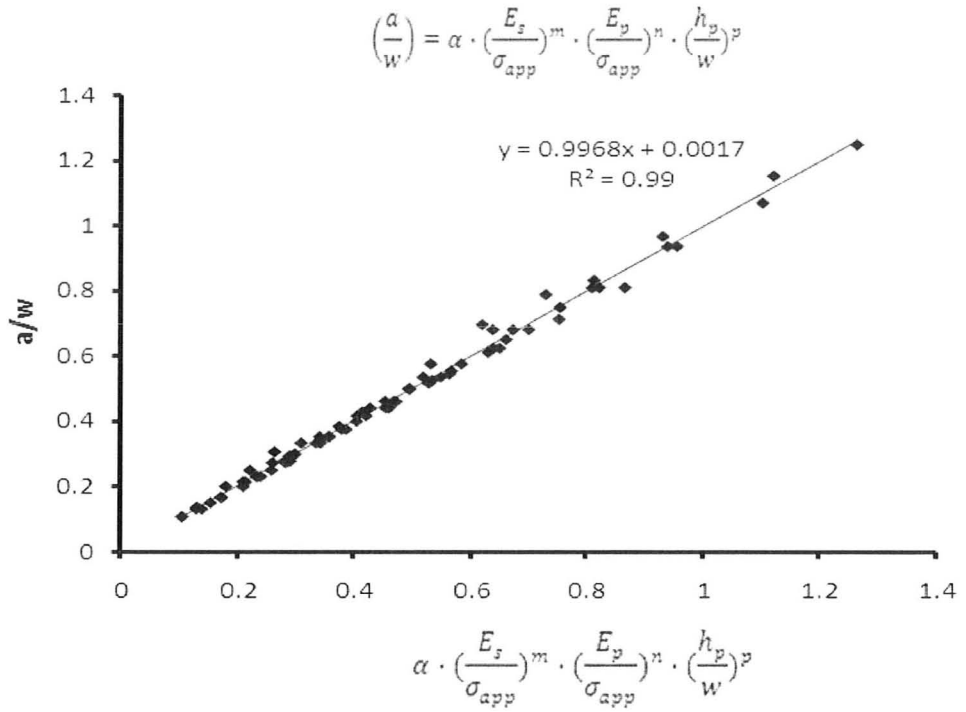

Figure 4.4- Condensation of π groups for FWD

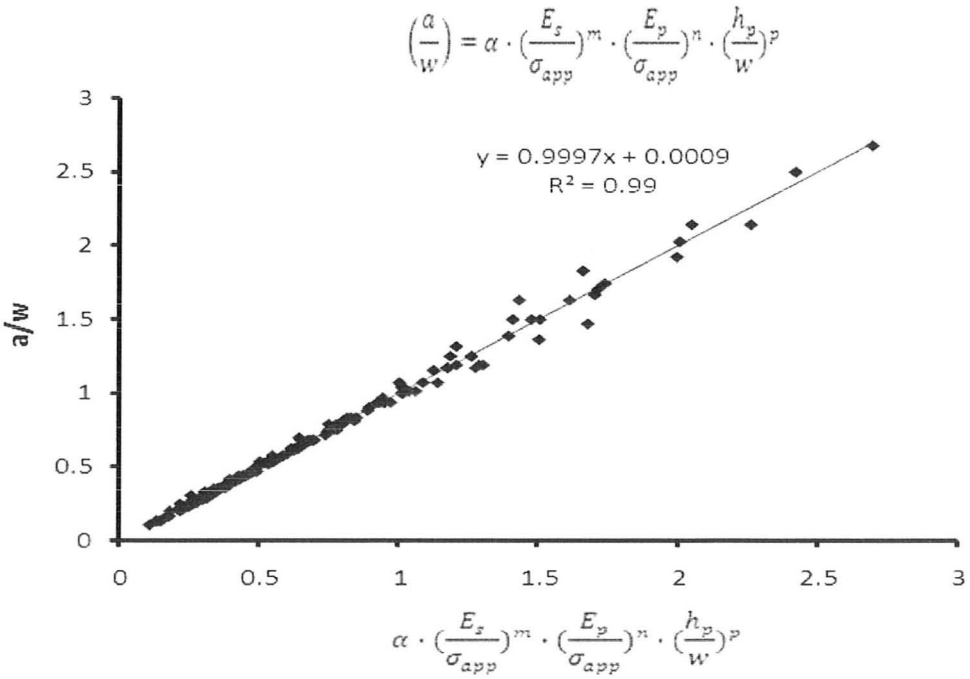

Figure 4.5- Condensation of π groups for combined FWD and LWD results.

Backcalculation of layer elastic moduli E_p and E_s from Eqn. (4.12) requires an additional piece of information. The zero frequency response (elastostatic stiffness) $S(0)=K$ discussed in Section 2.5.1 can be obtained from Eqn. (4.12). After extracting the maximum load applied P from the variable of the maximum applied pressure $\sigma_{app} = P/(\pi a^2)$ presented in Table 4.1 and taking into account that $K=P/w$ one ends up with the relation for the combined case of the LWD and FWD simulations shown in Fig. 4.6. To provide one with extra equation for backcalculation, dimensional analyses are further carried out in Sections 4.4.3 and 4.4.4 using the components of the impedance function.

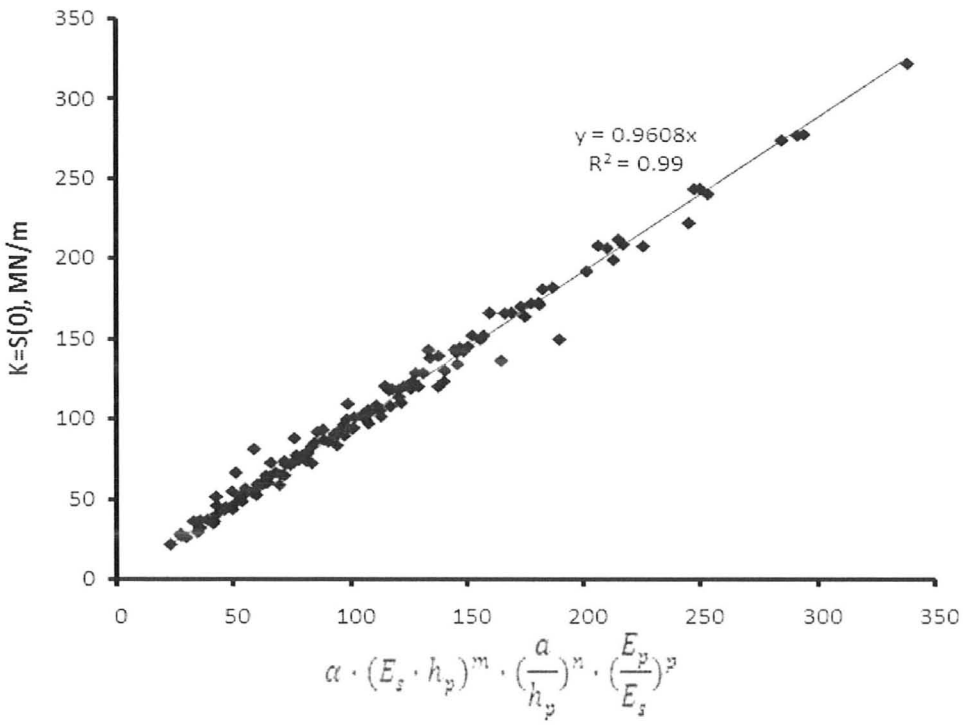

Figure 4.6 - Application in backcalculation for elastostatic stiffness K=S(0). Combined results for the LWD and FWD (α=1.66; m= 1; n=0.25; p= 0.37)

4.4.3 Frequency Domain Analysis

Let us now consider the dynamic nature of LWD and FWD in the backcalculation. This will allow us to estimate the layer moduli from LWD or FWD in-situ test data using only deflection and load histories from directly under the load. As mentioned in Section 2.4 this is mainly important for the LWD device typically limited to the deflection histories collected from one sensor located in the centre of the loading plate.

The focus of the current section is on frequency domain analysis being a promising tool for elastodynamic backcalculation. Real and imaginary components of dynamic impedance for the Mindlin plate idealization were calculated following FDA technique developed by Peiravian (1994) and extended in Section 2.5.1 (Fig. 2.3). The results of Mindlin theory approximation, allowing for shear deformations between the plate and the subgrade layer, were compared to those, calculated for elastodynamic isothermal FEM simulations (see Fig.4.1). The synthetic deflection data from FEM computer simulations were converted to the frequency domain using FFT. Discretization of the model and boundary conditions were discussed in Section 4.4.1.

Normalized real and imaginary components of the dynamic impedance were calculated using frequency domain MATLAB code developed by Peiravian (1994) and presented in Appendix B. For this study only loading frequencies up to 50 Hz were considered to have an appreciable effect on impedance characteristics. Therefore, angular frequencies ω up to 306.8 rad/s were taken into account providing 11 data points of real

and imaginary component for each simulation. The results of 75 simulations giving 825 data points for real and imaginary components of dynamic impedance are shown in Fig. 4.7.

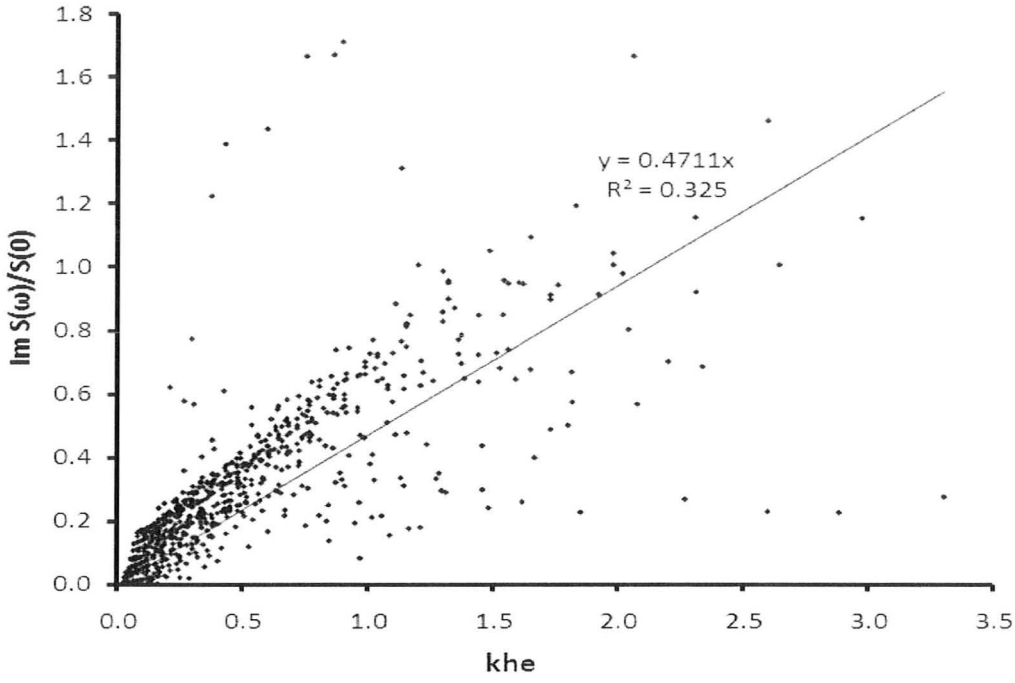

a)

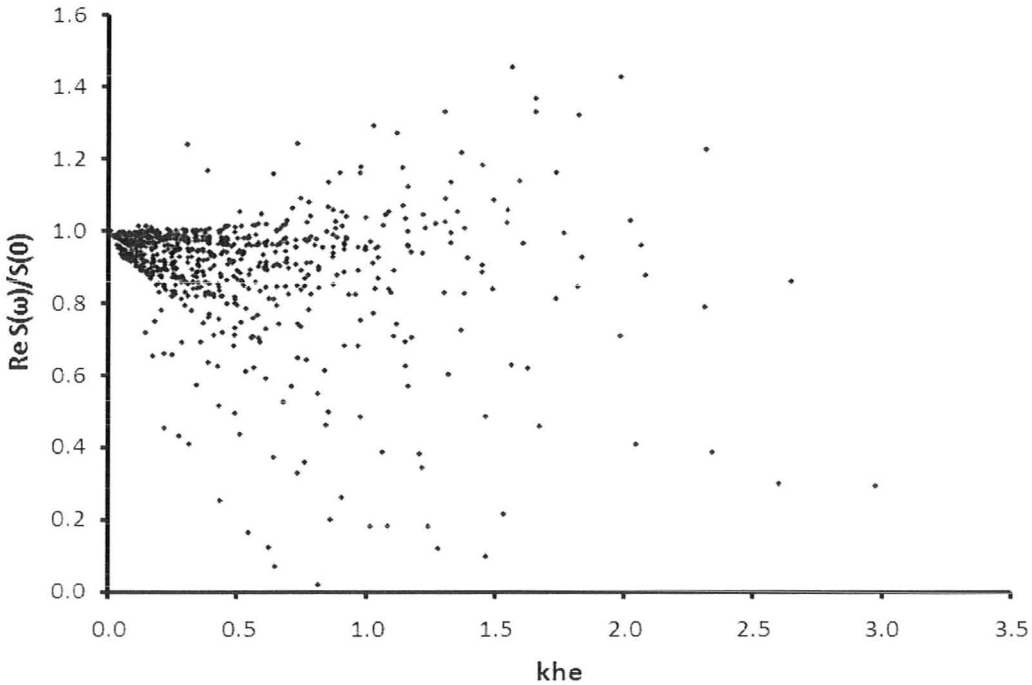

b)

Figure 4.7- Graph of normalized imaginary (a) and real (b) components of dynamic impedance for FWD isothermal simulated synthetic data versus dimensionless group kh_e

As one can see, there is a considerable scatter for both real and imaginary components of the dynamic impedance, compared to the idealized trends for the Kirchhoff and Mindlin plate theory approximations (Fig.2.3). The data points–outliers were analyzed and the results were summarized as follows:

- negative value of imaginary component was observed for the cases when elastic modulus of subgrade *Es* was 150-250 MPa and the angular frequency was at its low end (ω=30.7 rad/s).

- imaginary component was also negative for the pavements with h_p=0.05 and 0.2 m, stiff subgrade (*Es*=250 MPa) and frequency at its high end (ω=306.8 rad/s) as well as for the thick pavements of 0.3 m and angular frequency of 61.4 rad/s

- thick pavements of 0.3 m and E_s=150-250 MPa were giving most of the scatter at both high and low end of the frequency resulting in a limiting ω to a "safe" range of frequencies of 61.4-184.1 rad/s (10-30 Hz).

The anomalies in the impedance functions together with the observations mentioned above question the applicability of the SDOF model approximation presented in this study for the cases where the presence of the bedrock appears at shallow depth (4 m for these simulations). As indicated in Sections 2.5.1 and 2.5.2 both real and imaginary components are sensitive to the location of bedrock, especially the imaginary part. When the thickness of the subgrade decreases, the relation of normalized imaginary component of dynamic impedance plotted vs. ω^2 deviates from being linear and at low frequencies

becomes negative indicating that the damping coefficient C also becomes negative, which is unacceptable. Negative imaginary component indicates that the bedrock may be located at shallow depth.

In order to verify this hypothesis, elastodynamic simulations were performed using 4-noded FEM frequency domain FORTRAN program developed by Parvini (1997). The dynamic finite element model is presented in Fig. 4.1 with the only difference being the size of the mesh. As mentioned by Parvini (1997), the dynamic problems are very sensitive to the mesh discretization and the location of artificial boundaries. In order to avoid any problems, the model shown in Fig.4.1 and presented in Section 4.4.1 had a finer mesh. 4-noded quadrilateral elements were organized in 32 rows and 33 columns (FWD). Overall number of elements in the mesh used for the FWD simulations was 1056 and the total number of nodes- 1122. Simulations were performed for 18 cases described in Table 4.5. The damping ratio was assumed to be ξ=0.5 % to compare the results with the Mindlin plate approximation.

Table 4.5- Finite element discretization for FWD and LWD isothermal elastodynamic simulations

Parameter	FWD simulations	LWD simulations
Radius R, m	4.0	4.0
Depth to bedrock, m	4.05-4.30	4.05-4.30
Radius of loading plate, m	0.15	0.075
Distributed load, kPa	565.9	441.4
AC layer thickness h, m	0.05; 0.15; 0.3	0.05; 0.15; 0.3
Modulus of elasticity of AC layer, E_p, MPa	2000; 4000	2000; 4000
Modulus of elasticity of subgrade, E_s, MPa	75; 150; 250	75; 150; 250
Poisson's ratio of AC layer and subgrade, $\nu_p=\nu_s$	0.3	0.3
Unit weight of AC layer and subgrade, $w_p=w_s$, kN/m^3	20.0	20.0

Elastodynamic FE simulations were performed in the frequency range up to 314 rad/s (50 Hz). Real and imaginary components were calculated for the angular frequencies with a 5 Hz interval providing 11 data points for every case. Dynamic impedance at a low 2 Hz loading frequency (close to steady-state) was used to normalize real and imaginary components of $S(\omega)$, assuming that such loading would provide "near" elastostatic approximate solution. It should be noted that to have a non-singular matrix some dynamic component is necessary. The plots of normalized real and imaginary components of dynamic impedance are presented in Fig. 4.8 and 4.9.

As expected, introducing viscous dampers on the bottom boundary and, therefore, simulating elastic half-space with an infinite bedrock improved the trends. As one can see, up to $kh_e \approx 2$ imaginary component follows a near linear pattern for both LWD and

FWD devices. This is reasonable, as at higher frequency range the wavelengths are getting shorter compared to the asphalt-concrete layer thickness and for $kh_e > 2$, dynamic impedance begins to be dominated by the properties of the pavement layer resulting in a lot of scatter. Results of elastodynamic simulations support the notion that the existence of bedrock close to the surface has a major effect on the imaginary component behavior.

The slopes of the normalized imaginary components of dynamic impedance for the LWD and FWD frequency analysis (FA) simulations (Figs. 4.8 and 4.9 (a)) are compared to the Mindlin plate approximations shown in Fig. 2.3 (a). As one can see, the simulated results for the LWD (1:3 slope) and FWD (1:2.5) lie close to the Mindlin plate having 1:2 slope, suggesting that shear deformations typical for the real pavement-subgrade problems should not be neglected, indicating the Mindlin plate as a more realistic and accurate simplified model for a pavement-subgrade system. The differences between the FA simulations and Mindlin plate approximation may be explained as follows. Some energy still reflects back into domain, as the silent boundaries assumed for the FA simulations are not perfect. Furthermore, normalization of dynamic impedance for the FA simulations was performed at 2 Hz loading frequency compared to the steady-state normalization (zero frequency) for the Mindlin plate. Therefore, had stiffness been less, slope of the normalized imaginary component would have be greater.

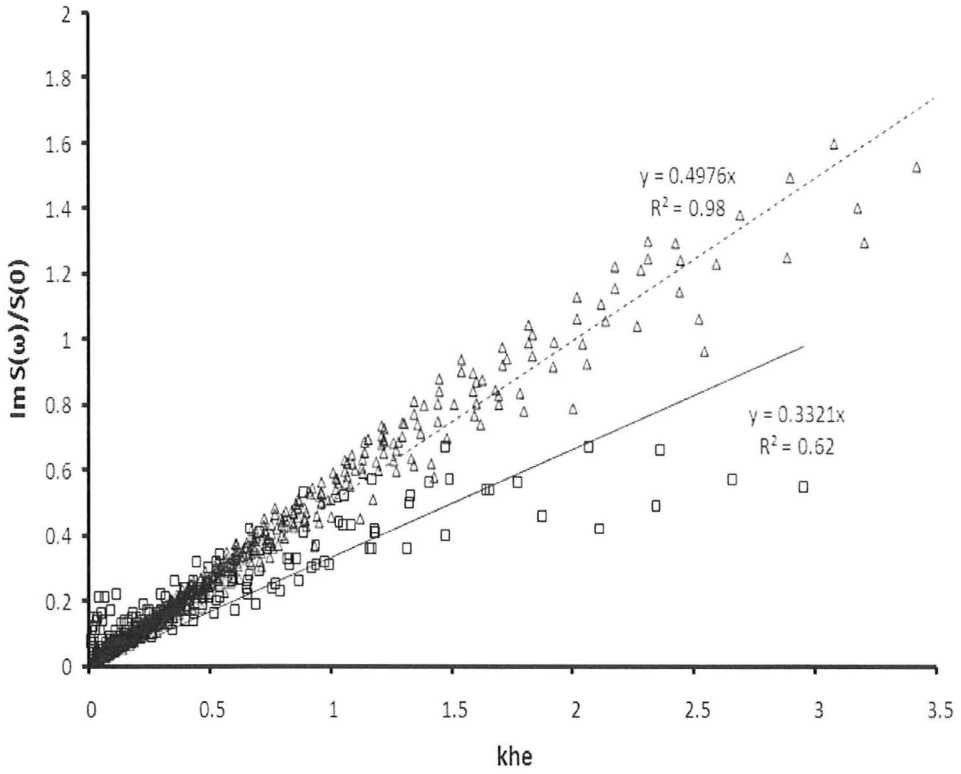

a)

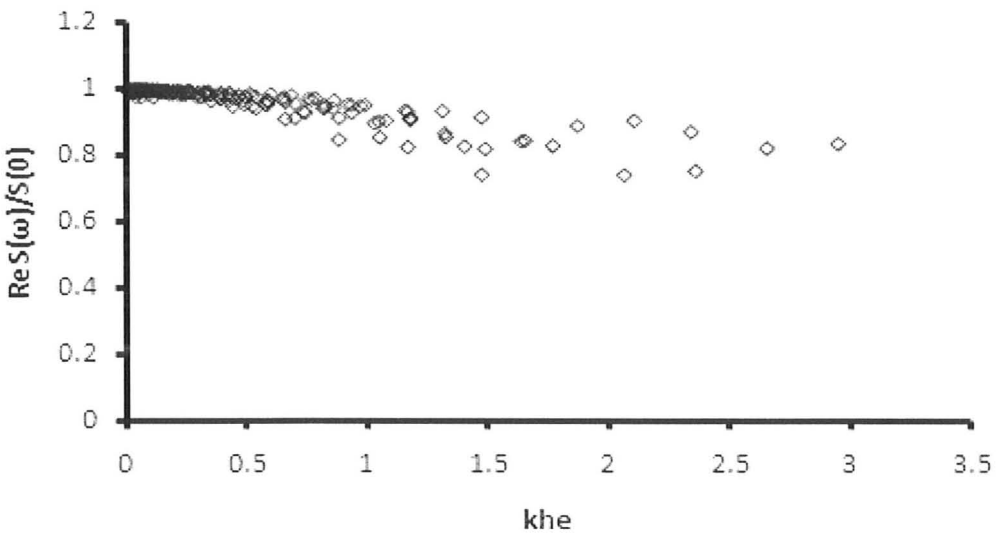

b)

Fig 4.8 - Normalized imaginary (a) and real (b) components vs. kh_e for LWD (0.5% damping) using 4-noded elastodynamic finite element program (--- Mindlin plate, — LWD, FA)

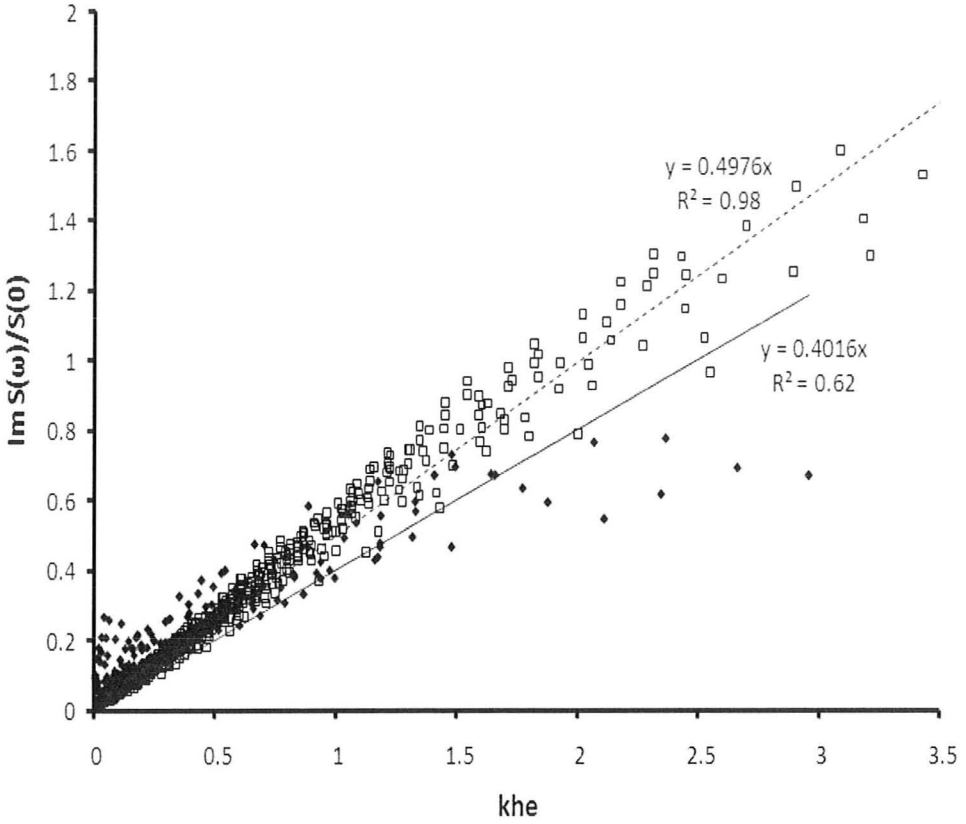

a)

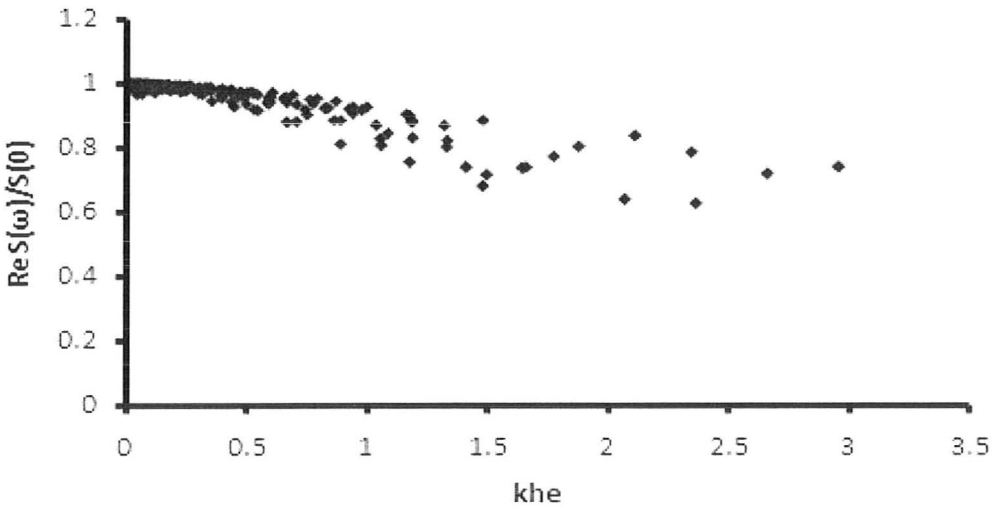

b)

Fig 4.9 - Normalized imaginary (a) and real (b) components vs. kh_e for FWD (0.5% damping) using 4-noded elastodynamic finite element program (--- Mindlin plate, — FWD, FA)

4.4.4 Dimensional Analysis: Elastodynamic. Backcalculation Strategy

To reduce the scatter shown in Figs. 4.8 and 4.9 dimensional analysis was performed on synthetic data used in the analysis that is presented in Section 4.4.3. The analysis was performed for data points in the range of $kh_e < 2$. Other points were eliminated due to the reasons discussed in Section 4.4.3.

Let us assume that the dynamic load test on a pavement-subgrade system is fully defined by the set of primitive variables listed in the Table 4.6. After performing the same steps as presented in Section 4.4.2 and assuming shear wave velocity, v_s , and elastic modulus of subgrade, E_s, to be the normalizing variables one comes up with four dimensionless groups presented in Table 4.7.

Table 4.6 Primitive set of variables for pavement-subgrade system under dynamic FWD (LWD) loading (Isothermal-Elastodynamic Analysis)

	variable		units	dimensions
A_1	ω	Angular frequency of loading	rad/sec	T^{-1}
A_2	v_s	Shear wave velocity	m/sec	LT^{-1}
A_3	E_p	Pavement elastic modulus	MPa	$ML^{-1}T^{-2}$
A_4	E_s	Subgrade elastic modulus	MPa	$ML^{-1}T^{-2}$
A_5	h_p	Pavement thickness	m	L
A_6	ρ_s	Density of pavement and subgrade	$kg \cdot m^{-3}$	ML^{-3}
A_7	$Im(S(\omega))/S(0)$	Normalized imaginary component of dynamic impedance function ($S(\omega)=P(\omega)/u(\omega)$; $K=P/w=S(0)$)	dimensionless	-
A_7*	$Re(S(\omega))/S(0)$	Normalized real component of dynamic impedance function	dimensionless	-

Table 4.7 π Groups for pavement-subgrade system under dynamic FWD(LWD) loading (Isothermal-Elastodynamic Analysis)

π_1	$\frac{Im(S(\omega)}{S(0)}$	Normalized imaginary component of dynamic impedance
π_2	$\frac{\omega h_p}{v_s}$	Normalized angular frequency
π_3	$\frac{E_p}{E_s}$	Normalized elastic modulus of pavement
π_4	$\frac{{v_s}^2 \rho_s}{E_s}$	Normalized shear wave velocity

Dimensionless group $\frac{{v_s}^2 \rho_s}{E_s} = \frac{1}{2(1+v_s)}$ is a constant and, as a result, was omitted in the functional relation which yields:

$$\frac{Im(S(\omega))}{S(0)} = \alpha(\frac{\omega h_p}{v_s})^m(\frac{E_p}{E_s})^n \tag{4.13}$$

Figures 4.10-4.12 show the results of the condensated π groups for the elastodynamic frequency domain FE simulations discussed in Section 4.4.3 and the Mindlin plate plots data set discussed in Section 2.5.1. Coefficients *α, m, n* for the LWD, FWD, combined LWD + FWD and Mindlin cases are summarized in Table 4.8.

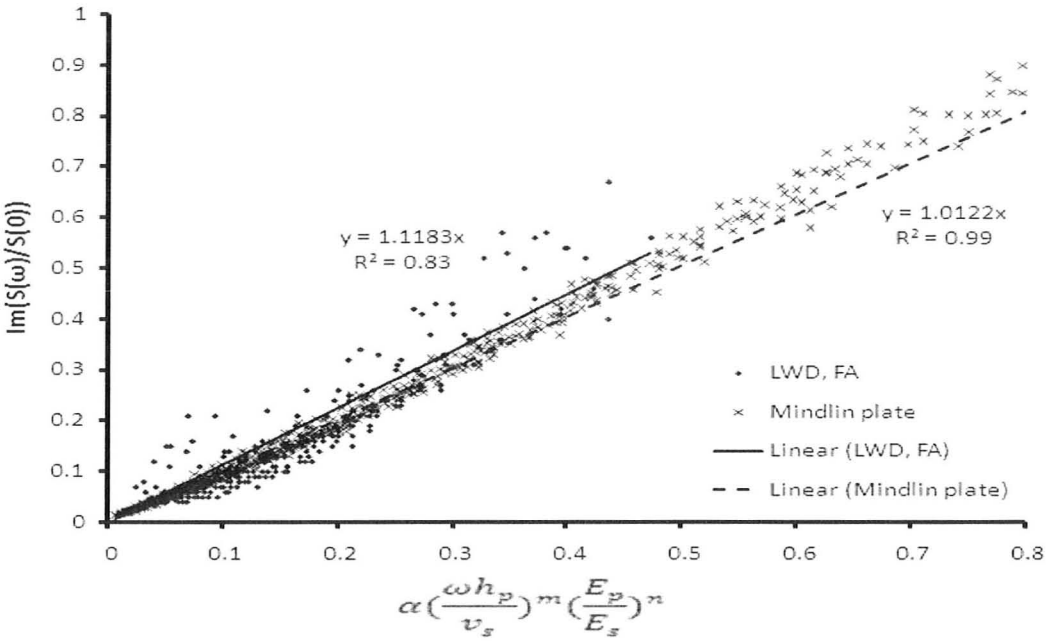

Figure 4.10 - Normalized imaginary component vs. dimensionless groups for LWD (0.5% damping)

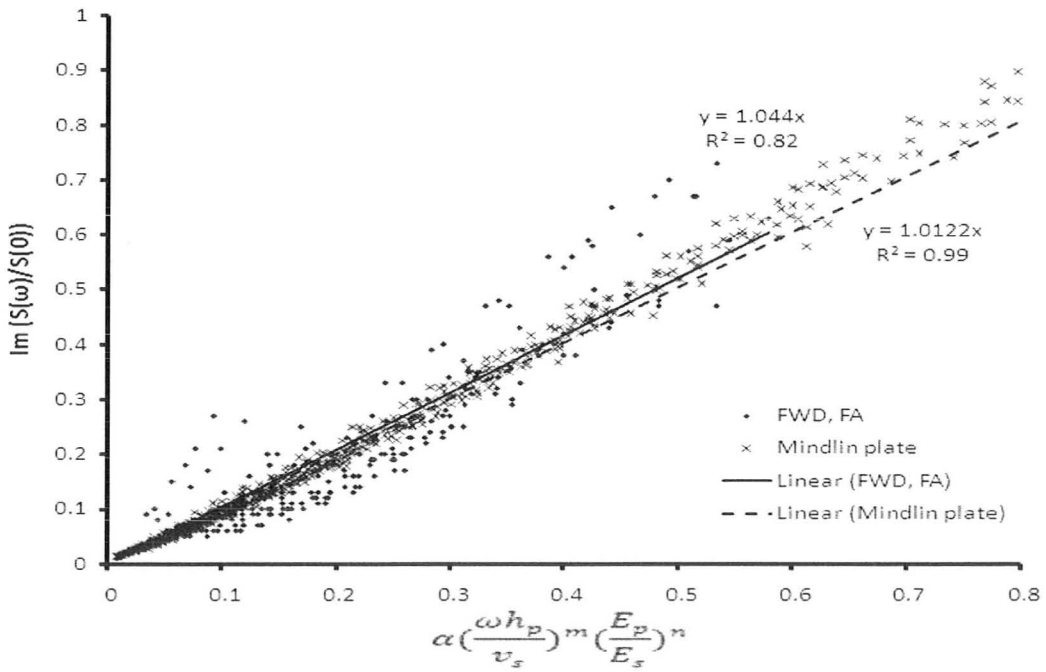

Figure 4.11 - Normalized imaginary component vs. dimensionless groups for FWD (0.5% damping)

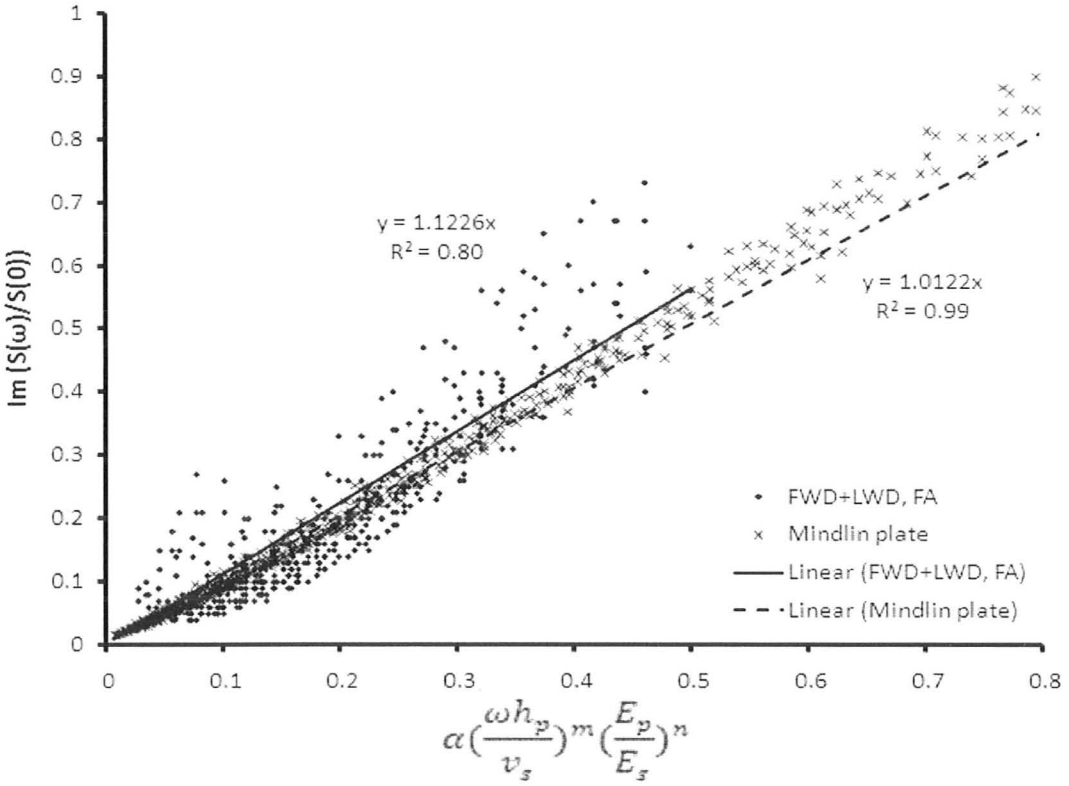

Figure 4.12 - Normalized imaginary component vs. dimensionless groups for LWD and FWD combined case (0.5% damping)

Table 4.8- Coefficients, standard deviation and standard error of the estimate for functional

Parameter	LWD	FWD	LWD and FWD combined case	Mindlin plate
α	0.17	0.27	0.21	0.37
m	0.45	0.45	0.45	0.92
n	0.35	0.25	0.3	0.4
standard deviation	0.10	0.123	0.106	0.30
standard error of the estimate	0.054	0.064	0.064	0.033

All cases (Figs. 4.9-4.11) show a good agreement with the Mindlin plate theory plots. This fact supports the applicability of the simplified Mindlin plate approximation for backcalculation of material properties of the real pavement-subgrade structures assuming that the bedrock is not close. Backcalculation of the unknown layer elastic moduli (E_s and E_p) can be performed from Eqn. (4.13) and the plot of the normalized imaginary component of dynamic impedance for the Mindlin plate (Fig. 4.10-4.12) together with the relation for elastostatic stiffness *S(0)* presented in Section 4.4.2 (Figs. 4.3-4.5). Imaginary component of the dynamic impedance can be found using FFT performed on the recorded load and deflection histories.

Chapter 5 EFFECT OF TEMPERATURE ON PAVEMENT RESPONSE

5.1 General

Factors that affect the magnitude of the elastic moduli of pavements are temperature, freeze-thaw cycles, moisture conditions and drainage, and compaction of different layers of the asphalt structure. Research in the past has often assumed average constant values of the resilient modulus within an asphalt concrete layer. The reason for this simplification was the lack of adequate analytical tools. Ullidtz et al. (1999) suggested using "relative modulus", which eliminates the effects of temperature or any other seasonal changes.

Deflections are highly sensitive to variations in elastic moduli of the pavement system layers. It is well known that the temperature of the asphalt concrete (AC) layer is a key aspect affecting the elastic modulus of asphalt concrete and, thus the deflection of flexible pavements. An important concern of highway engineers is to know how to deal with the interpretation of test data taken under various weather (temperature) conditions.

Among researchers who worked on the effect of temperature on flexible pavement behavior and sensitivity of FWD device over the past decade are:

- Chen et al. (2000)- finding temperature correction procedures for FWD deflections for cracked and intact pavements;
- Park et al. (2002), Fernando (2003)- establishing temperature correction factors and equations for FWD deflection data;

- Ali and Parker (1996), Herb et al. (2006) – performing simulations to predict asphalt pavement temperatures.

Temperature profiles within a pavement structure are influenced by the air temperature near the surface, as well as the solar radiation and the geothermal flux. Temperature fluctuations on the surface and within the pavement structure have a significant impact on the elastic properties of the pavement materials, specifically that of the asphalt concrete (AC) layer. The magnitude of the variations is greater near the surface and decreases with depth. Binder materials depend highly on temperature changes with the viscosity being inversely proportional to temperature. As expected, elastic moduli are low for high temperatures typical of summer conditions, which leads to decreased structural capacity and rutting. On the other hand, cold temperatures result in an increased elastic modulus of the asphalt, but at temperatures below zero the AC layer becomes more brittle, which can lead to premature cracking.

In either case, extreme temperatures are a source of pavement distress and therefore a good understanding of temperature influences helps pavement engineers better design pavements for specific weather conditions. For this reason it is important that any approach to predict pavement performance and behavior should make allowances for temperature changes. Furthermore, the backcalculation of elastic moduli should take into account for short-term and long-term temperature variations, namely daily and seasonal.

Averaging the resilient modulus over the different layers of the pavement structure for typical weather conditions is not considered a suitable approach as this does not take into proper account the influence of temperature changes. For example, the resilient modulus usually reaches its highest value when the pavement is completely frozen or during the early part of the stage when the pavement begins to partially thaw. As thawing continues the resilient modulus drops dramatically (Steinert et al. 2006).

Generally, the pavement temperature variation of a structure can be divided into four periods (Scrivner et al. 1969):

1) a period of deep frost and high strength;
2) a period of rapid strength loss;
3) a period of rapid strength recovery;
4) a period of slow strength recovery (also see Alkasawneh et al. 2007).

The second and third periods together represent critical periods for flexible pavements. (Scrivner et al. 1969).

5.2 Background

Among early research on asphalt pavement temperature changes was that carried out by Barber (1957). Others working on asphalt concrete temperature distributions in the northern and central parts of the USA in late 1960s, include Straub, et al. (1968), Demsey and Thompson (1970), Geiger (1959), and Vehrencamp (1953). In their work they tried to

develop better correlations between the pavement temperature on the surface of the asphalt layer and temperatures at specific depths, taking into account most temperature-related effects, as noted above.

At later stages, research propagated to the other parts of USA (Rumney and Jimenez 1971) and countries where the main concern and interest of the road engineers were the influence of hot climate and maximum pavement surface temperatures; see, for example Williamson (1972) in South Africa. The focus of this group of researchers was primarily on the thermal properties of the pavement (radiative absorption coefficient, surface emissive power, convection coefficient, thermal conductivity of the pavement material, pavement density) and climatic parameters such as air temperature.

Another group of pavement researchers was interested in studying the behavior of asphalt concrete pavements under the effect of low temperatures and frost penetration; see, for example, Christison and Anderson (1972) in Canada, and Noss (1973) in Norway, The pavement engineers of this group used input variables such as the geometry of asphalt pavements and thermo-physical properties including mean air temperature (normal air temperature), relative difference between the normal air, temperature and the recorded temperature, cloud cover, relative humidity, precipitation, wind velocity, and solar radiation.

Using air temperature to predict the temperature of the asphalt concrete layer has been quite popular among the pavement researchers. The limitations of these models are their complexity and applicability to one specific geographical location, which maybe not

representative for different conditions at the other sites. A general observation is that better temperature models usually require many input parameters that are often unavailable to the average practitioner. Well-known pavement temperature prediction models include: Asphalt Institute Model (1982), BELLS Equations (Stubstad et al. 1994, Stubstad et al. 1998, and Lukanen et al. 2000), the IPAT (Idaho Pavement Temperature) Model (Abo-Hashema and Bayomy 2002) and LTPP High & Low Pavement Temperature Models (Mohseni and Symons 1998).

Specific aspects of non-isothermal problems were:

- transient thermal response of AC pavements: Deen and Southgate (1975) , Berg (1974) , Wilson (1976) , Spall (1982), Highter and Wall (1984), Wolfe et al. (1987);
- relationship between the maximum surface temperatures and maximum air temperatures as a function of latitude - Solaimanian and Kennedy (1993) ;
- assessment of AC middepth temperature - Inge and Kim (1995) ;
- choice of asphalt binder based on pavement temperatures - Voller et al. (1998), Lukanen et al. (1998) and Mohseni (1998) ;
- assessment of temperature fluctuations in asphalt pavements due to thermal environmental conditions using a two-dimensional, transient finite-difference approach - Yavuzturk et al. (2002).

Models have been developed that relate temperature variation and other parameters (like air temperature, viscosity of AC layer, depth at which temperature is to

be predicted and so on) to the elastic modulus of asphalt concrete. For instance, Rada et al. (1991) proposed the SHRP's (Strategic Highway Research Program) equation to relate temperature variations to AC layer elastic modulus. This model takes into account material characteristics of asphalt concrete (percent air voids, viscosity and others) and testing conditions (test frequency and temperature profile) via

$$\log_{10}(E_{ac}) = a_1 + a_2 \cdot P_{200} \cdot f^{a_3} - a_4 \cdot V_a + a_5 \cdot \eta_{70,10^6} + a_6 \cdot \left[t_p^{(1.3+a_7 \cdot \log(f))} \cdot P_{ac}^{0.5} \cdot f^{-1.1}\right] + a_8 \cdot f^{a_9} \quad (5.1)$$

where E_{ac} - AC modulus, x 10^5 psi;

V_a - Percent air voids in mix, %;

f - Test frequency, cps or Hz;

t_p - Mid depth AC layer temperature, °F;

P_{200} - Percent aggregate weight passing # 200 sieve, %;

$\eta_{70,10}{}^6$ - Asphalt viscosity at 70 F, x10^6 poises;

P_{ac} - Percent asphalt content by volume of mix, %.

and coefficients a_1=0.553833; a_2= 0.28829; a_3= -0.17033; a_4= 0.03476;

a_5= 0.070377; a_6=0.000005; a_7=0.498251; a_8=0.931757; a_9= -0.02774.

Asphalt cement viscosity changes influence shear resistance of asphalt concrete. Equation (5.1) explains why the elastic modulus of AC decreases when the temperature in the pavement increases. This model is not used in the present study because of insufficient experimental data.

Several simplified models can be found in the literature to approximate the resilient modulus as a function of temperature. Equations relating the pavement elastic modulus with variation of pavement temperatures, include:

1) Lee (1976): Relationship between resilient modulus $log_{10}(M_R)$ and temperature between 0 and 50°C is approximately inversely linear. He also suggested that the decrease of 10°C resulted in the increase in M_R of more than three times the initial value.

2) Ullidtz (1987):

$$E = 15000 - 7900 \cdot \log(T) \tag{5.2}$$

3) Witczak (1989):

$$\log(E) = 6.53658 - 0.006447T - 0.00007404 \cdot T^2 \tag{5.3}$$

4) Janoo and Berg (1991):

$$E = 5994 - 242 \cdot T \tag{5.4}$$

5) Ali and Lopez (1996) found that the AC elastic modulus could be well correlated (R^2= 0.72) to the AC layer temperature:

$$E = e^{9.372-0.0361 \cdot T} \tag{5.5}$$

where for all cases, E is the asphalt concrete elastic modulus (MPa) and T is the pavement temperature at a depth 25 mm in the asphalt layer (°C).

Alkasawneh et al. (2007) compared the four different models shown in Fig. 5.1. By comparing these four models, one can see that three out of four relations provide similar predictions; i.e., Ullidtz's, Witczak's, and Ali and Lopez's models. The present study considers the model suggested by Ali and Lopez (1996) as it provided a good correlation factor (R^2=0.72) between the resilient modulus and temperature as reported in the case study by Bayomy et al. (2005). Ullidtz's model also provides a good compromise.

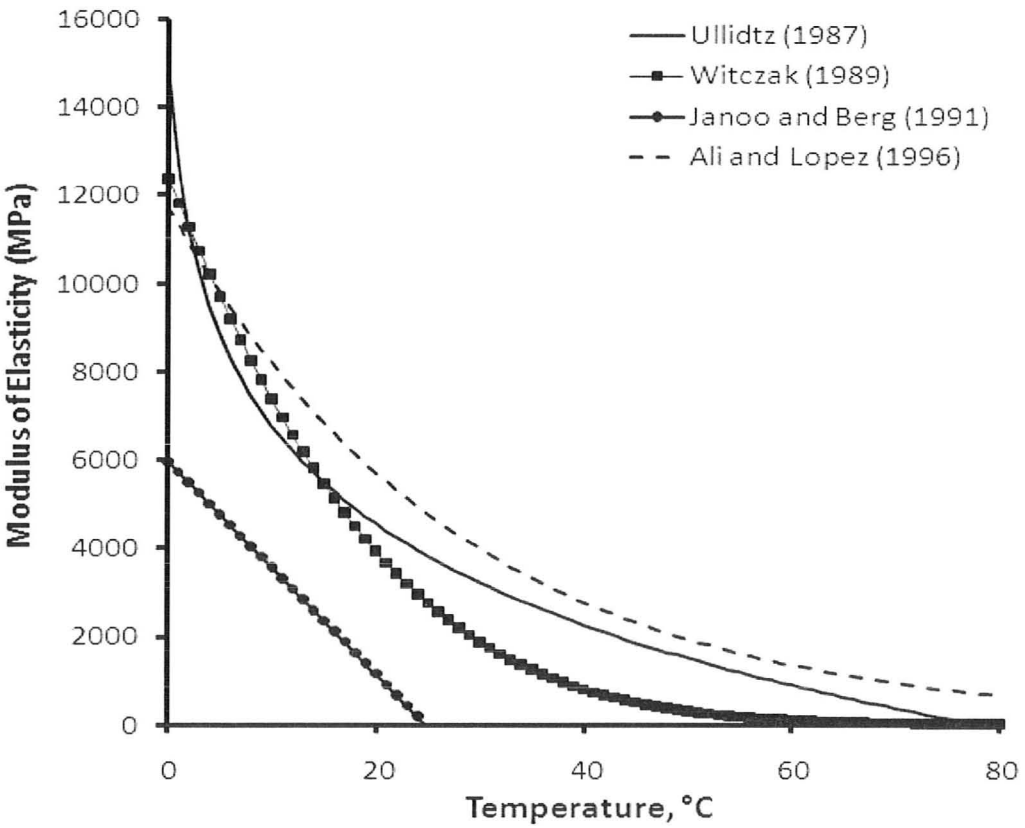

Figure 5.1- Resilient modulus vs. temperature. Comparison of various models of elastic modulus variation with temperature (Alkasawneh et al. 2007)

The Poisson's ratio of asphalt concrete is also known to be sensitive to temperature. For instance, Lee (1976) reported that Poisson's ratio varies from 0.24 to 0.46 for a temperature change from 10 to 42°C.

5.3 Objective of the Temperature Study

This chapter addresses the impact of temperature changes on pavement response for FWD and LWD to find the answers to the following questions: Are the subgrade modulus estimates sensitive to surface fluctuations in temperature? How does backcalculated layer stiffness vary as temperature changes in terms of what one measures using the various tests? What is the impact of temperature variation on the engineers' ability to backcalculate subgrade moduli? Material presented in this section will also give better understanding in terms of what a pavement engineer actually measures when FWD and LWD tests are performed. In this thesis temperature considerations were evaluated given limited experimental investigation with the results being analyzed using a one-dimensional finite difference model. The temperature profiles were subsequently used to determine how backcalculated pavement stiffness is influenced by non-isothermal conditions.

5.4 Temperature measurements

A limited experimental program was conducted on the Applied Dynamics Laboratory at McMaster (ADL) grounds to measure temperature profiles on three prototypes of pavement structures during August 2008. Temperatures were measured at different depths within the pavements. Readings were taken during 10 days at 10 minute intervals. The three pavement prototypes B-D with the thermocouples location are listed in Table 5.1. Pavement sample on station A was damaged at the time the experiment was carried out and, therefore, not considered.

Table 5.1- Thermocouple location

Thermocouple	Thermocouple depth from the top, mm		
	Station B	Station C	Station D
1	-	-	10
2	80	80	110
3	160	160	200
4	240	240	275
5	320	320	355

5.5 Temperature profile

Temperature conditions recorded at Hamilton Intl. Airport, ON, Canada (Latitude: 43.10N, Longitude: 079.56W, Altitude: 237m) are summarized in Table 5.2 (http://www.theweathernetwork.com/statistics/C01996/caon0289).

Table 5.2- Temperature profile near Hamilton Airport, ON, Canada

Temperature, °C												
	Jan	Feb	Mar	Apr	May	Jun	Jul	Aug	Sep	Oct	Nov	Dec
Maximum	-2	-1	4	11	19	24	26	25	21	14	7	1
Minimum	-9	-9	-4	1	7	12	15	14	11	5	0	-6
Mean	-5	-5	0	6	13	18	21	20	16	9	4	-2

According to the four periods classification of Scrivner et al. (1969) the temperature-related measurements in this research study correspond to the fourth period - period of slow strength recovery. It is worth noting that asphalt temperatures at depth 10 mm were recorded with maximum of 43.7° C and a minimum of 15.1° C, while the air temperatures in August varied from a maximum 51.8° C to a minimum of 10.0° C.

Taking into account that the pavement temperature is linked to the air temperature, one would expect the periodic temperature fluctuations during the day as well as over the year. As suggested by Ali (1996), the elastic modulus of asphalt pavements follows a sinusoidal pattern throughout the year:

$$E_{AC} = A + B\sin(2\pi \cdot f \cdot T + \theta) \tag{5.6}$$

where E_{AC} (or E_1) - elastic modulus of the asphalt concrete layer;

A - average value;

B - amplitude of the wave (if the dependent variable is constant then B equals 0);

T - time of observation (e.g., month of the year 1 to 12);

f - frequency (number of increments per cycle equals 1/12 in case of using month increments, and there is one cycle per year); and

θ - phase angle which controls the starting point on the curve and the peak month(s).

This model was adjusted and applied to the data collected in-situ near ADL. For this study five consequent days in August 2008 were selected when the temperature changes were quite smooth and the peak temperatures could be assumed as constant. According to the 1986 AASHTO guide temperature prediction procedure, monitoring the average air temperature for the subsequent five days is required for predicting pavement temperatures with depth. Based on the field data monitored near ADL, the averaged AC layer temperature sinusoidal function of time at depth 10 mm was found to be:

$$T(t) = A + B \sin [\theta(t - t_0)] = 13*\sin(6.02*(t-12))+28 \quad (5.7)$$

where t-time (hours).

Averaged temperature predictions calculated using Eqn. (5.7) are shown in Fig. 5.2 together with the surface temperature time history. As shown in the figure, the surface temperature measurements followed a sinusoidal pattern, although it was not as smooth as the simulated one. This was due to the various rate of temperature rise during the heating (morning) and cooling (afternoon) cycles, making averaging and determining an equation for temperature fluctuations somewhat problematical.

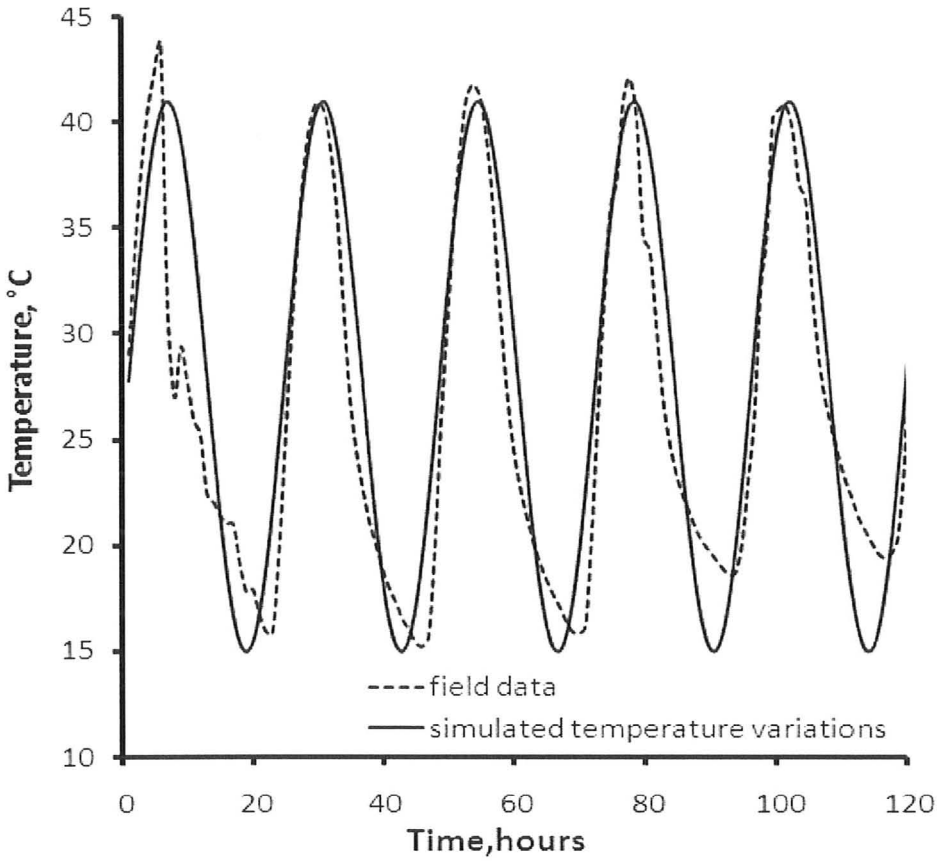

Figure 5.2 – Daily temperature fluctuations monitored at 10 mm depth in August, 2008 (collected near ADL building, McMaster University, Hamilton, ON, Canada) and simulated temperature variations. .

5.6 Heat transfer model

According to Yavuzturk et al. (2002) and Herb et al. (2006) several environmental aspects can affect pavement temperature: solar radiation, wind, precipitation, thermal and atmospheric long wave radiation between the pavement surface and the sky, back radiation, convection within the asphalt concrete and evaporation. These factors affect the

surface energy balance and the direction of the heat flux, which could lead to cooling or heating of the AC surface, depending on the difference between air and pavement surface temperatures. At a certain depth, depending on a season, the temperature in the pavement remains fairly constant. For the analytical evaluation of temperature profiles, this depth was assumed to be approximately 600 mm, which is consistent with the measurement of the deepest thermocouples that measured little fluctuation in temperature during the 5 days. Temperature measurements carried out near ADL were discussed earlier in Sections 5.4 and 5.5.

To be able to estimate the temperature distribution of the asphalt concrete layer, one must take into account the diffusion of the heat through the pavement and soil, which may be represented by the heat equation:

$$\frac{\partial T(t,x)}{\partial t} = \alpha \frac{\partial^2 T(t,x)}{\partial x^2} \tag{5.8}$$

where $T(t,x)$ - the temperature of the pavement at time t and depth x; and α - thermal diffusivity of asphalt concrete layer and base (m^2/s). The *thermal diffusivity* is "the coefficient that expresses the rapidity of temperature change when a unit volume of asphalt concrete is exposed to a fluctuating thermal environment. " It is related to the *thermal conductivity,* which is "the rate at which heat energy is transferred across unit area of asphalt concrete" and the *specific heat capacity,* that is "the amount of heat that must be added or removed from a unit mass of asphalt concrete to change its temperature

by one degree" (Mrawira et al. 2006). The relation between the various thermal properties is given by:

$$C = \frac{\lambda}{\rho\alpha} \tag{5.9}$$

where C- specific heat capacity (J/(kg•K); λ - thermal conductivity (W/(m•K)); α - thermal diffusivity (m^2/s); and ρ- density (kg/m^3)

Equation (5.8) becomes:

$$\frac{\partial T(t,x)}{\partial t} = \frac{\lambda}{\rho \cdot C}\frac{\partial^2 T(t,x)}{\partial x^2} \tag{5.10}$$

Using forward difference approximation one can develop with an explicit method for solving the 1D heat equation, which is known to be conditionally stable (the time step for simulations was specified 60 minutes):

$$\frac{T_j^{n+1} - T_j^n}{\Delta t} = k\frac{T_{j+1}^n - 2T_j^n + T_{j-1}^n}{(\Delta x)^2} \tag{5.11}$$

with Δt- time increment , Δx-displacement increment, n- corresponding to time , j- to location

. The objective of the theoretical heat conduction simulations was to determine temperature profiles within the pavement-subgrade structure to confirm the agreement with the thermocouple temperature measurements, as well as to obtain a better understanding of the temperature dynamics. Two sets of simulations were performed with different base layer materials, gravel and clay, with various thermal diffusivities to see how sensitive the results are to these differences. Based on brief literature review the thermal conductivity and heat capacitance values for asphalt concrete layer, (Luca et al., 2005) are: thermal conductivity is λ=1.5 W/m∘K, specific heat capacity C=1,500 J/kg∘K, and density is ρ=2,300 kg/m^3 then thermal diffusivity $K_1=\lambda/(\rho \circ C)=0.4348*10^{-6}$ m^2/s. For gravel the thermal values, see Table 4 of Luca et al. (2006): λ=1.96 W/m∘K, C=1,700 J/kg∘K, ρ= 2,400 kg/m^3, $K_2= \lambda/(\rho \circ C)= 0.4804* 10^{-6}$ m^2/s. For clay layer, see British Geological Survey (2007): thermal diffusivity – K_2=0.042 m^2/day=0.5324*10^{-6}m^2/s. For the node on the border between asphalt concrete layer and base layer (silt or gravel) thermal diffusivity was assumed to be the average between K_1 and K_2.

A pavement-base layer section 600 mm deep was assumed for the temperature analysis of the stations B to D (100-200 mm thick). The model did not take into account thermal properties of pavement layers related to moisture content. There were 61 nodes in the vertical direction with the spacing between the nodes of 10 mm. For all analyses, the grid was the same. For instance, for a pavement of 200 mm there are 21 uniformly distributed nodes, with one of them at the interface between materials (pavement-base layers). The boundary conditions were specified as follows: the asphalt layer surface

(corresponding to 10 mm depth) and the bottom boundary (600 mm depth) with the initial temperature distribution with depth being assumed constant and equal to 22.5°C. The temperature within the asphalt concrete and base layers was estimated using the explicit finite difference scheme for calculating transient temperature variations with depth and time. The surface of the system was subjected to a temperature variation characterized by the averaged sinusoidal function (Eqn. (5.7)), while the bottom of the system had a constant fixed value of temperature (22.5°C). The simulations were performed based of the assumption that temperature at the initial time t_0 (12 am) and after 5 days no longer had an important influence on the predictions. Since the analysis covered five days of time stepping, the predicted values were believed to be not very sensitive to the condition of uniformly distributed initial temperature with depth. The MATLAB code for Eqn. (5.11) used for the simulations is provided in the Appendix B.

5.7 Results from Thermal Analysis

Based on the results from simulations with different granular base materials (clay and gravel) and, therefore, various thermal diffusivities, it was found that the properties did not have a noticeable effect on the temperature profiles in the asphalt concrete. Therefore, only simulated profiles corresponding to gravel at the base (Figs. 5.3 (1,3,5)) are compared to the measured ones (Figs. 5.3 (2,4,6)). Figure 5.4 shows predicted changes in temperature and elastic modulus over a day. The elastic modulus of subgrade

was believed to be slightly affected by temperature variations in the pavement layer with depth and, therefore, simulations were performed only within the asphalt concrete and base layers of the pavement-subgrade system. A comparison of measured and predicted temperature profiles in Fig. 5.3 shows reasonable agreement.

The temperature changed quite rapidly in the upper layers of the asphalt pavement layer during the day while it remained almost constant in the underlying layers. This profile is characteristic for summer conditions.

According to Herb et al. (2006) temperature gradients due to heating exceed those due to cooling and the surface temperature gradients are larger than the gradients across the depth of the asphalt concrete layer. In this study surface temperature amplitudes for measured profile varied from 19.6°C to 40.5°C. For the simulated profile, surface temperature values were calculated using Eqn. (3.18) with fluctuations from 21.3°C to 40.9°C. Measured temperature variations at the bottom of AC layer were wider than predicted by the Ali and Lopez model:

a) 19-34.8°C and 24.5 - 33°C respectively for station B (h_p=100mm);

b) 22.7-26.9°C and 26-31°C for station C (h_p=150mm);

c) 22-28°C and 26-29°C for station D (h_p=200mm).

For asphalt concrete pavements up to 100 mm thick, the simple model has shown some limitations. Thus, elastic moduli variations cannot be properly accounted for when the pavement layer is thin. On the other hand, for thicker pavements (stations C and D) the simple temperature model provides better results.

The measured temperature profile at location C (h_p=150 mm) is different than the other two at 12 pm (see Fig.5.3 (2,4,6)). It is possible that the thermocouple was not working properly at that station. It might also have been the consequence of backfilling the drilled holes with non-original material after installation of the thermocouples. Thermocouples, which were assumed to face and touch one side of the pavement layer in the hole, might have been measuring the temperature of the improper filling or air void. From Fig.5.3 (4) one can see that the temperature at noon changes gradually up to 100 mm depth and then remains constant up to 150 mm. It is well-known that viscoelastic properties of the asphalt concrete and physical nature of the bottom layers affect the temperature fluctuations in flexible pavements. This will lead to changes of the elastic modulus distribution with depth making the pavement softer during the hot temperatures which will effect the pavement response due to loading (deflections). Also, larger temperature deviation can be observed within the pavement layer compared to the granular base layer as the temperature gradients tend to decrease with depth.

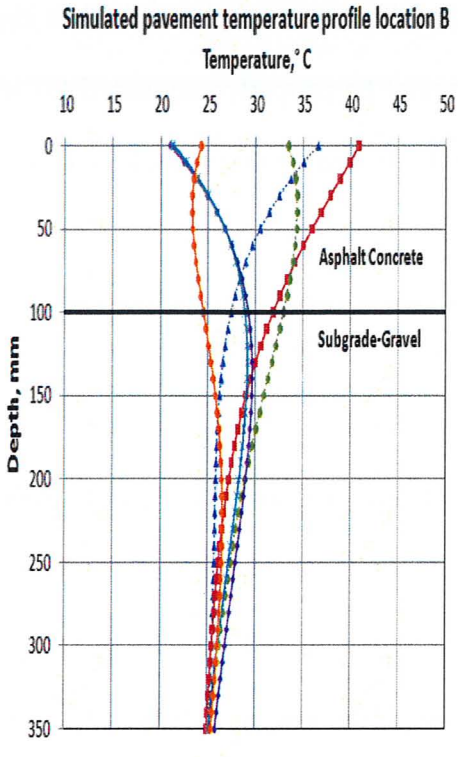
Simulated pavement temperature profile location B
Temperature,°C
10 15 20 25 30 35 40 45 50
0 50 100 150 200 250 300 350
Depth, mm
Asphalt Concrete
Subgrade-Gravel

(1)

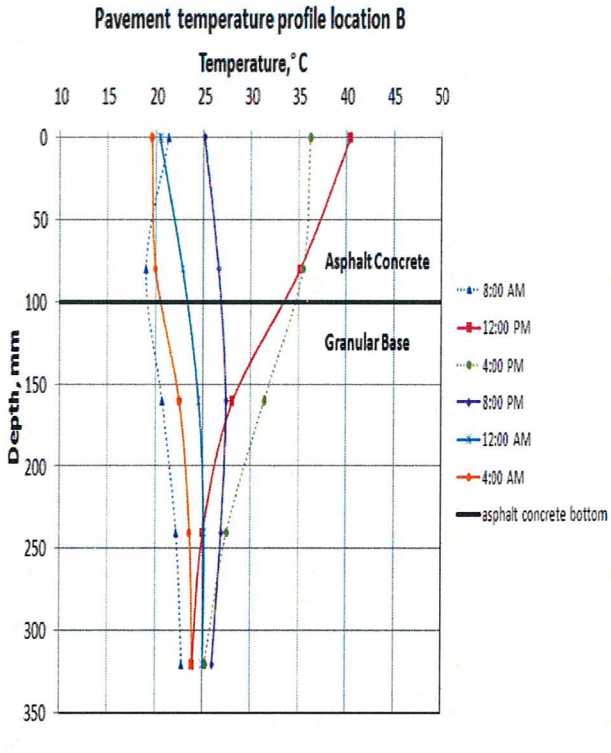
Pavement temperature profile location B
Temperature,°C
10 15 20 25 30 35 40 45 50
0 50 100 150 200 250 300 350
Depth, mm
Asphalt Concrete
Granular Base
8:00 AM
12:00 PM
4:00 PM
8:00 PM
12:00 AM
4:00 AM
asphalt concrete bottom

(2)

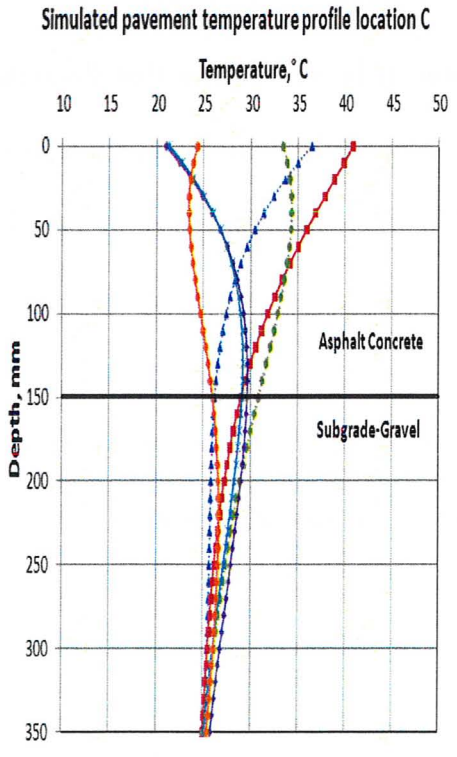
Simulated pavement temperature profile location C
Temperature,°C
10 15 20 25 30 35 40 45 50
0 50 100 150 200 250 300 350
Depth, mm
Asphalt Concrete
Subgrade-Gravel

(3)

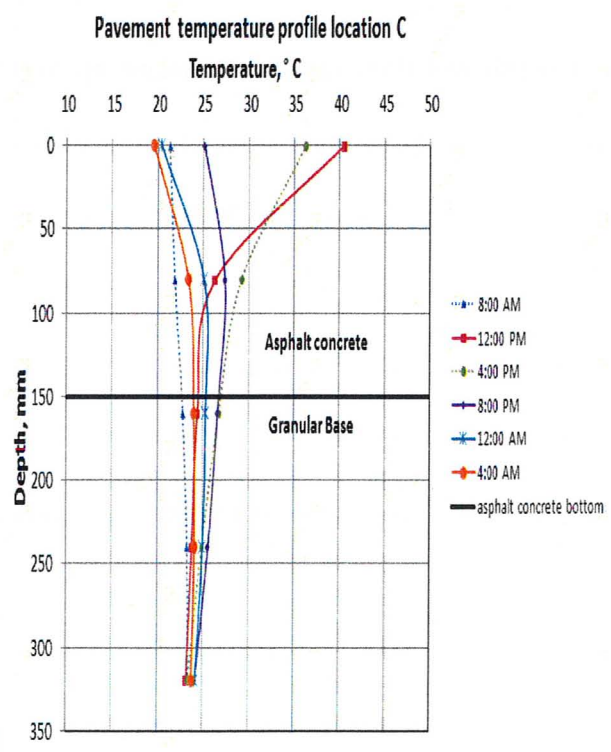
Pavement temperature profile location C
Temperature,°C
10 15 20 25 30 35 40 45 50
0 50 100 150 200 250 300 350
Depth, mm
Asphalt concrete
Granular Base
8:00 AM
12:00 PM
4:00 PM
8:00 PM
12:00 AM
4:00 AM
asphalt concrete bottom

(4)

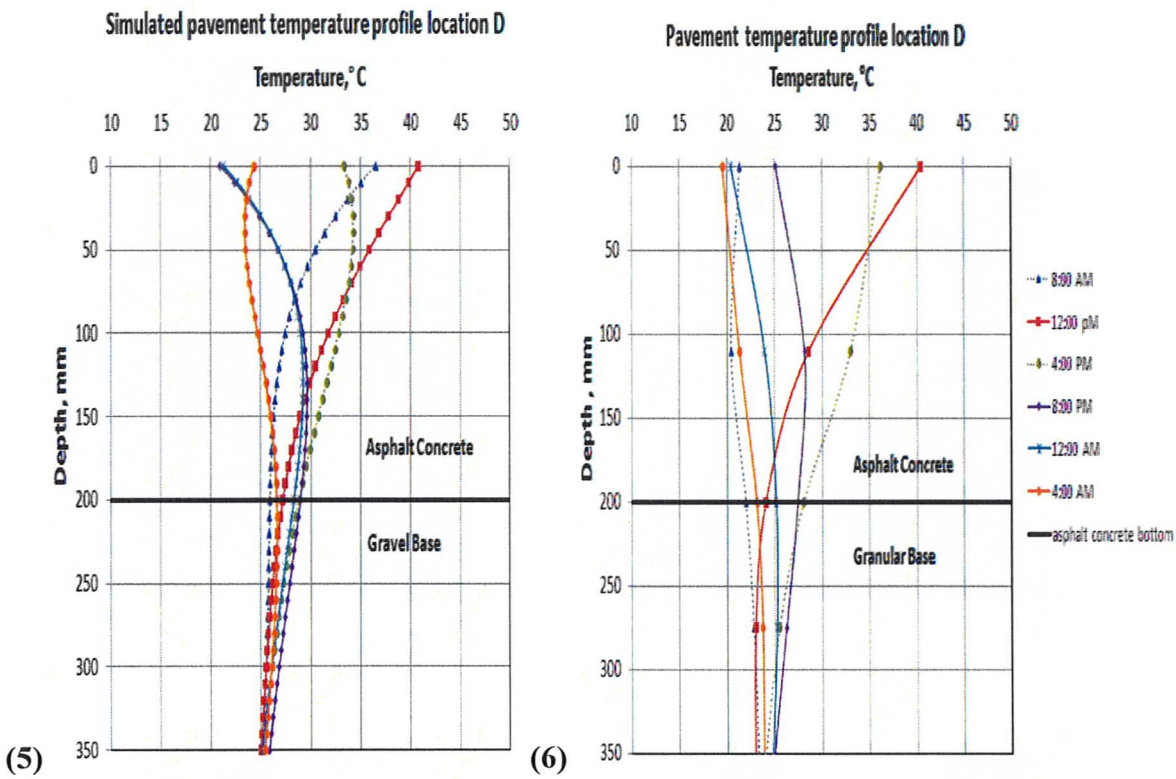

Figure 5.3- Simulated temperature profiles for gravel (1,3,5) base materials and actual daily (2,4,6) temperature profiles.

Figure 5.4 shows temperature and elastic modulus simulated variations over time and depth in the asphalt concrete layer. 12 am is specified as the initial and final time points. The simulations for all three stations look alike and therefore simulations for Section C were not presented in the current study. Temperature on the surface of the asphalt layer fluctuates from 21°C at 8 pm-12 am to 36-41°C at 8am-12 pm (Fig. 5.4 (a) and (c)). At noon heat propagates 0.17 m deep, while during the nights the depth of temperature propagation is about 0.11 m. The asphalt concrete temperature decreases with depth and reaches its constant value of approximately 27°C at a depth of 0.18 m deep.

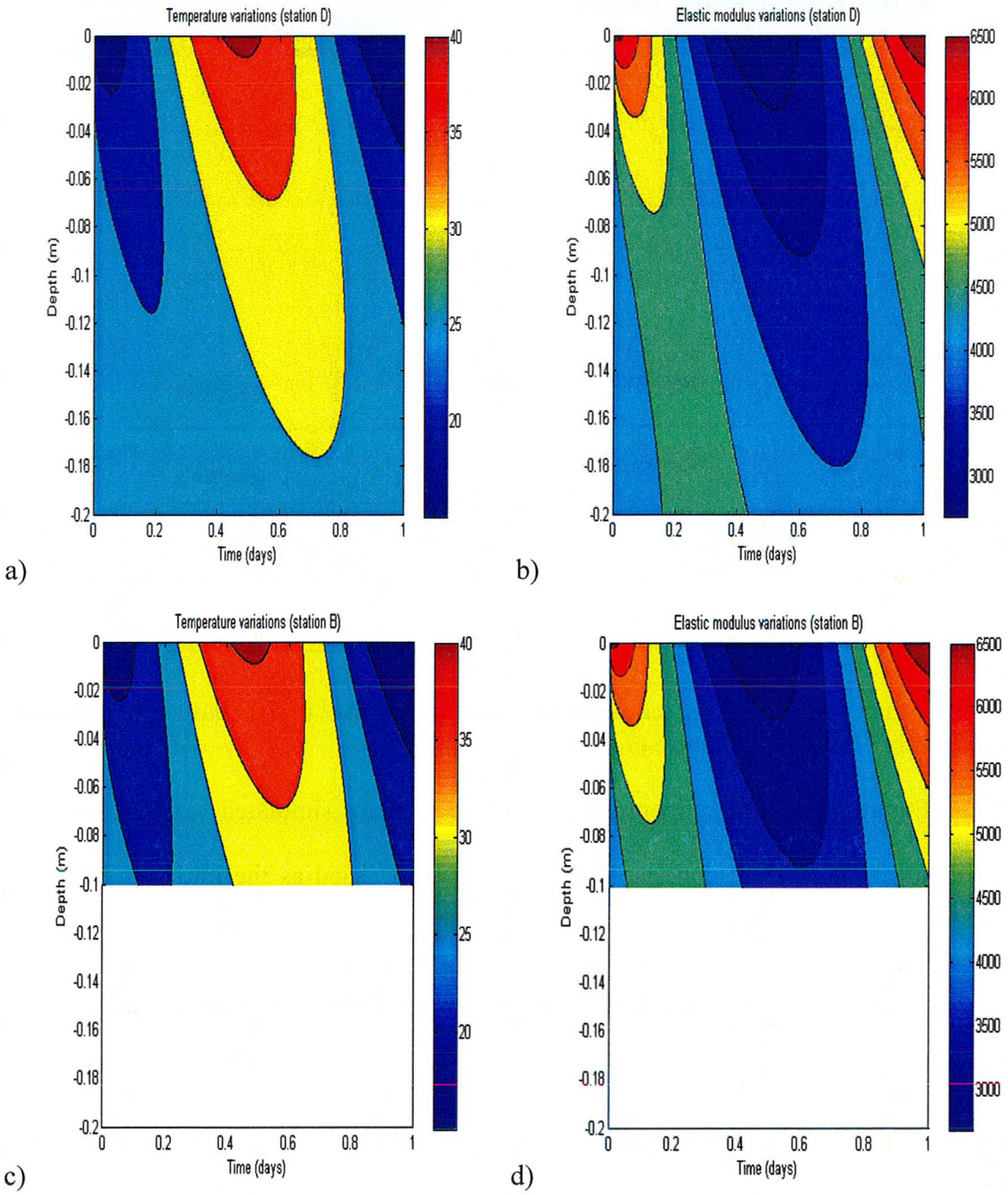

Figure 5.4- 1D Daily temperature (a, c) and elastic moduli (b, d) variations in the AC layer with gravel base for stations D and B (1 day simulation in August)

On the surface of pavement layer elastic modulus reaches its maximum value of 5500 MPa at 8 pm-12 am and its minimum value of 2700 MPa at 12 pm (Figs. 5.4 (b) and (d)). Rapid changes of the elastic modulus during the day can be observed within approximately the top 0.07 m. Elastic modulus decreases with depth at nights, while in the middle of the day when temperature reaches its highest value and pavement becomes softer elastic modulus values increase with depth. For both cases, the elastic modulus of asphalt concrete layer reaches its average value of 4250-4500 MPa at approximately 0.2 m depth and thus proving that the temperature of the asphalt layer at this depth stays constant.

5.8 Finite Element Model For FWD and LWD Simulations

Non-isothermal simulations, in which the elastic modulus of asphalt concrete is non-uniform, depending on surface temperature of pavement layer during the day, were performed to capture the effect of temperature changes in pavements on the response of the pavement-subgrade system to loading. The variation of the resilient modulus of asphalt concrete layer with depth was calculated according to Eqn. (5.5) (Ali and Lopez 1996). Pavement layer was divided into several sublayers 50 mm thick to simplify the model. The value of elastic modulus of asphalt concrete was averaged and calculated at the mid-depth of each sublayer. Taking into account the field data collected near ADL building, three reference times during the day were chosen for temperature simulations -

4 am (lowest), 12 pm (highest) and 8 pm (average pavement surface temperatures). The finite element discretization for FWD and LWD is described in Section 4.4.1 (Fig.4.1) and summarized in Table 5.3. The boundary conditions were the same as shown in Fig. 4.1. The results of the simulations are presented in Tables A.4 and A.5 of the Appendix.

Table 5.3- Finite element discretization for FWD and LWD simulations

Parameter	FWD simulations	LWD simulations
Radius R, m	4.0	4.0
Depth to bedrock, m	4.10-4.20	4.10-4.20
Radius of loading plate, m	0.15	0.075
Distributed load, kPa	565.9	441.4
AC layer thickness h, m	0.1; 0.15; 0.2	0.1; 0.15; 0.2
Modulus of elasticity of AC layer, E_p, MPa (see range in Tables A.4,A.5)	varies during the day	varies during the day
Modulus of elasticity of subgrade, E_s, MPa	75; 100; 150; 200; 250	75; 100; 150; 200; 250
Poisson's ratio of AC layer and subgrade, $\nu_p=\nu_s$	0.3	0.3
Unit weight of AC layer and subgrade, $w_p=w_s$, kN/m^3	20.0	20.0

5.9 Results of LWD and FWD Simulations

5.9.1 Results of Elastostatic Data Interpretation

Backcalculation analysis was performed on synthetic load-deflection histories corresponding to FWD and LWD simulations to understand how temperature fluctuations in pavement layer affect the effective surface modulus predictions. The surface modulus

can be estimated from the load-deflection histories of FWD and LWD tests. It presents the weighted average modulus of pavement-subgrade system. The main idea of the analysis was to determine how the effective surface modulus varies with radius and at what offset E_{SM} represents the elastic modulus of the subgrade E_s. The idea was also to identify how sensitive backcalculated E_s is to the temperature changes in asphalt concrete.

Elastostatic backcalculation approach presented in Section 2.3 was implemented in the FORTRAN computer code MODULUS-Mac developed at McMaster. Effective surface moduli were backcalculated using Eqn. (2.1) using maximum surface displacements from simulated non-isothermal load-deflection histories for the FWD and LWD taken at various offsets (r = 0, 300, 400, 600, 900, 1300, 1600 mm and r = 0, 150, 300, 450, 600, 750, 900 mm for FWD and LWD, respectively). This was done corresponding to various times of the day (8 am, 12pm and 4pm). Representative effective surface modulus profiles are shown in Figs. 5.5-5.6 while profiles for all remaining cases are presented in Figs. C.1-C.4 of Appendix C.

Figure 5.5 shows effective surface moduli profiles (for the FWD and LWD, respectively) on one plot keeping the thickness of asphalt layer h_a constant (150 mm). This allows one to look at the influence of E_{SM} (as well as temperature) on profiles and backcalculated estimate for the subgrade modulus E_s.

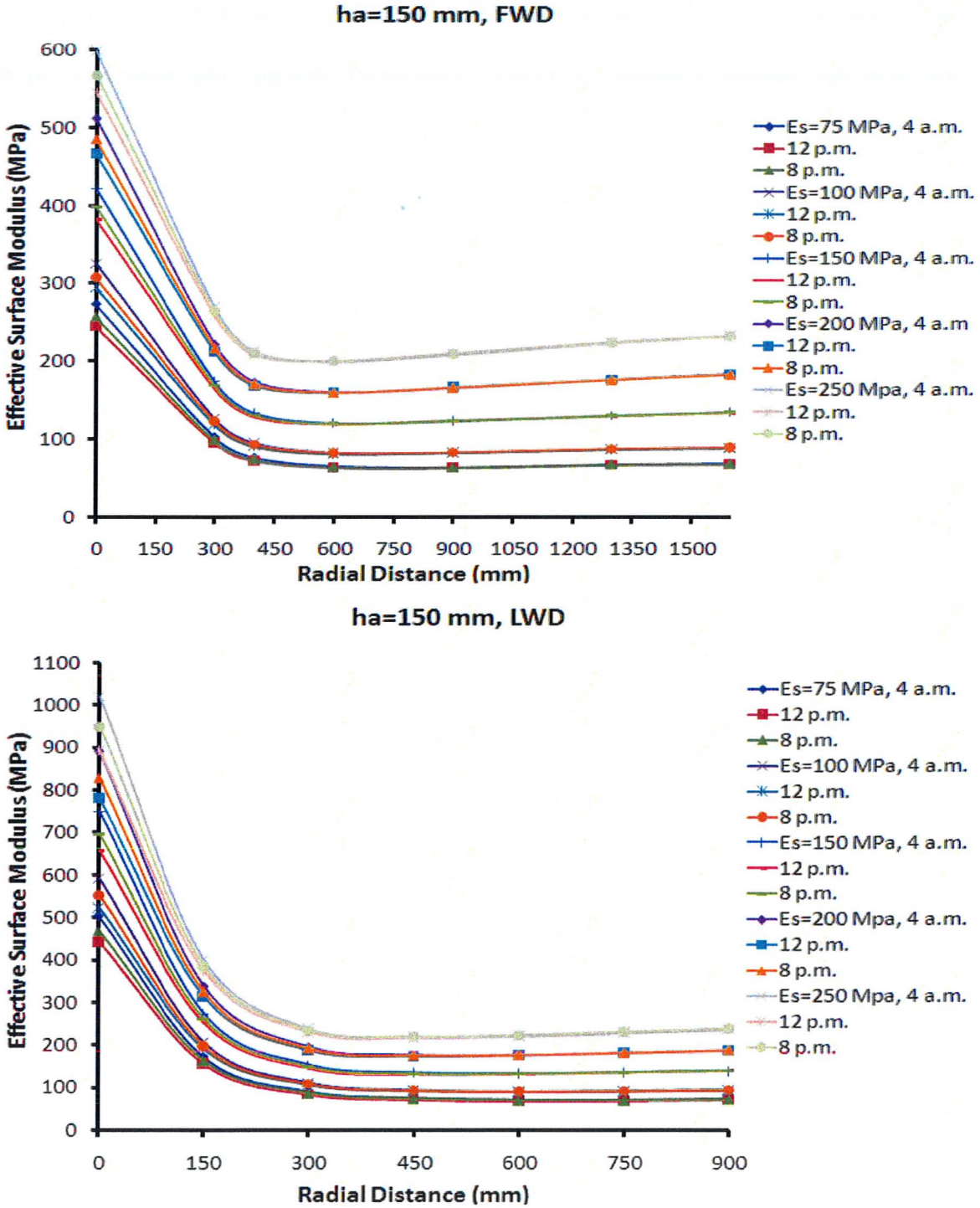

Figure 5.5- Influence of subgrade modulus and temperature on effective surface modulus measured by FWD and LWD

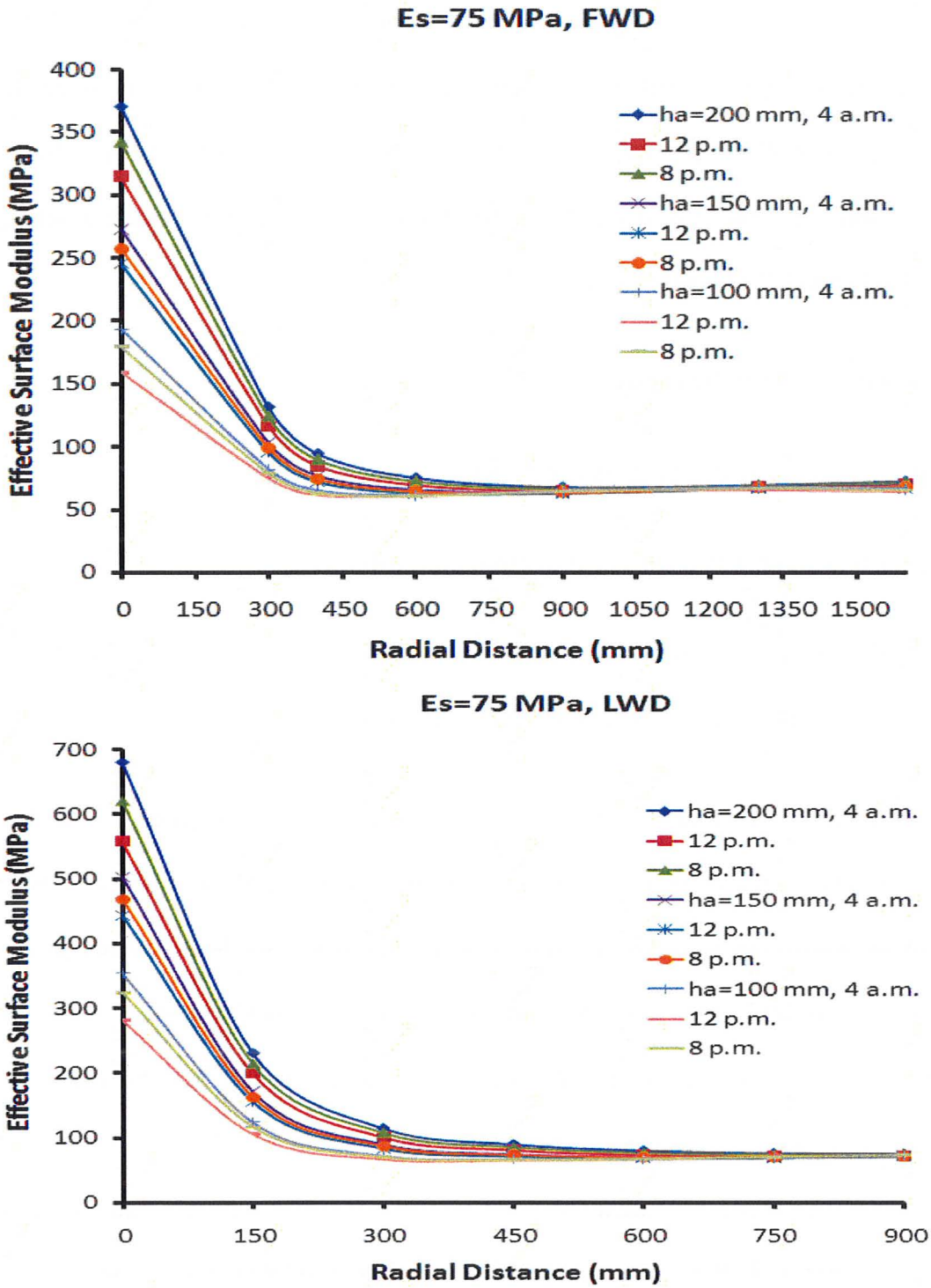

Figure 5.6- Influence of pavement thickness and temperature on effective surface modulus for FWD and LWD

Figure 5.6 represents effective surface modulus profiles (for FWD and LWD) keeping elastic modulus of subgrade E_s constant to study the influence of pavement thickness h_a (as well as temperature) on the profiles and the estimate for subgrade modulus. Tables A.7 and A.8 of the Appendix A summarize the same results in tabular form for FWD and LWD loading respectively.

The plots help to answer the questions:

1. How sensitive are backcalculated E_s values to temperature?

2. Do FWD and LWD results lead to different sensitivities?

3. Can one make any strong statements with respect to being able to backcalculate system parameters when using an "elastostatic" approach?

The trends for both devices (see Figs. 5.5, 5.6) look similar. Figures 5.5 and C.1-C.2 of Appendix C clearly show that an increase in pavement thickness (h_a) affects the growth of the maximum value of effective surface moduli E_{SM} for both devices (at zero offset), as one might expect. Another common observation for both devices is that the value of the effective surface modulus E_{SM} increases with an increase in the stiffness of a subgrade layer E_s. This is reasonable as the surface modulus at zero offset (r=0) represents the stiffness of the entire pavement-subgrade system. E_{SM} has a higher value at 4 am when the temperature in the AC layer reaches its minimum, while the drops down as the day temperature reaches its peak at noon. From Fig. 5.5 one also clearly observes that the

value of effective surface modulus E_{SM} at zero offset corresponding to the LWD is consistently higher than the value predicted by FWD.

For example, backcalculated E_{SM} (r=0m, 4 am) for the LWD is higher than that of the FWD by the factor of approximately 1.7 for E_s=250 MPa and 1.84 for E_s=75 MPa (Fig. 5.5). The LWD and FWD devices excite different volumes of the pavement-subgrade system. As mentioned in Section 1.4, for the LWD one would expect the influence depth of about 225 mm, which is 1.5 times the loading plate diameter (Nazzal et al., 2007). Therefore, the LWD is mostly capturing the stiffness of the pavement-base layers which is higher than that of the subgrade resulting in the higher E_{SM} at zero offset than that of the FWD. Variations of effective surface modulus E_{SM} at zero offset shown in Fig.5.6 are significant during the day. For the FWD simulations with E_s=75 MPa, E_{SM} backcalculated for r=0 increases up to 23.3; 11.2 and 18% for h_a=100; 150 and 200 mm respectively from 12 pm (when its value is the lowest) to 4 am (highest). As for the LWD, temperature-related simulations, the increase in the effective surface modulus E_{SM} backcalculated under the load is higher and is 25.6; 13.5 and 21.8% respectively (E_s=75 MPa). Therefore, LWD results seem to be more sensitive to temperature changes in asphalt concrete layer, as one might expect.

As one can see from Figs. 5.5-5.6, effective surface modulus decreases with increase of the distance from a load centre as it starts to represent the stiffness of the lower layers, which have smaller elastic moduli values (Jung, 1993). At some point E_{SM}

changes become negligible forming a single relation. The radial distance (offset) where the effective surface modulus becomes constant is approximately 400-800 mm for the FWD and 300-600 mm for the LWD. The load plate radius is believed to have some impact on this characteristic distance. The backcalculated effective surface moduli E_{SM} at this offset seem to underestimate the real values of elastic modulus of subgrade E_s assumed for the simulations. At farther offsets (900 and 1600 mm for the LWD and FWD, respectively) E_{SM} approaches the value of E_s though still underestimates it. Backcalculated effective subgrade moduli (E_{eff}) for the FWD are less than the actual values (E_s) by 12.3; 9.0 and 4.8% for h_a=100; 150 and 200 mm respectively (Fig.5.6). For the LWD these errors are smaller and are 2.2; 4.5 and 2.2% respectively. Overall, the values of the effective subgrade moduli (E_{eff}) backcalculated at far distances from the applied load showed less agreement with the actual value of elastic moduli of subgrade (E_s) for the FWD than those backcalculated for the LWD. According to Stolle and Jung (1992) the distance where E_{eff} reaches its minimum value is approximately equal to equivalent thickness h_e for two-layer pavement-subgrade approximation. This statement has a good correlation with the backcalculated values of effective thickness for both devices presented in Tables A.7-A.8 of the Appendix. In their research, Stolle and Jung (1992) showed that the geophones located at far offsets from the load are more susceptible to deep subgrade material properties resulting in an increase of effective modulus at larger offsets. Therefore, each offset reflects the pavement-subgrade system properties at different depths. Rising of the effective surface moduli (Fig.5.5) at the

farther distances from the load centre indicates the existence of a shallow bedrock location (see, i.e. Jung, 1993). Theory originally developed for the FWD perhaps needs some alternative calibration for the LWD. However, it can be clearly seen in Figs. 5.5-5.6 that the backcalculated surface elastic moduli E_{SM} representing E_s at far distances from the load are not sensitive to the temperature changes in the pavement layer (and thus, to the time of the day the test was carried out) and merge into one almost horizontal straight line. A significant conclusion of the detailed analysis of the backcalculated synthetic non-isothermal data is that, although not perfect, the elastostatic approach is a valuable tool for interpretation LWD and FWD load-deflection histories. One observes that the insensitivity of E_{SM} at larger offsets indicates that the backcalculated subgrade modulus is not sensitive to temperature fluctuations in the asphalt layer, as one might expect.

The elastic modulus of pavement layer E_p was backcalculated on simulated (synthetic) deflection basin and compared to the average input asphalt concrete layer moduli E_p. The results are shown in Fig. 5.7. Overall, a good linear agreement exists between backcalculated and input parameters for both LWD and FWD. Furthermore, Fig. 5.8 shows the minimum backclaculated elastic modulus of subgrade against input E_s. Although not perfect, there appears to be a reasonable one-to-one relation. The equivalent thickness of the asphalt layer h_a was calculated using Eqn. (2.2) (assuming that E_p of the hot mix is 4000 MPa and constant with depth) and compared to the input pavement thickness in Fig. 5.9. For all figures, linear trends are observed for the LWD and FWD as

one would expect, with quite a bit of scatter. One must take into account that the simulated data is elastodynamic though the interpretation of the results is simplified to be elastostatic. This crude tool of data backcalculation is, however, sensitive and shows a good agreement, though it may cause systematic modeling errors. Obvious data point groups can be observed in Figs. 5.8 and 5.9 corresponding to the variation in the backcalculated subgrade modulus E_s (five different cases) and equivalent thickness of the asphalt layer h_a corresponding to three stations of various thicknesses.

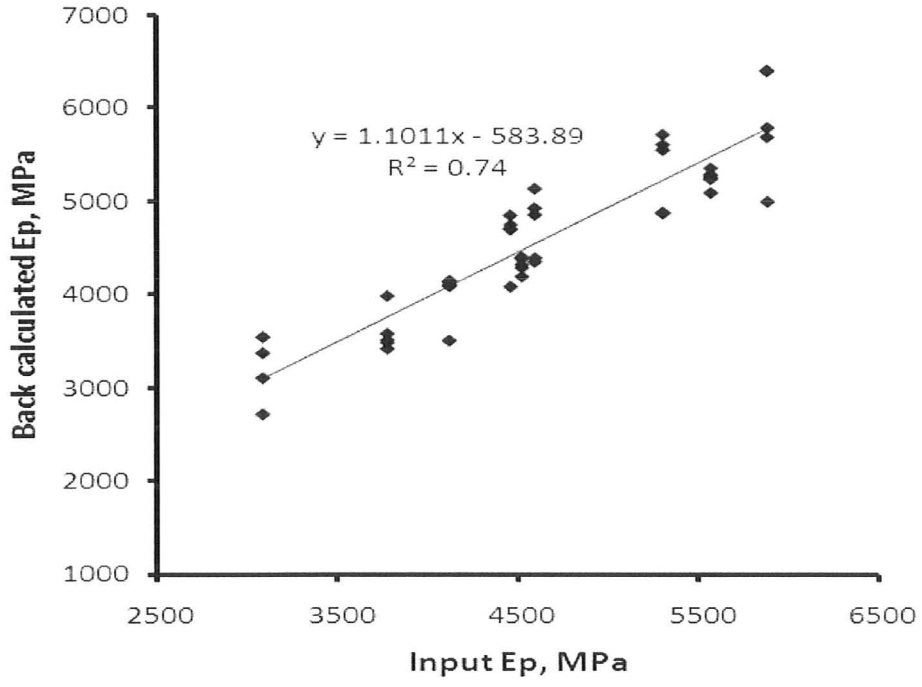

a)

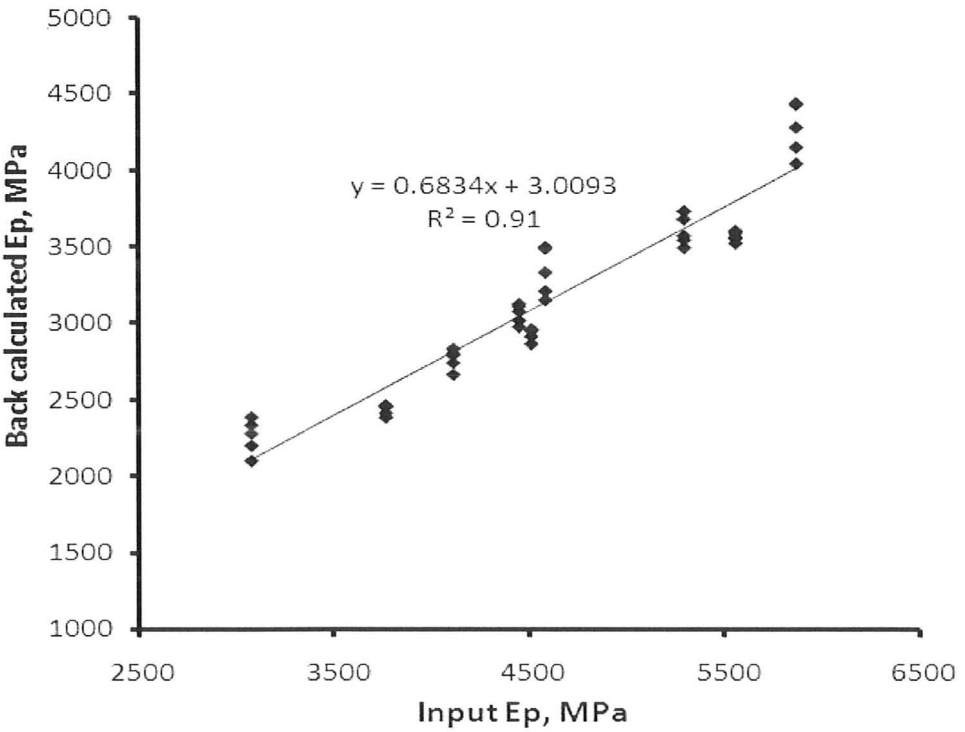

b)

Figure 5.7- Backclaculated E_p vs. average input E_p for FWD (a) and LWD (b)

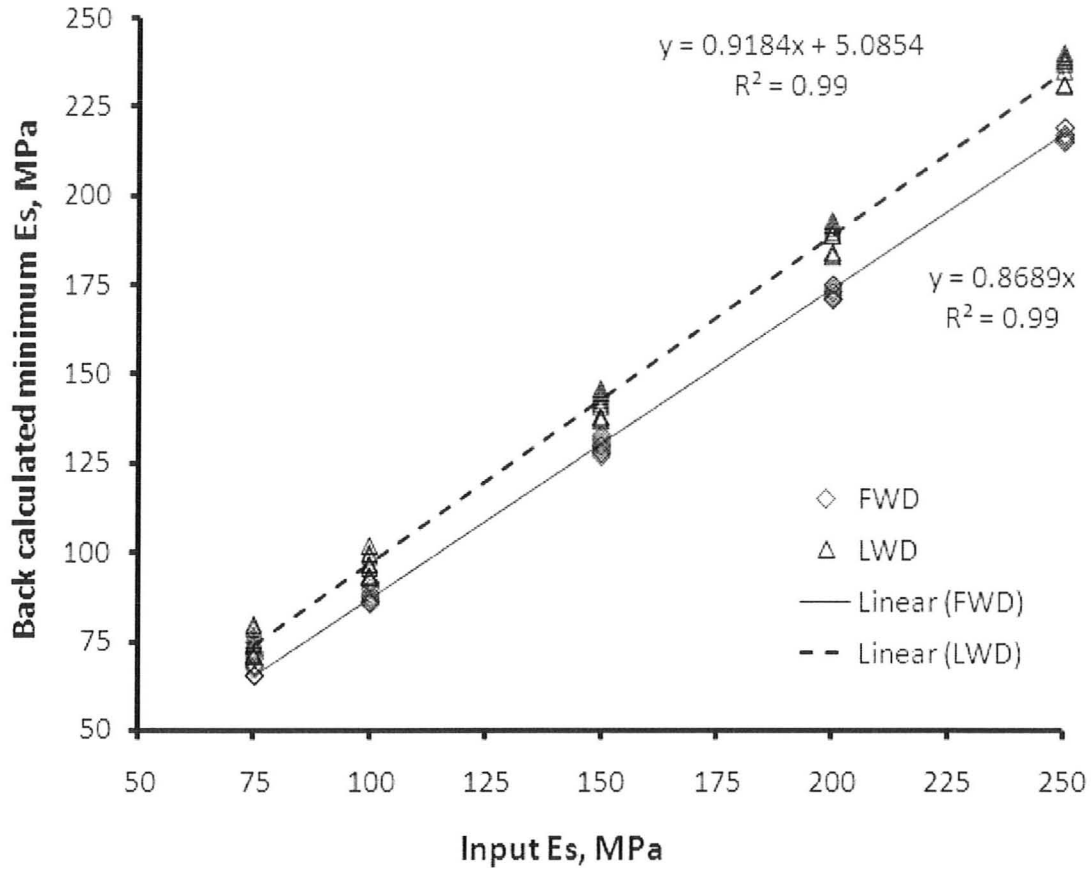

Figure 5.8- Minimum backclaculated Es vs. input Es for FWD and LWD

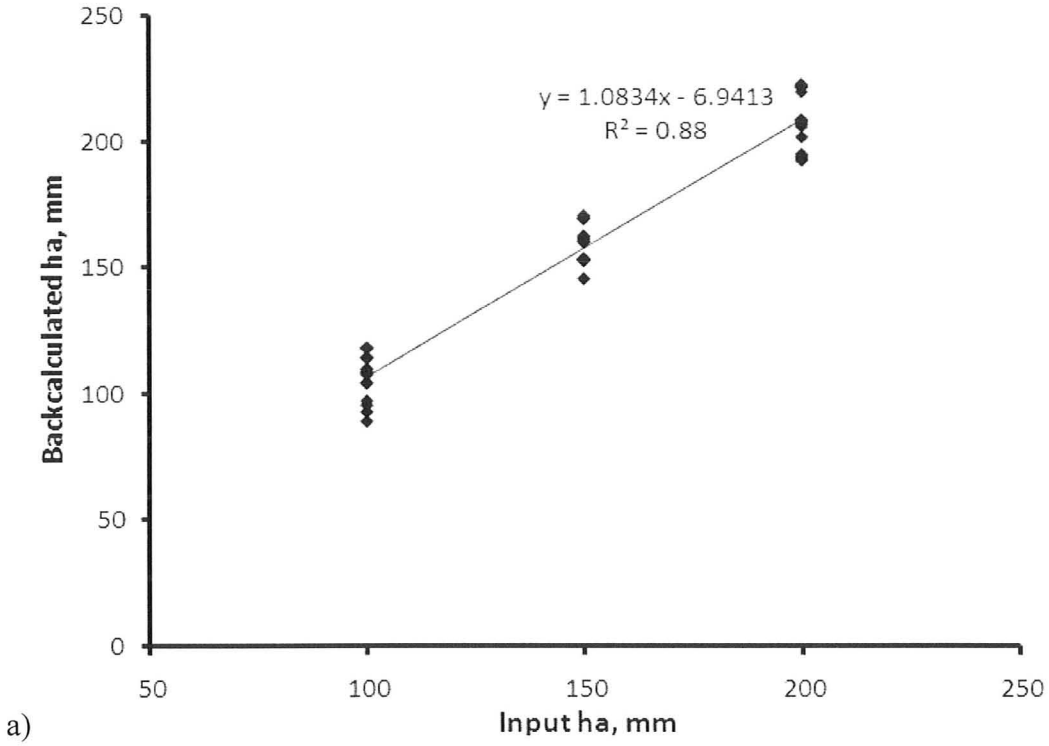

a)

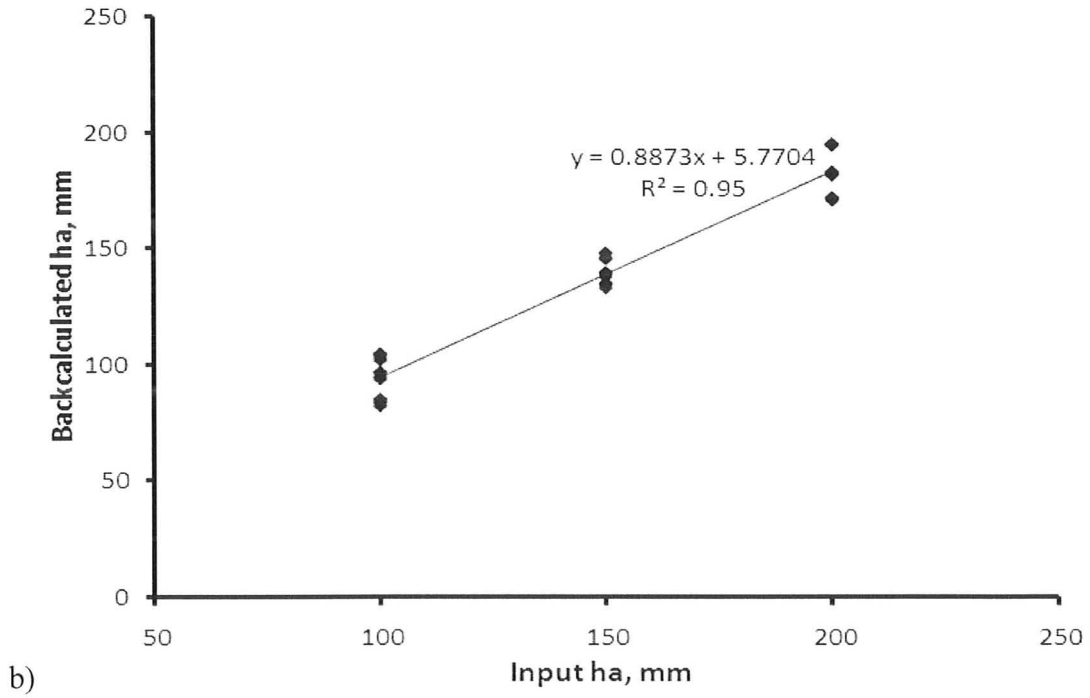

b)

Figure 5.9- Backclaculated h_a vs. input h_a for FWD (a) and LWD (b)

5.9.2 Results of Elastodynamic Data Interpretation

Typical simulated load-deflection histories for FWD measurements are presented in Fig. 5.10. These trends reflect those observed when testing flexible pavements during an average hot summer day while the surface of the asphalt concrete pavement layer reaches its minimum (at 4am) and maximum (at 12pm) temperatures. As expected, the asphalt layer becomes softer at noon when the air (and thus, surface) temperature is at its highest which leads to larger deflections. On the contrary, if a test were to be performed in the early morning, say at 4 am when the asphalt surface temperature reaches its minimum, the deflections would be smaller as the decrease of air temperature increases elastic modulus of AC layer, making the pavement stiffer. As mentioned before, one is interested in getting as much information as possible from the load-deflection history of the LWD recorded typically for one central sensor. Therefore, elastodynamic approach discussed in Section 2.4 becomes a valuable tool for data backcalculation.

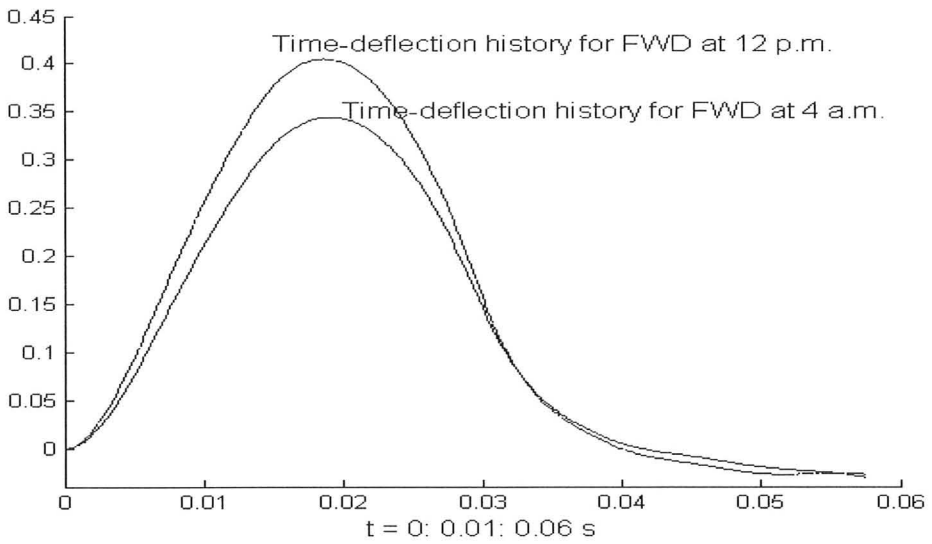

Figure 5.10 - Time-deflection history for the various time of the day (typical hot summer day)

Figure 5.11 shows normalized time-deflection histories with respect to peak deflections for isothermal (a) and non-isothermal (b) simulations. In the set of plots, displacement history is presented for the case when E_s is constant but h_a varies with all displacements being normalized with respect to the peak deflection. One can identify similarities with regard to how the deflections evolve for different pavement thicknesses. An important observation is that there is a shift in the peak values, depending on temperature or thickness of pavement. The shift influences the value of the damping coefficient C. However, an important observation is that the shapes of the normalized deflection histories for both isothermal and non-isothermal parameters are similar. Thus, one cannot really make a statement about variations in asphalt concrete modulus based on the deflection histories.

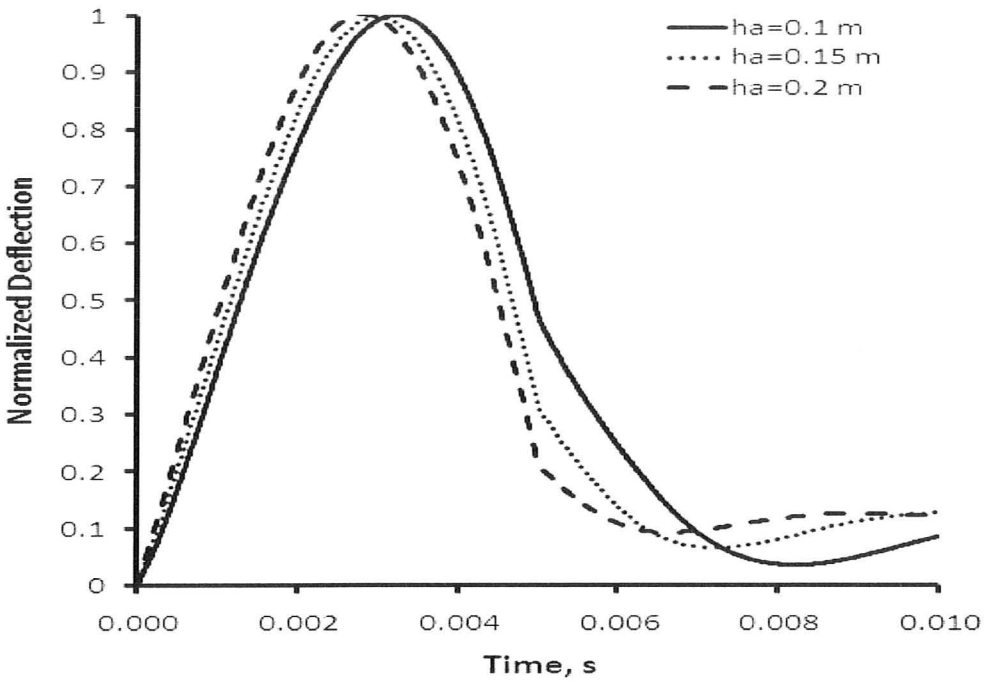

a)

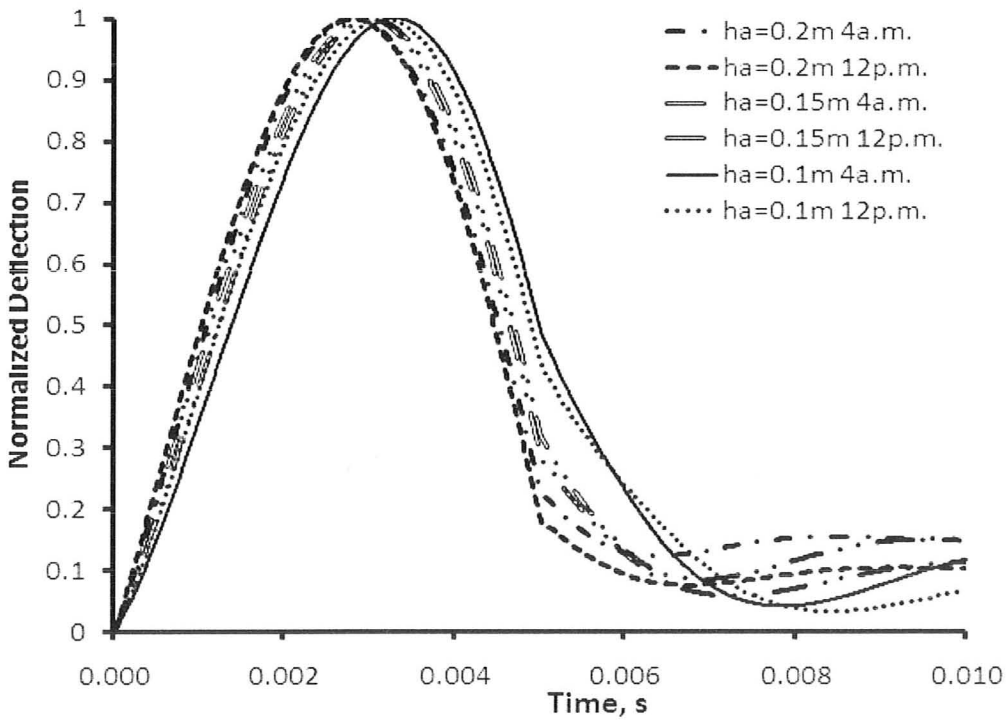

b)

Figure 5.11- Representation of normalized time-deflection histories with respect to peak deflections. a) isothermal case; b) non-isothermal case.

In the present study TDA was used to evaluate *M, C* and *K* corresponding to a SDOF approximation for the FWD and LWD simulations in which temperature within the asphalt layer varied with depth. *M, C* and *K* values were backcalculated using the synthetic load-displacement histories according to the procedure described in Section 2.5.2. Figures 5.12-5.19 show representative trends for *K* and *C* for all FWD and LWD isothermal and non-isothermal simulations, with the actual values summarized in Tables A.4 -A.5 that appear in the Appendix A.

The static stiffness is commonly estimated using peak displacements of the time-deflection history and the peak load (Hoffman et al., 2004) according to:

$$K_{peak} = \frac{F_{peak}}{w_{peak}} \tag{5.12}$$

K_{peak} values were calculated for all simulations using equation (5.12) as well as the average value of K_{aver} adding all forces over time and dividing by a number of readings over time, which corresponds to the steady-state (zero frequency) (Stolle and Guo 2005). Comparison of *K* and *C* values with those calculated using only peaks (K_{peak}) or average values (K_{aver}) is presented in Figs. 5.12-5.15. A good correlation is observed between the two stiffnesses for both isothermal and non-isothermal simulations when plotting K_{aver} versus K_{peak} and K_{aver} versus *K* (Tables A.4-A.5 of Appendix A). Figures 5.12-5.15 (c) show a stable increase of the damping coefficient *C* with an increase of the average stiffness K_{aver}. Quite a bit of scatter might be a result of the presence of the bedrock. Five almost linear patterns appearing on every plot (Figs. 5.12-5.15 (c)) may be due to the five

sets of subgrade moduli E_s assumed for the simulations. It should be noted, that no attempt was made to develop a functional relation between C and K_{aver} .

The results of K and C coefficients for isothermal and non-isothermal simulations are summarized and plotted in Figs. 5.16-5.19. The non-isothermal simulations were performed using the Ritz vector method and TDA to find M, C and K values. The equivalent mass M values were found to be very small and were omitted in the thesis as they are not required for backcalculation. The results were summarized in the bar plots provided for the case where thickness is held constant and E_s is allowed to vary and vice versa- E_s is held constant while thickness of the pavement layer changes (Figs. 5.16-5.19). These graphs help answer the questions: "How do C and K change for varying E_s and constant h_a (and varying h_a and constant E_s)?" "Are the trends here the same as for the FWD and LWD tests?" "Changes in temperature or changes in thickness are reflected in changing C and K?"

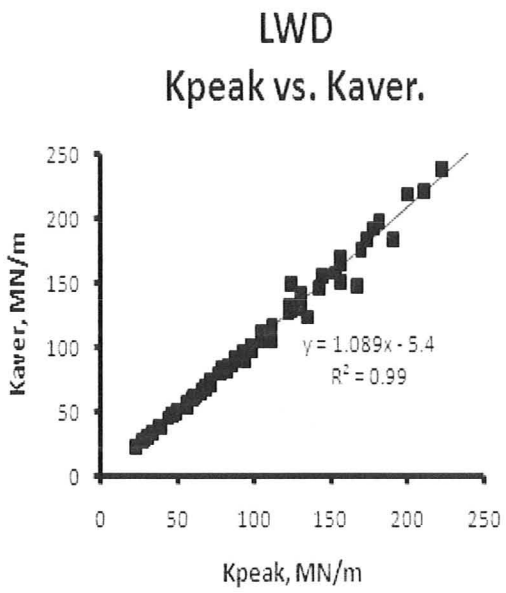

a)

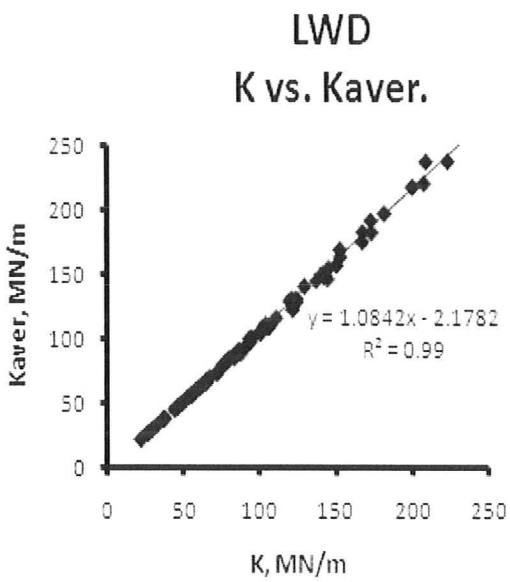

b)

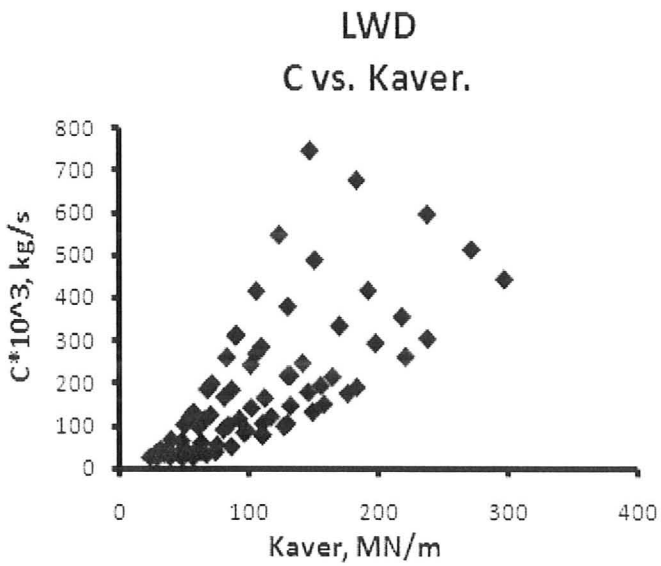

c)

Figure 5.12: LWD non-isothermal simulations: (a) K vs. K_{aver}; (b) K_{peak} vs. K_{aver}; (c) C vs. K_{aver} .

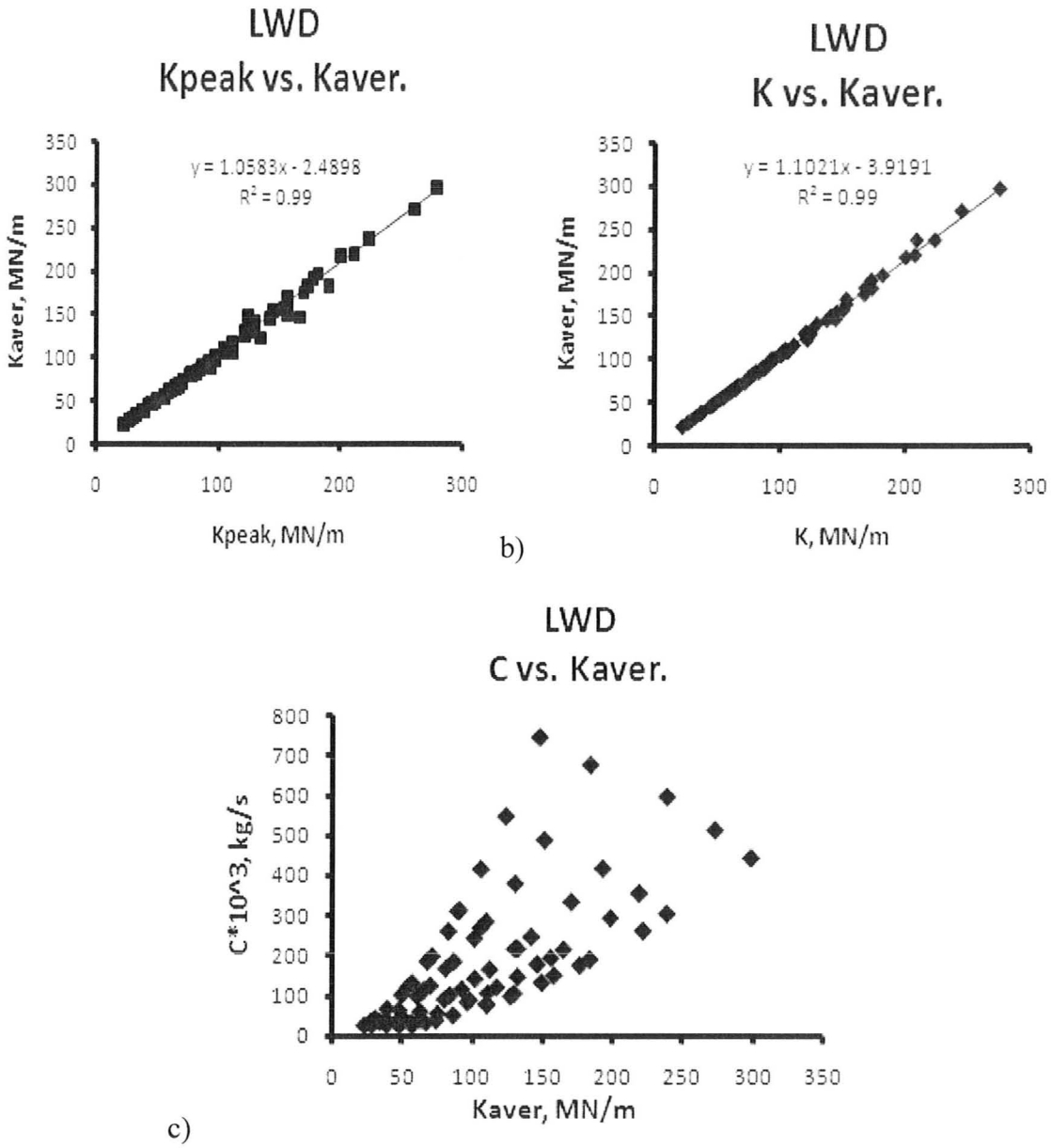

Figure 5.13- LWD isothermal simulations (a) K vs. K_{aver}; (b) K_{peak} vs. K_{aver}; (c) C vs. K_{aver} .

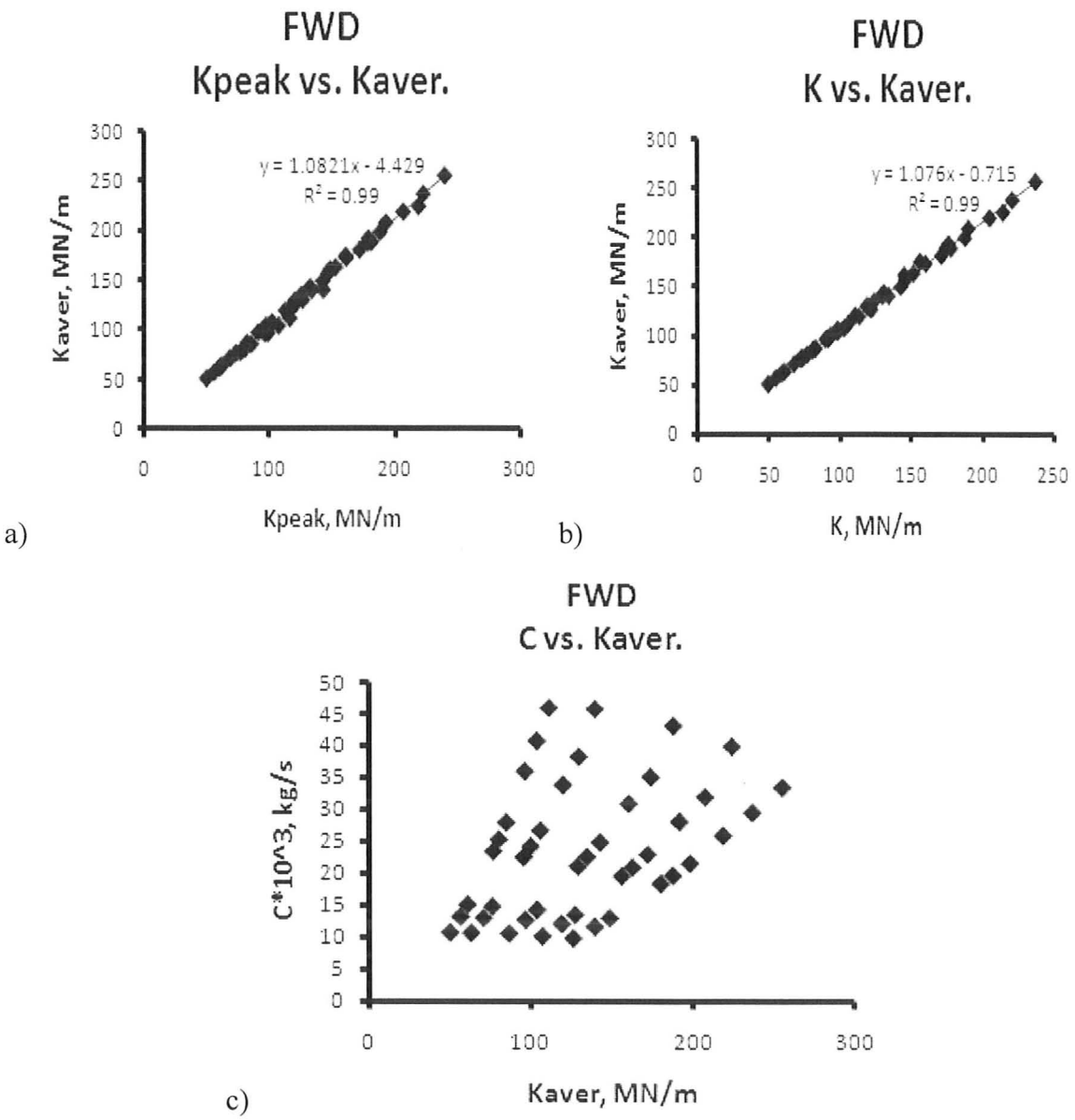

Figure 5.14: FWD non-isothermal simulations: (a) K vs. K_{aver}; (b) K_{peak} vs. K_{aver}; (c) C vs. K_{aver} .

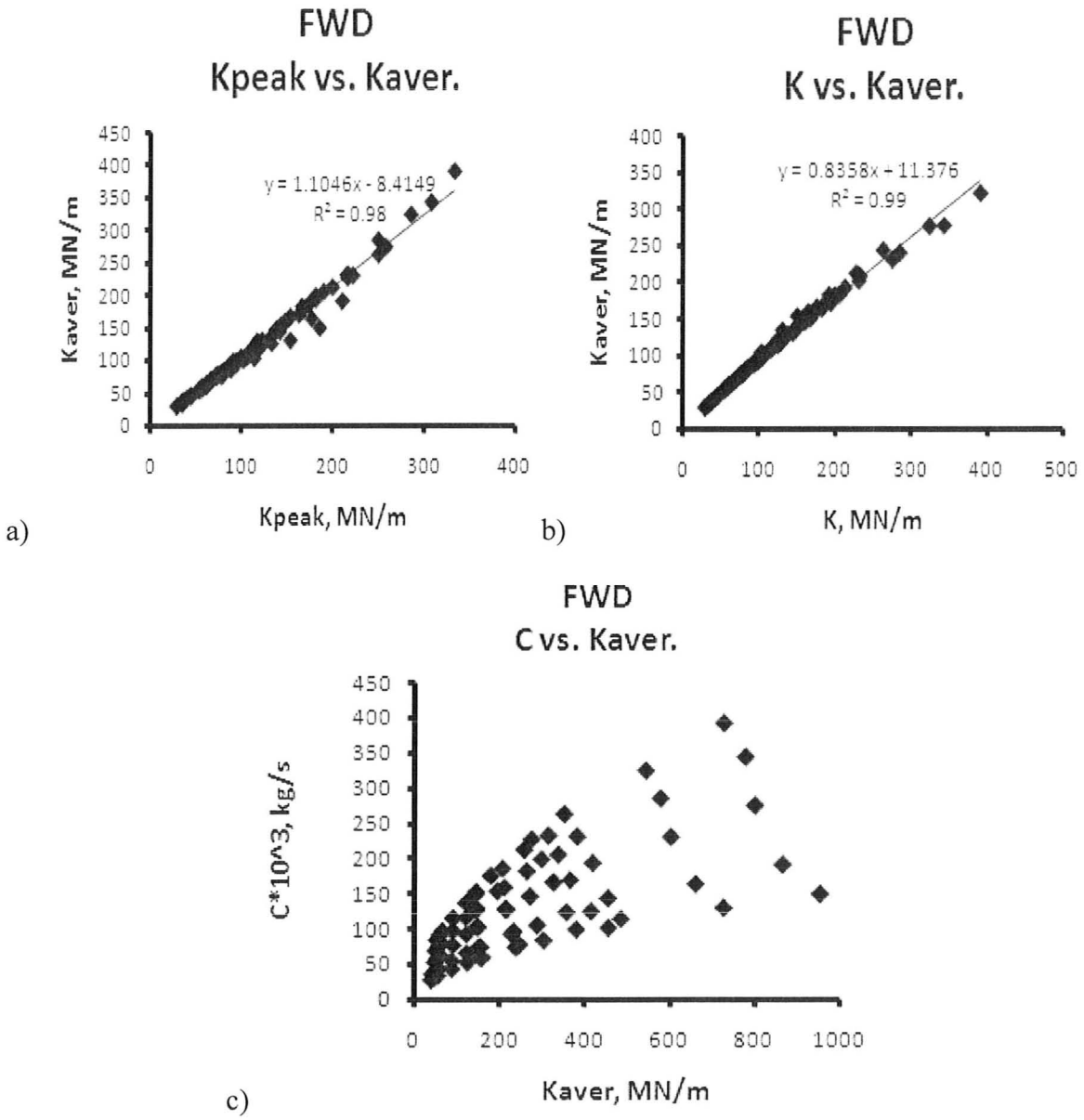

Figure 5.15: FWD isothermal simulations: (a) K vs. K_{aver}; (b) K_{peak} vs. K_{aver}; (c) C vs. K_{aver}.

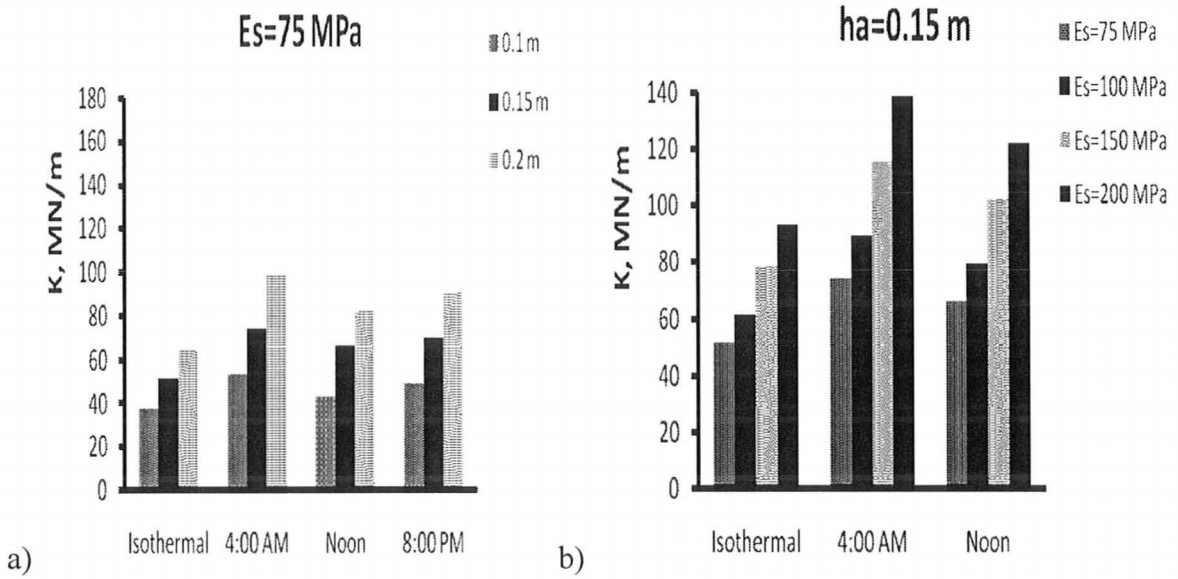

Figure 5.16- Stiffness coefficients for LWD corresponding to E_s = 75 MPa (a) and h_a=0.15 m (b)

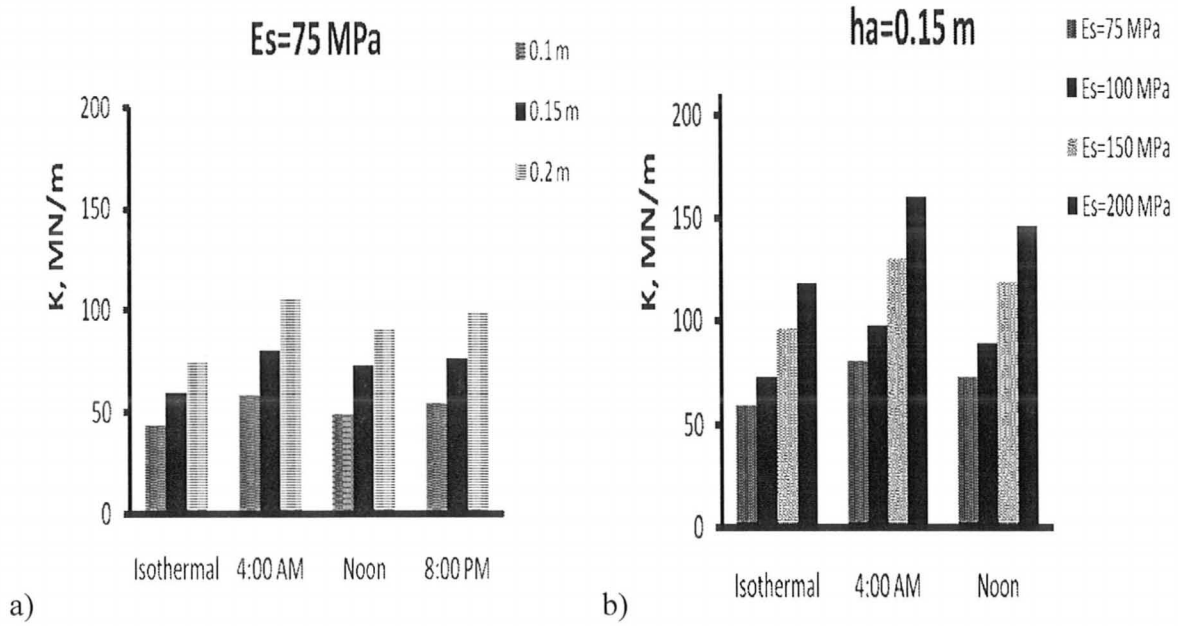

Figure 5.17- Stiffness coefficients for FWD corresponding to E_s = 75 MPa (a) and h_a = 0.15 m (b)

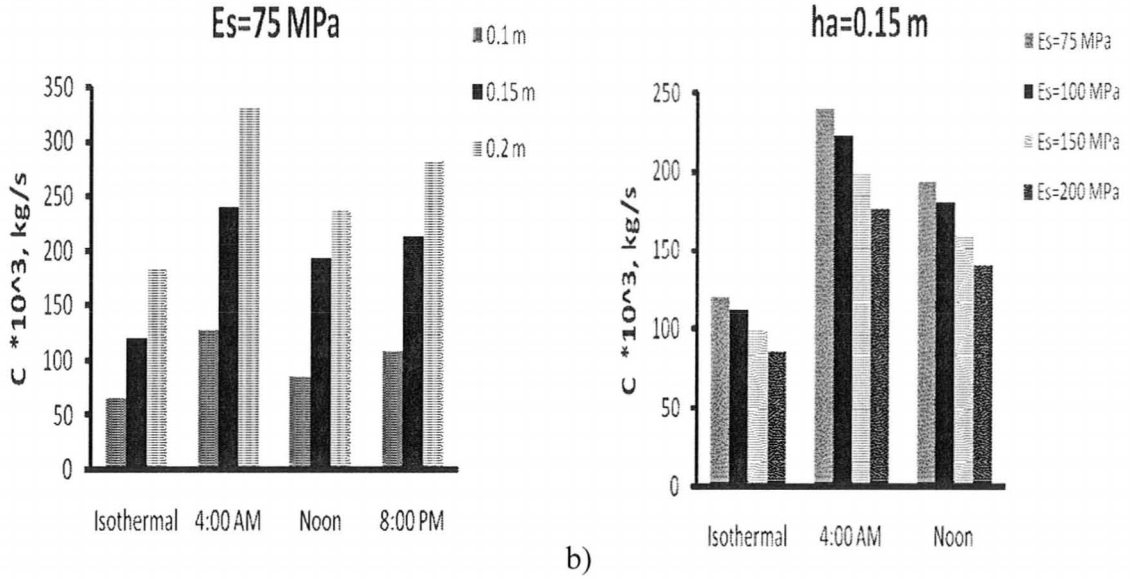

Figure 5.18- Damping coefficients for LWD corresponding to E_s = 75 MPa (a) and h_a = 0.15 m (b)

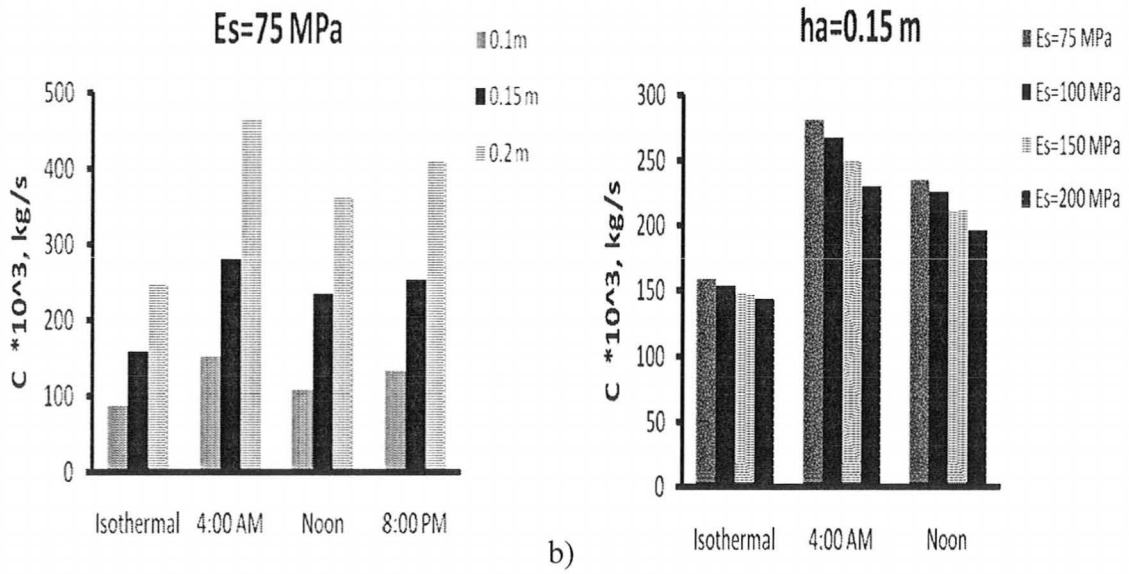

Figure 5.19- Damping coefficients for FWD corresponding to E_s = 75 MPa (a) and h_a = 0.15 m (b)

The main observations for the stiffness coefficient K (Fig.5.16 -LWD, Fig.5.17 - FWD and Figs. C.5-C.8 in the Appendix) are:

- K increases with an increase of the subgrade modulus E_s for the pavement with the constant h_a (Figs. 5.16-5.17 (b));
- K increases with an increase of the pavement thickness h_a (Figs. 5.16-5.17 (a));
- K increases with a decrease of the pavement surface temperature. For example, for the LWD test carried out at 4 am when the pavement surface temperature reaches its lowest value, K values are expected to be 1.24; 1.12 and 1.20 times higher (for pavement layer 0.1; 0,15 and 0.2 m thick, respectively) than those collected at noon (Fig. 5.16 (a)). Reduction in K value for the same cases measured by FWD is smaller and is 1.20; 1.10 and 1.15 times for E_s=75 MPa.

The main observations for the damping coefficient C (Fig.5.18 -LWD, Fig.5.19 - FWD and Figs. C.9-C.12 in the Appendix) are:

- For the pavement with the same thickness of asphalt concrete layer C decreases with an increase of the subgrade modulus E_s (Figs. 5.18-5.19 (b));
- C increases with an increase of the pavement thickness h_a (Figs. 5.18-5.19 (a));
- As the pavement surface temperature increases (which implies decreasing elastic modulus of asphalt concrete E_p) the damping coefficient C decreases. One can note that the damping coefficients for the isothermal case (E_p = 4000 MPa) are

the smallest and can be compared to the case for the modulus distribution E_p = 2969 to 4496 MPa corresponding to noon. For example, for LWD (E_s=75 MPa) C values are found to be 1.50; 1.24 and 1.40 times higher for tests carried out at 4am compared to those measured at noon for h_a=0.1; 0,15 and 0.2 m, respectively. Reduction in C value for the same cases measured by FWD is smaller and is 1.40; 1.20 and 1.28 times for E_s=75 MPa, respectively.

One can observe that LWD results of backcalculation for C and K values are more sensitive to temperature as well as subgrade stiffness changes than those backcalculated from the FWD data. Backcalculation of the effective subgrade modulus E_s and equivalent pavement thickness h_e can be performed using elastodynamic approach equations by Parvini and Stolle (1996):

$$K = 0.67\pi E_s\sqrt{(0.81h_e^2 + a^2)} \tag{5.13}$$

$$C = 0.73Kh_e\sqrt{\frac{3\rho_s}{E_s}} \tag{5.14}$$

or Eqns. (3.2) and (3.4) introduced in Section 3.2.1. One must remember that in spite of how good the model assumptions may be, the system parameters are not the real material properties but rather low-order approximations of the E_s and h_e. A two-layer model approximation used in this study introduces large systematic errors to the backcalculated variables. Stolle (1996) showed that the relative error of the pavement modulus is a summation of the relative errors for the displacement histories, pavement thickness h_a,

and elastic modulus of subgrade E_s. Considerable scatter is observed when using the Ritz vector solution with the fixed boundary conditions on the bottom. Semi-infinite half-space assumption for the subgrade layer is not met if a subgrade layer is located several meters deep from the pavement surface. Such factors as a shallow stiff layer, bedrock or water table implement significant errors in the backcalculated pavement-subgrade elastic moduli. Irwin (2002) suggested that bedrock located deeper than 12 meters has insignificant influence of the backcalculated moduli and may be assumed to be infinite.

CHAPTER 6 SIMULATIONS OF IE TEST

6.1 General

Strictly speaking, the Impact Echo (IE) test is based on analyzing wave propagation. The emphasis in this chapter for the performed FEM analysis for a "fictitious" impact echo (IE) test was to investigate in a forward analysis the sensitivity of response to changes due to temperature gradients, etc, at a higher frequency of loading. A problem was solved that was similar to that for the LWD and FWD simulations in Chapter 5. In other words, the finite element method (FEM) analysis was identical to the previous two tests (FWD and LWD), only the scale and frequency range were different. The main idea of performing the IE simulations was to analyze the response corresponding to a higher frequency range. An important factor was that a much smaller volume was being excited compared to that of the LWD or FWD. No attempt was made to look at the wave propagation characteristics. Analysis interpretation focused on what was happening as a response problem, looking at the temperature sensitivity of the *M, C* and *K* values.

6.2 Finite Element Model

The behaviors of the isothermal and non-isothermal pavement were modeled with the 0.2125x0.25m two-dimensional elastodynamic axisymmetric finite element grid

shown in Fig. 6.1. As one can see, the dimensions of the grid are much less than encountered for the LWD and FWD simulations.

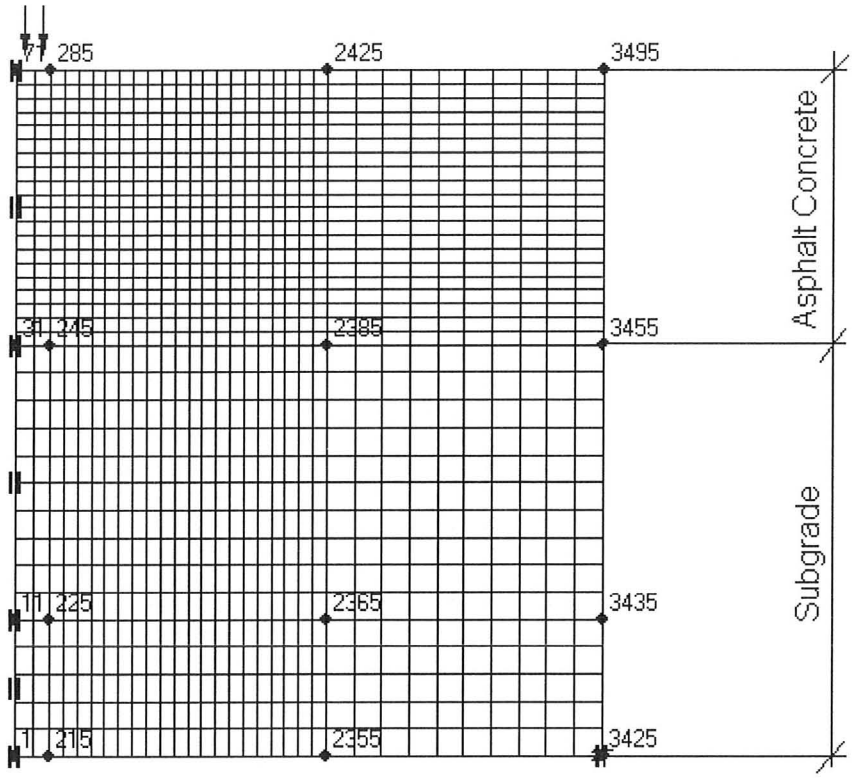

Figure 6.1- FE mesh for isothermal and non-isothermal simulations for IE.

The finite element model was discretized via eight-noded quadrilateral elements for which the node spacing is half the actual size of the element. On the right bottom where numarical filtering of frequencies occurs, the maximum size of the elements was 0.01x0.01m. Thus, the node spacing was equal to 0.005m, which was within the required element size for maximum frequency equal to 20 kHz. The model shown in Fig. 6.1 was discretized into 32x35 eight-noded elements. Overall, there were 1120 elements with the

smaller elements (0.00625x0.005m) under the applied load and bigger ones (0.005x0.01m) farther from the load, to meet the computer memory requirements. The damping ratio corresponding to the dominant frequency was assumed to be approximately 5%. The details on IE model discretization, parameters and material properties are summarized in Table 6.1. For the simulations dealing with non-isothermal conditions, the elastic modulus of the pavement layer E_p varied with depth (see Table A.6 of the Appendix). Variation of E_p with depth, as well as subdivision of the pavement layer into smaller sublayers, was assumed to be the same as for the LWD and FWD non-isothermal simulations described in Section 5.8.

The silent boundary conditions (dashpots) were placed at the bottom and right-hand side of the model (Fig. 6.1) to reduce wave reflection from the boundaries. The left-hand side boundary allowed sliding in the vertical direction via rollers. Referring to Fig. 6.1, there was a roller at node 1 (bottom left) and full fixation at node 3425 (bottom right). Results of the isothermal simulations for IE are summarized in Table A.3 of the Appendix, with those for the non-isothermal simulations being summarized in Tables A.4 and A.6 of the Appendix.

Table 6.1- Finite element discretization for IE isothermal simulations

Parameter	IE simulations
Radius R, m	0.20
Thickness of the pavement-subgrade system, m	0.25
Radius of steel ball, m	0.0125
Distributed load, kPa	2.04
AC layer thickness h_a, m	0.10; 0.15; 0.2
Subgrade layer thickness h_s, m	0.15; 0.10; 0.05
Modulus of elasticity of AC layer, E_p, MPa	4000
Modulus of elasticity of subgrade, E_s, MPa	100; 150; 200
Poisson's ratio of AC layer and subgrade, $\nu_p=\nu_s$	0.3
Unit weight of AC layer and subgrade, $w_p=w_s$, kN/m^3	20.0

The impact due to the 2.5 cm diameter steel ball being dropped on the pavement surface was modeled as a circular uniformly distributed dynamic load, details given in Table 6.1. Goldsmith (1965) suggested that the impact length is proportional to the diameter of the impactor, with Cheng and Sansalone (1993) indicating that the duration of the impact generated by current IE devices typically varies from 10 to 80μs. Lin et al. (1990) recommended that the contact time should be ~30μs to make sure that most of the energy lies in the frequency range less than 50 kHz. In the current study, the load was, however, applied over 0.03s, which is much greater than the recommended one, as shorter load duration caused problems when running the FE program, resulting in meshes that exceeded computer memory. The duration is important for capturing wave propagation,

which was not the focus of the present study. The analysis completed here, nevertheless, allowed us to look at the dynamic behavior at a much smaller scale and higher frequency.

Typical frequency range used for IE testing lies between 5 and 40 kHz. In this thesis, frequencies were considered in the range up to 20 kHz. Given the excitation frequency of 20 kHz, the expected wavelength was approximately 0.082 m, which implied that time step should be less than 2.5μs to provide an accurate numerical solution, with the element size not exceeding 0.005 m. Simulations were performed for the full system of equations using a Newmark time-stepping FORTRAN finite element code developed at McMaster.

6.3 Results of Elastodynamic Data Interpretation

The elastodynamic time domain analysis approach presented in Section 2.4 was used for the IE simulations to evaluate *M, C* and *K* values related to a SDOF oscillator approximation. For non-isothermal simulations, temperature was allowed to vary with depth within the pavement layer. The simulated load-displacement histories were used to backcalculate *M, C* and *K* values following to the technique described in Section 2.5.2. Characteristic trends for *K* and *C* for isothermal and non-isothermal IE simulations are summarized in Figs. 6.2-6.4, Figs. C.13-C.16 and Tables A.3 and A.6 of Appendix. Only representative plots are presented in the main body of this thesis. It should be emphasized that the analysis of the IE test data does not use this approach. Instead, the data is analyzed using wave propagation techniques, as indicated previously.

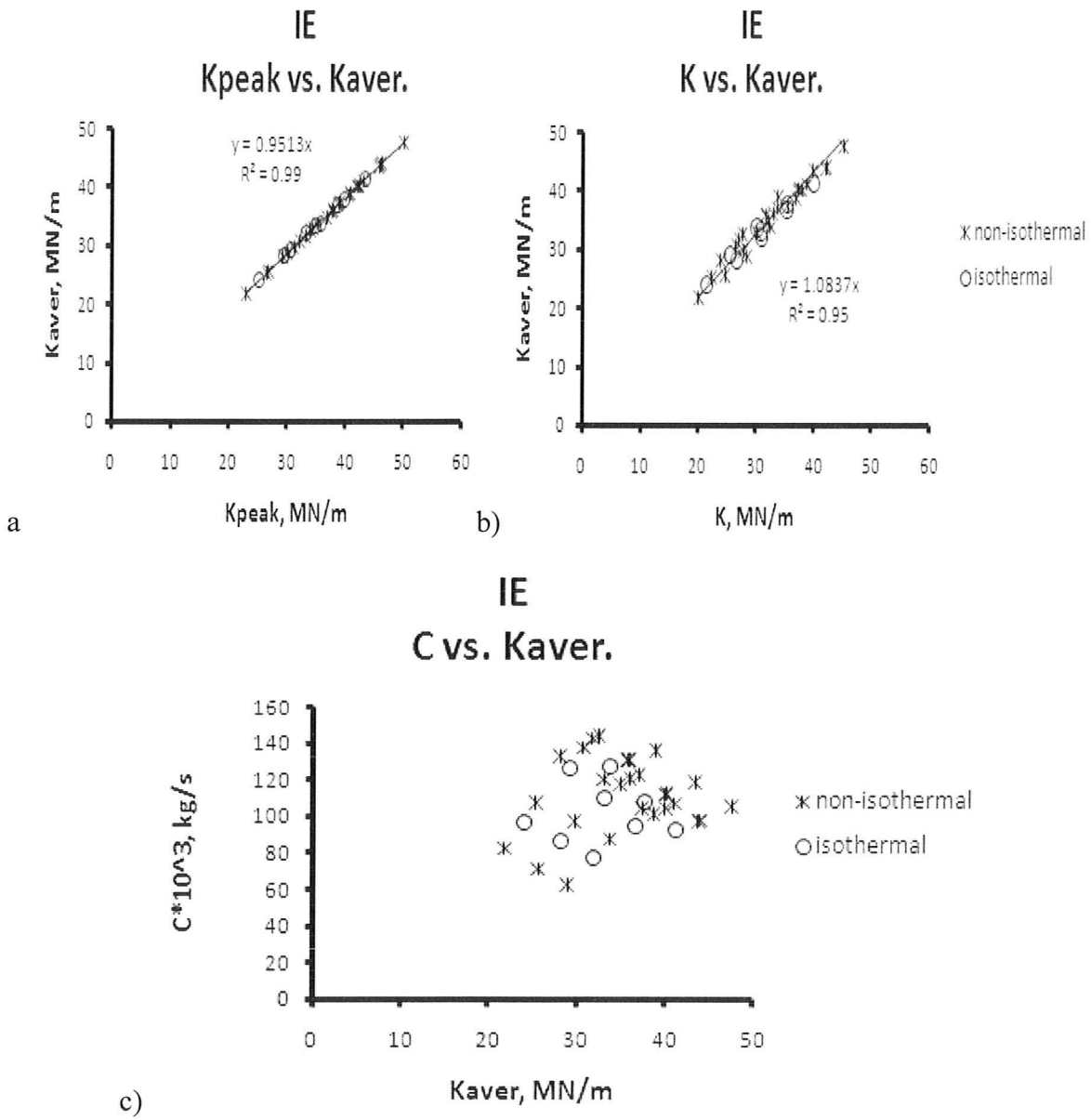

Figure 6.2: IE simulations: a) K vs. K_{aver}; b) K_{peak} vs. K_{aver}; c) C vs. K_{aver}

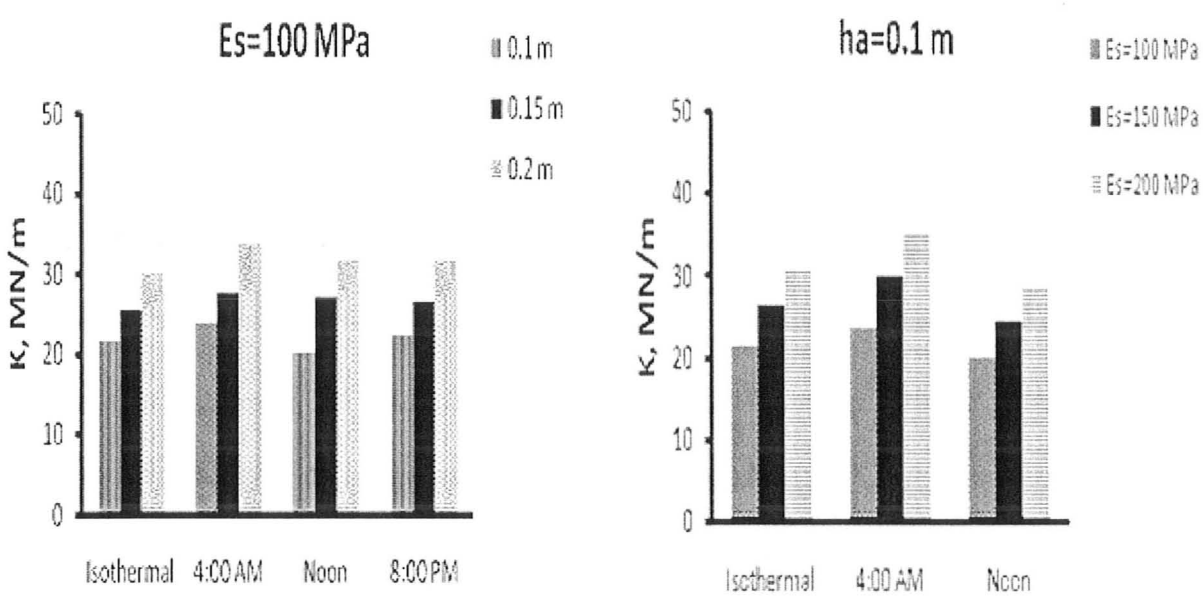

Figure 6.3- Stiffness Coefficients for IE corresponding to E_s = 100 MPa and h_a= 0.10 m

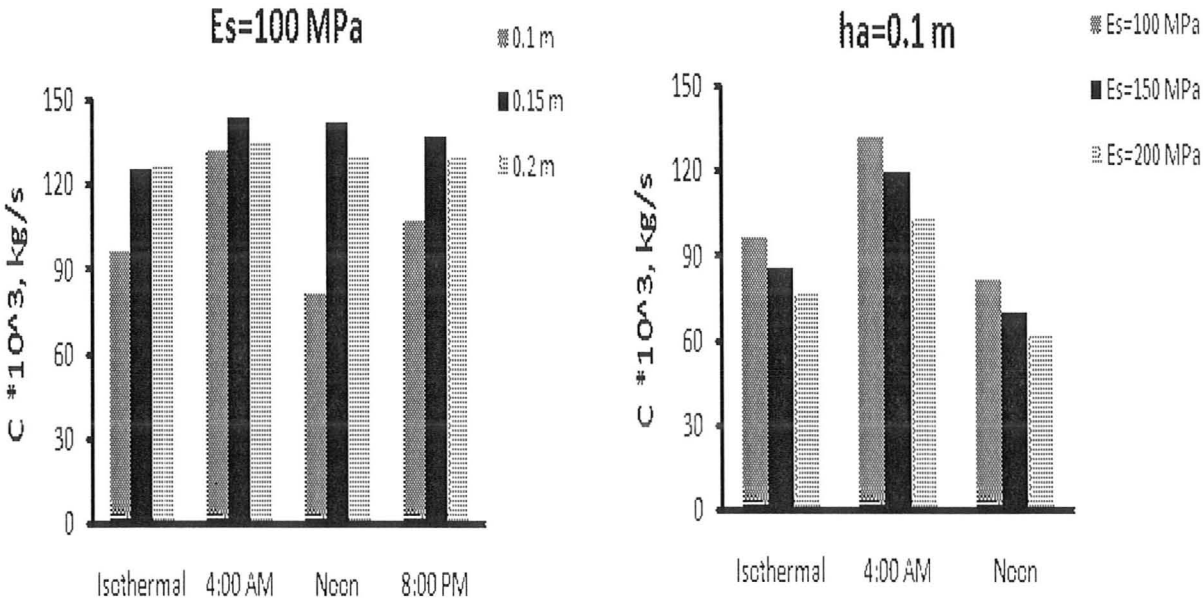

Figure 6.4- Damping Coefficients for IE corresponding to E_s = 100 MPa and h_a= 0.15 m

One observes from Fig. 6.2 that a good linear relation exists between the backcalculated K values and the static stiffness K_{peak} calculated using Eqn. (5.12) or the average value of $K_{aver}=S(0)$ that corresponds to the steady-state (zero frequency) for both isothermal and non-isothermal cases. A lot of scatter is observed when plotting the damping coefficient C versus the average stiffness K_{aver}, which indicates that the damping coefficient C for the impact echo test is not directly related to the structural stiffness.

As mentioned above, the interest of this chapter was in high frequency response of the IE test compared to the LWD and FWD with no attempt made to simulate the actual IE test. The fast Fourier transform (FFT) analysis was performed on the synthetic load-deflection histories to identify which frequency range was expected to dominate the response. The result showed that most of the energy was in the 0 to 4 kHz range, while the information pertaining to frequencies greater than that could not be properly captured. The characteristic wavelength for the dominant frequency 4 kHz is:

$$\lambda_p = \frac{C_p}{f} = \frac{1640}{4 \cdot 10^3} \approx 0.4m$$

Heukelom and Foster (1960) showed that for a high frequency range when the dominating wavelengths approach the thickness of the pavement, the response is mainly affected by the properties of the asphalt concrete layer. Taking into account that the dominating wavelength (0.4 m) was 2-4 times larger than the thickness of the asphalt concrete layer of pavement models (h_a=0.1; 0.2m), the waves generated by the IE propagated in the lower layers. Thus, the overall response was more affected by the

subbase-subgrade than the asphalt concrete layer properties. Moreover, in order to detect flaws in the pavement layer the wavelength should be much smaller than the size related to the flaws.

The results of K and C coefficients shown on Figs. 6.3-6.4 and Figs. C.13-C.16 of Appendix C follow the similar trends as for LWD and FWD devices. The mass coefficient values M were very small in value and, therefore, were not taken into account in the present study. The K values change with temperature, thickness of the pavement and elastic modulus of subgrade:

- Stiffness coefficient K increases with an increase of the subgrade modulus E_s holding h_a constant (Figs. 6.3 (b))
- Stiffness coefficient K increases with an increase of the asphalt layer thickness h_a (Fig. 6.3 (a))
- A minor increase is observed in K values with decrease of the pavement surface temperature for thick pavements (h_a=0.15 and 0.2 m) (Figs. 6.3 and C.14 of the Appendix). Stiffness increase was more apparent in thin pavements (h_a=0.1m). For instance, for different pavement samples with h_a=0.1; 0,15 and 0.2 m (E_s=100 MPa) K values are observed to be 1.19; 1.02 and 1.06 times larger at 4 am than those, measured at noon, respectively (Fig. 6.3).

As for the damping coefficient C, main trends are similar to those observed for the LWD and FWD with some differences:

- For thin pavements (h_a=0.1m) damping coefficient C appears to be influenced more by pavement temperature changes than stiffness K, which for larger thicknesses is not the case.
- C increases as the elastic modulus of subgrade E_s decreases for the pavements with the same thickness of asphalt concrete layer h_a.
- Damping coefficient C in the thin pavements (0.1 m) rapidly decreases as the pavement surface temperature increases (corresponding to decrease in E_p). C values for the thicker pavements (0.15 and 0.2 m) remain almost constant during the day with a slight decrease at noon. For example, C values for pavement samples with h_a=0.1; 0.15 and 0.2 m respectively, E_s=100MPa are 1.61; 1.01 and 1.04 times larger at 4am compared to noon (Fig. 6.4).

The IE can identify that changes take place due to changing E_p as a result of a variation in temperature, but more sophisticated analysis techniques are required to extract details. Both K and C data analyses indicated that "fictitious" IE device measurements are sensitive to temperature changes in thin pavements (0.1m) with smaller changes in thicker pavements. This suggests that fictitious IE device is not able to capture the full picture in the thick pavements. Therefore, the IE device might have a limited applicability in real pavements, thicker than 100 mm, being not practical for typical pavement structures representative for highways. The impact echo device cannot provide information about E_s. It must be stressed that at more realistic frequencies the details may be very different, however, the conclusion regarding information about E_s will likely remain the same.

Furthermore, the wave propagation characteristics might provide additional information not captured in the analysis of this Chapter since the wavelength of the present analysis was much greater than for real impact echo test.

One must take into account that simplified SDOF approximation of the dynamic response of a real pavement-subgrade system initially intended for the FWD and LWD, might cause systematic errors and inconsistencies for IE data interpretation. SDOF assumption for the IE tests most likely does not reflect the real pavement-soil system dynamic characteristics. Because of much shorter dominant wavelengths (0.4 m), the way the wave interacts with layered pavement-subgrade system is different than encountered for the FWD and LWD tests, which have excited wavelengths exceeding 3-4 m. Nevertheless, one can still identify sensitivities of the IE response to asphalt concrete layer temperature changes though K and C have different meanings. Stiffness and damping coefficients depend on the vibration mode and, thus, vary with higher frequency of the IE test.

Chapter 7 CONCLUSIONS

7.1 General

Dynamic backcalculation technique for the FWD suggested by Peiravian (1994) and based on the impedance functions was extended and applied to the LWD test. Two pieces of information can be extracted from each geophone in dynamic backcalculation, allowing one to backcalculate an additional pavement-subgrade parameter. This is particularly significant for the LWD test, as it is restricted to a maximum of three geophone measurements. It was shown that elastostatic backcalculation, although neglecting damping and inertia effects, can be a simple effective tool for pavement-subgrade system identification. Using advantages of both elastostatic and dynamic methods, one can accurately identify system characteristics at offsets greater than zero.

Based on the elastostatic and elastodynamic backcalculation analysis results, an attempt was made to develop an understanding of applicability of the LWD and IE in testing real pavements. Owing to the choice of the diameter of the load plate affecting its influence depth, the LWD was found to be picking up the response of the upper base-subgrade layers in thin pavements. Results from simulations for a fictitious IE device are inconclusive. Nevertheless, temperature sensitivity was observed and it is clear that information about E_s cannot be extracted from the IE.

The sensitivity of the LWD, FWD and IE devices to pavement layer properties, affected by changes in the surface temperature, were investigated. In principle, large

differences in backcalculated parameters should not exist between the LWD and FWD tests if diameter of the load plate is the same and only energy input (applied load) varies. Differences in backcalculated parameters can be attributed to the various radii of the load plates adopted for the FWD and LWD simulations; smaller plate radius for the LWD has an impact on the volume of material tested.

This study answered the questions raised in Sections 5.3 and 5.9:

1. How sensitive is backcalculated subgrade modulus E_s to surface temperature variations in pavement layer?

It was shown, that the backcalculated surface elastic moduli E_{SM} representing E_s at far distances from the load are not sensitive to the temperature changes in the pavement layer.

2. How does backcalculated layer stiffness vary as temperature changes in terms of what one measures using the FWD and LWD tests?

Relative differences in stiffness K with the increase of asphalt layer thickness matched well for the FWD and LWD tests in pavements thicker than 0.15 m. The bigger differences in relative stiffness increase were encountered when testing thinner (0.1 and 0.15m thick) pavements with the LWD.

3. What a pavement engineer actually measures when FWD and LWD tests are performed? Do FWD and LWD results lead to different sensitivities?

The LWD is mostly capturing the complex stiffness of the pavement-base layers which is typically higher than that of the subgrade. This results in the higher E_{SM} value at zero offset for the LWD than that for the FWD. Variations of effective surface modulus E_{SM} at zero offset showed that the LWD results are more sensitive to temperature changes in asphalt concrete layer than the FWD ones. The values of the effective subgrade moduli (E_{eff}) backcalculated at far distances from the applied load showed less agreement with the actual values of elastic moduli of subgrade (E_s) for the FWD than those backcalculated for the LWD.

4. Can one make any strong statements with respect to being able to backcalculate system parameters when using an "elastostatic" approach?

The detailed analysis on the backcalculated non-isothermal synthetic data showed that the elastostatic approach is a valuable tool for interpretation LWD and FWD load-deflection histories given that the backcalculated subgrade modulus is not sensitive to temperature fluctuations in the asphalt layer.

7.2 On Backcalculation

Following Peiravian (1994), an assumption of the infinite bedrock location was made to extend backcalculation elastodynamic technique presented in this thesis. Therefore, the subgrade was modeled as an elastic halfspace assuming no sudden changes in its stiffness with depth.

For a Kirchhoff plate on elastic halfspace shear deformations are neglected in the plate. Taking into account the additional flexibility of a plate due to shear deformation allows one to more accurately model the pavement-subgrade system behavior. A more sophisticated approach to model real thick flexible pavement-subgrade structures known as the Mindlin plate was presented in this study. It was found that the Mindlin plate is a realistic and accurate simplified model for pavement-subgrade system modeling and backcalculation.

The experimental results and accompanying analysis of the case studies discussed in Chapter 3 showed some problems with the experimental test setup for the LWD. The LWD tests were carried out on the small pavement samples with close edge boundary conditions deviating from a two-layer idealization. A rough back-of-the-envelope calculation indicates that the relation between maximum pressure of the subgrade at the bottom of asphalt pad (q_{sub}) and maximum pressure applied under the loading plate (q_{app}) for the LWD field test was $\frac{q_{sub}}{q_{app}} \sim \frac{1}{20}$. As a result, the edge boundary effects, together with the possible movement of the device after the drop, had a negative impact on the recorded load-deflection histories and, therefore, on backcalculated system parameters in general.

An important limitation of elastodynamic backcalculation revealed in Chapter 4 was the presence of the nearby bedrock. The FWD and LWD computer simulations were performed for the case of a shallow bedrock (4 m deep) modeled by the fixed bottom

boundary. Real and imaginary components of the dynamic impedance function showed considerable scatter. Hypothesis was further supported by the results of frequency analysis simulations carried out for the case of infinite bedrock modeled by introducing transmitting boundary on the bottom. The normalized imaginary component of dynamic impedance showed a good agreement with the Mindlin plate approximation, with considerably reduced scatter. A combined elastostatic and elastodynamic backcalculation of the unknown layer elastic moduli was adopted in Chapter 4 for the cases where the bedrock is deep. One can use the plot of the normalized imaginary component of dynamic impedance for the Mindlin plate approximation up to $kh_e \approx 2$ together with the relation for elastostatic stiffness K=S(0) using relations from the dimensional analysis to backcalculate "effective" equivalent asphalt thickness h_a and subgrade elastic moduli E_s, provided that the conditions in the field do not deviate strongly from the two-layer idealization.

7.3 On Sensitivity of LWD, FWD and IE Tests to Temperature Variations

Temperature analysis, elastostatic and elastodynamic backcalculation on the non-isothermal synthetic data presented in Chapters 5 and 6 for the LWD, FWD and IE devices allowed one to undertsand the influences of temperature changes in the upper layer of the pavement, thickness of the asphalt-concrete pavement and subgrade modulus on the response.

Based on the results of the temperature analysis performed for the summer conditions, the following conclusions and observations are made based on an elastostatic data interpretation of the LWD and FWD simulated data:

1- Increases in pavement thickness, as well as increase in the stiffness of subgrade layer, increase the maximum value of effective surface moduli.

2- Existence of elastic moduli variations in pavement layer cannot be accurately accounted for in the thin pavements (less than 100 mm thick) as most of the rapid temperature fluctuations occur near the surface affecting rapid elastic modulus changes during the day.

3- LWD response is more sensitive to temperature fluctuations in the pavement layer than the FWD.

4- For the LWD a higher surface modulus is observed at zero offset than that of the FWD. This fact supports the notion that the LWD influence depth reaches the pavement-base layers capturing their stiffness, which is higher than that of the subgrade reached by the FWD testing.

5- Theory originally developed for the FWD perhaps needs some alternative calibration for the LWD, which can use maximum up to three geophones to record load-deflection histories.

6- Backcalculated surface elastic modulus, representing elastic modulus of subgrade, at far distances from the load is not sensitive to the temperature changes in the asphalt concrete layer.

Main conclusions from elastodynamic data interpretation for the LWD, FWD and IE devices:

1- LWD device results of elastostatic backcalculation are more sensitive to temperature as well as subgrade stiffness changes than those backcalculated from the FWD data.

2- Significant errors in the backcalculated pavement-subgrade elastic moduli can be introduced by using a two-layer model approximation, as well as by presence of a shallow stiff layer or a bedrock.

3- Impact echo measurements are sensitive to temperature changes in thin pavements (less than 100 mm). No strong statement can be made about thick pavements.

7.4 Further Research Recommendations

The experimental study and the backcalculation techniques developed herein can be improved and extended as follows:

1- Larger pavement pads should be tested with the LWD to reduce edge boundary effects on the test response. Geophones should also be placed farther from the load, to allow full application of the elastostatic backcalculation presented in this study.

2- Numerical simulations should be completed to study what happens during the winter and early spring as the stiffness profile undergoes changes.

3- The presence of moisture should be accounted for, its effect on elastic moduli of pavement-subgrade layers and, as a result, on the sensitivity of the response of the NDT devices discussed in this study.

4- Backcalculation approach presented in this study should be adjusted for layer elastic moduli estimation of the deteriorated pavements.

APPENDIX A

Table A.1 -Results of FWD Isothermal Computer Simulations using Ritz method and Time Domain Analysis (P=40 kN)

#	E_p (MPa)	E_s (MPa)	h_p (m)	C 10^3 (kg/s)	K (MN/m)	K_{peak} (MN/m)	K_{aver} (MN/m)	w under the plate (mm)
1	2000	75	0.05	38.891	28.542	28.57	28.68	1.4
2	2000	75	0.1	87.832	43.961	44.44	44.371	0.9
3	2000	75	0.15	159.30	59.728	61.54	60.49	0.65
4	2000	75	0.2	246.59	74.795	80.00	78.7	0.5
5	2000	75	0.3	454.30	103.73	114.29	102.32	0.35
6	2000	100	0.05	41.162	36.421	36.36	37.01	1.1
7	2000	100	0.1	87.834	54.447	57.14	55.69	0.7
8	2000	100	0.15	154.40	72.921	72.73	74.91	0.55
9	2000	100	0.2	233.48	90.494	94.12	96.75	0.425
10	2000	100	0.3	413.64	122.95	133.33	125.33	0.3
11	2000	150	0.05	46.703	51.755	53.33	53.64	0.75
12	2000	150	0.1	89.794	74.014	74.07	77.65	0.54
13	2000	150	0.15	148.35	96.800	100.00	102.87	0.4
14	2000	150	0.2	213.25	118.69	117.65	128.58	0.34
15	2000	150	0.3	364.41	155.11	163.27	169.49	0.245
16	2000	200	0.05	49.648	66.760	66.67	69.49	0.6
17	2000	200	0.1	90.004	92.282	90.91	97.50	0.44
18	2000	200	0.15	144.15	118.35	117.65	127.17	0.34
19	2000	200	0.2	194.01	143.56	145.45	153.88	0.275
20	2000	200	0.3	336.72	183.00	190.48	205.29	0.21
21	2000	250	0.05	52.475	81.513	81.63	84.64	0.49
22	2000	250	0.1	90.878	109.72	111.11	115.52	0.36
23	2000	250	0.15	141.23	138.48	140.35	148.11	0.285
24	2000	250	0.2	178.93	166.22	166.67	175.44	0.24
25	2000	250	0.3	313.99	208.08	216.22	232.08	0.185
26	4000	75	0.05	48.039	32.213	34.78	32.40	1.15
27	4000	75	0.1	123.98	52.830	53.33	53.48	0.75
28	4000	75	0.15	238.32	73.848	78.43	74.84	0.51
29	4000	75	0.2	379.60	94.383	102.56	99.84	0.39
30	4000	75	0.3	725.85	134.27	153.85	130.22	0.26
31	4000	100	0.05	49.975	40.677	40.00	41.44	1
32	4000	100	0.1	122.29	65.091	66.67	66.83	0.6
33	4000	100	0.15	228.30	90.008	94.12	92.89	0.425
34	4000	100	0.2	356.47	114.09	123.08	124.15	0.325

35	4000	100	0.3	660.26	159.24	177.00	163.89	0.226
36	4000	150	0.05	54.619	57.012	57.14	59.19	0.7
37	4000	150	0.1	121.25	87.786	88.89	92.84	0.45
38	4000	150	0.15	216.46	119.09	123.08	128.32	0.325
39	4000	150	0.2	326.16	150.05	153.85	166.49	0.26
40	4000	150	0.3	601.48	201.78	222.22	230.22	0.18
41	4000	200	0.05	57.121	72.830	72.73	75.97	0.55
42	4000	200	0.1	120.70	108.84	111.11	116.08	0.36
43	4000	200	0.15	210.55	145.52	148.15	159.15	0.27
44	4000	200	0.2	297.71	182.51	181.82	198.92	0.22
45	4000	200	0.3	576.80	240.64	250.00	284.55	0.16
46	4000	250	0.05	60.038	88.351	88.89	91.92	0.45
47	4000	250	0.1	121.24	129.01	133.33	137.04	0.3
48	4000	250	0.15	206.16	170.47	173.91	185.54	0.23
49	4000	250	0.2	275.03	212.24	216.22	226.76	0.185
50	4000	250	0.3	542.26	277.08	285.71	324.03	0.14
51	6000	75	0.05	55.798	34.970	34.78	35.22	1.15
52	6000	75	0.1	153.72	59.162	61.54	59.97	0.65
53	6000	75	0.15	303.15	83.854	88.89	84.77	0.45
54	6000	75	0.2	483.73	108.21	117.65	114.40	0.34
55	6000	75	0.3	951.33	153.50	186.05	149.64	0.215
56	6000	100	0.05	57.456	43.900	44.44	44.79	0.9
57	6000	100	0.1	150.26	72.679	74.07	74.82	0.54
58	6000	100	0.15	287.96	101.97	106.67	105.51	0.375
59	6000	100	0.2	453.49	130.41	142.86	143.61	0.28
60	6000	100	0.3	863.62	182.48	210.53	191.16	0.19
61	6000	150	0.05	61.228	61.028	61.54	63.47	0.65
62	6000	150	0.1	146.94	97.596	100.00	103.80	0.4
63	6000	150	0.15	271.32	134.58	137.93	146.49	0.29
64	6000	150	0.2	417.27	171.62	181.82	193.64	0.22
65	6000	150	0.3	798.61	231.25	258.06	274.68	0.155
66	6000	200	0.05	63.424	77.469	78.43	80.95	0.51
67	6000	200	0.1	145.46	120.59	123.08	129.54	0.325
68	6000	200	0.15	263.81	164.27	166.67	182.15	0.24
69	6000	200	0.2	380.98	209.16	216.22	230.81	0.185
70	6000	200	0.3	776.69	277.79	307.69	343.25	0.13
71	6000	250	0.05	66.236	93.562	94.12	97.54	0.425
72	6000	250	0.1	145.15	142.61	142.86	152.61	0.28
73	6000	250	0.15	257.67	192.47	200.00	212.25	0.2
74	6000	250	0.2	351.19	243.92	250.00	262.65	0.16
75	6000	250	0.3	725.82	322.31	333.33	391.03	0.12

Table A.2-Results of LWD Isothermal Computer Simulations using Ritz method and Time Domain Analysis (P=7.8 kN)

#	E_p (MPa)	E_s (MPa)	h_p (m)	C 10^3 (kg/s)	K (MN/m)	K_{peak} (MN/m)	K_{aver} (MN/m)	w under the plate (mm)
1	2000	75	0.05	23.882	22.016	22.29	22.36	0.35
2	2000	75	0.1	65.201	37.584	39.00	38.68	0.2
3	2000	75	0.15	120.50	51.759	55.71	53.72	0.14
4	2000	75	0.2	183.50	64.611	67.83	67.2	0.115
5	2000	75	0.3	308.41	87.357	93.98	88.99	0.083
6	2000	100	0.05	23.974	27.289	27.86	27.87	0.28
7	2000	100	0.1	62.480	45.486	45.88	47.13	0.17
8	2000	100	0.15	111.81	61.693	65.00	64.78	0.12
9	2000	100	0.2	165.79	76.012	78.00	80.12	0.1
10	2000	100	0.3	267.19	100.12	105.41	105.12	0.074
11	2000	150	0.05	24.821	37.106	37.14	38.11	0.21
12	2000	150	0.1	58.736	59.467	60.00	62.06	0.13
13	2000	150	0.15	98.896	78.668	78.00	83.25	0.1
14	2000	150	0.2	140.12	94.918	97.50	101.23	0.08
15	2000	150	0.3	215.33	120.59	121.88	129.62	0.064
16	2000	200	0.05	24.238	46.304	45.88	47.39	0.17
17	2000	200	0.1	53.584	71.824	70.9i	74.46	0.11
18	2000	200	0.15	86.837	93.103	97.50	97.55	0.08
19	2000	200	0.2	119.03	110.54	111.43	116.66	0.07
20	2000	200	0.3	176.58	136.80	141.82	145.44	0.055
21	2000	250	0.05	23.588	55.053	55.71	56.13	0.14
22	2000	250	0.1	49.538	83.021	82.11	85.44	0.095
23	2000	250	0.15	77.654	105.71	105.41	109.57	0.074
24	2000	250	0.2	103.74	123.80	123.81	129.01	0.063
25	2000	250	0.3	148.82	150.06	152.94	157.22	0.051
26	4000	75	0.05	33.100	26.471	26.90	26.98	0.29
27	4000	75	0.1	100.33	47.315	48.75	49.13	0.16
28	4000	75	0.15	196.19	66.987	70.91	70.40	0.11
29	4000	75	0.2	311.39	85.739	86.67	89.78	0.09
30	4000	75	0.3	545.55	121.24	134.48	122.95	0.058
31	4000	100	0.05	32.943	32.630	33.19	33.49	0.235
32	4000	100	0.1	96.038	57.352	59.09	60.09	0.132
33	4000	100	0.15	182.94	80.280	84.78	85.88	0.092
34	4000	100	0.2	283.02	101.62	108.33	109.16	0.072
35	4000	100	0.3	486.37	140.11	156.00	150.36	0.05

36	4000	150	0.05	33.201	44.035	43.33	45.45	0.18
37	4000	150	0.1	89.252	75.224	76.47	79.49	0.102
38	4000	150	0.15	162.95	103.53	104.00	111.59	0.075
39	4000	150	0.2	244.75	128.95	130.00	141.03	0.06
40	4000	150	0.3	415.22	172.45	177.27	191.89	0.044
41	4000	200	0.05	31.905	54.656	55.71	56.15	0.14
42	4000	200	0.1	81.466	91.236	91.76	95.46	0.085
43	4000	200	0.15	144.87	123.81	123.81	131.46	0.063
44	4000	200	0.2	212.68	152.44	156.00	163.99	0.05
45	4000	200	0.3	353.17	199.61	200.00	218.10	0.039
46	4000	250	0.05	30.979	64.738	65.00	66.17	0.12
47	4000	250	0.1	75.773	105.90	106.85	109.70	0.073
48	4000	250	0.15	130.96	141.92	123.81	148.57	0.063
49	4000	250	0.2	188.37	172.95	173.33	182.77	0.045
50	4000	250	0.3	302.23	222.59	222.86	237.92	0.035
51	6000	75	0.05	40.719	29.650	30.00	30.32	0.26
52	6000	75	0.1	129.32	54.087	55.71	56.50	0.14
53	6000	75	0.15	258.28	77.509	82.11	82.10	0.095
54	6000	75	0.2	413.69	100.48	111.43	105.24	0.07
55	6000	75	0.3	742.73	144.15	166.67	146.83	0.0468
56	6000	100	0.05	40.323	36.444	37.14	37.55	0.21
57	6000	100	0.1	123.47	65.573	67.83	69.27	0.115
58	6000	100	0.15	241.07	93.032	97.50	100.79	0.08
59	6000	100	0.2	377.56	119.26	130.00	129.64	0.06
60	6000	100	0.3	673.80	167.21	190.24	182.97	0.041
61	6000	150	0.05	39.947	48.978	48.75	50.73	0.16
62	6000	150	0.1	114.00	86.121	86.67	91.77	0.09
63	6000	150	0.15	215.63	120.57	121.88	131.49	0.064
64	6000	150	0.2	332.12	152.35	156.00	169.54	0.05
65	6000	150	0.3	593.89	208.39	222.86	237.82	0.035
66	6000	200	0.05	38.006	60.602	60.94	62.42	0.128
67	6000	200	0.1	103.86	104.59	104.00	110.08	0.075
68	6000	200	0.15	192.15	144.85	144.44	155.06	0.054
69	6000	200	0.2	291.52	181.28	181.40	197.57	0.043
70	6000	200	0.3	510.85	243.88	260.00	271.97	0.03
71	6000	250	0.05	36.724	71.604	70.91	73.30	0.11
72	6000	250	0.1	96.628	121.57	121.88	126.42	0.064
73	6000	250	0.15	174.01	166.76	169.57	175.66	0.046
74	6000	250	0.2	259.68	207.01	210.81	220.86	0.037
75	6000	250	0.3	441.03	274.24	278.57	297.57	0.028

Table A.3-Results of Isothermal Computer Simulations for IE using full system equations and TDA

#	E_p (MPa)	E_s (MPa)	h_p (m)	M 10^{-5} (kg)	C 10^3 (kg/s)	K (MN/m)	K_{peak} (MN/m)	K_{aver} (MN/m)	w under the plate (mm)
1	4000	100	0.1	3.3	96.7	21.5	25.2	24.0	.3964E-04
2	4000	100	0.15	3.8	126.3	25.5	30.7	29.1	.3261E-04
3	4000	100	0.2	4.5	127.2	30.1	35.7	33.7	.2802E-04
4	4000	150	0.1	4.0	86.3	26.6	29.6	28.2	.3383E-04
5	4000	150	0.15	2.5	110.1	30.8	34.9	33.1	.2865E-04
6	4000	150	0.2	5.5	107.3	35.4	39.8	37.7	.2511E-04
7	4000	200	0.1	4.5	77.1	30.9	33.3	31.9	.3006E-04
8	4000	200	0.15	3.5	94.5	35.2	38.5	36.7	.2596E-04
9	4000	200	0.2	6.0	92.2	39.7	43.3	41.2	.2309E-04

Table A.4-Results of Temperature Computer Simulations for FWD using Ritz method and TDA (P=40 kN)

#	Station, Time	h_p (m)	Average E_p (MPa) varies with h_p	E_s (MPa)	C 10^3 (kg/s)	K (MN/m)	K_{peak} (MN/m)	K_{aver} (MN/m)	w under the plate (mm)
1	4 a.m	0.2	5200-5992	75	46.056	105.31	116.36	111.8	0.344
2	12 p.m	0.2	2969-4496	75	36.069	91.279	98.96	96.96	0.40
3	8 p.m	0.2	4456-4662	75	40.827	98.280	107.52	104.32	0.372
4	4 a.m	0.15	4991-5791	75	28.021	80.512	85.64	85.44	0.467
5	12 p.m	0.15	3200-4730	75	23.534	73.089	77.08	77.4	0.519
6	8 p.m	0.15	4445-4619	75	25.346	76.285	80.48	80.8	0.497
7	4 a.m	0.1	5429-6018	75	15.116	58.408	60.68	61.52	0.659
8	12 p.m	0.1	2894-3261	75	10.791	48.916	49.94	50.97	0.801
9	8 p.m	0.1	4516-4661	75	13.255	54.545	56.1	57.19	0.713
10	4 a.m	0.2	5200-5992	100	45.872	129.62	142.86	140.22	0.28
11	12 p.m	0.2	2969-4496	100	33.924	110.40	116.62	120.39	0.343
12	8 p.m	0.2	4456-4662	100	38.368	118.73	126.58	130.13	0.316
13	4 a.m	0.15	4991-5791	100	26.761	98.134	102.56	106.33	0.39
14	12 p.m	0.15	3200-4730	100	22.626	89.291	96.62	96.1	0.432
15	8 p.m	0.15	4445-4619	100	24.283	93.057	96.62	100.38	0.414
16	4 a.m	0.1	5429-6018	100	14.817	71.839	73.66	76.68	0.543
17	12 p.m	0.1	2894-3261	100	10.726	60.401	61.54	63.65	0.65
18	8 p.m	0.1	4516-4661	100	13.063	67.175	68.73	71.33	0.582
19	4 a.m	0.2	5200-5992	150	43.195	174.71	181.00	188.53	0.221
20	12 p.m	0.2	2969-4496	150	30.975	145.37	148.15	160.97	0.27
21	8 p.m	0.2	4456-4662	150	35.176	156.42	160.64	174.48	0.249
22	4 a.m	0.15	4991-5791	150	24.889	130.64	132.45	143.16	0.302
23	12 p.m	0.15	3200-4730	150	21.160	119.04	120.48	129.5	0.332
24	8 p.m	0.15	4445-4619	150	22.642	123.95	125.39	135.13	0.319
25	4 a.m	0.1	5429-6018	150	14.315	97.435	97.32	104.27	0.411
26	12 p.m	0.1	2894-3261	150	10.628	82.270	82.30	87.13	0.486
27	8 p.m	0.1	4516-4661	150	12.737	91.219	91.12	97.24	0.439
28	4 a.m	0.2	5200-5992	200	39.956	214.67	218.58	224.52	0.183
29	12 p.m	0.2	2969-4496	200	28.150	176.59	178.57	192.14	0.224
30	8 p.m	0.2	4456-4662	200	32.036	190.26	192.31	208.03	0.208
31	4 a.m	0.15	4991-5791	200	23.007	160.22	161.29	172.53	0.248
32	12 p.m	0.15	3200-4730	200	19.610	146.16	146.52	156.58	0.273
33	8 p.m	0.15	4445-4619	200	20.956	151.89	152.67	163.11	0.262
34	4 a.m	0.1	5429-6018	200	13.535	120.66	120.12	127.61	0.333

35	12 p.m	0.1	2894-3261	200	10.198	102.44	102.04	107.57	0.392
36	8 p.m	0.1	4516-4661	200	12.116	113.28	112.68	119.42	0.355
37	4 a.m	0.2	5200-5992	250	33.520	237.63	239.52	255.51	0.167
38	12 p.m	0.2	2969-4496	250	25.963	205.27	206.19	218.89	0.194
39	8 p.m	0.2	4456-4662	250	29.566	221.23	222.22	236.94	0.18
40	4 a.m	0.15	4991-5791	250	21.589	187.83	187.79	198.67	0.213
41	12 p.m	0.15	3200-4730	250	18.448	171.31	171.67	180.69	0.233
42	8 p.m	0.15	4445-4619	250	19.692	178.09	178.57	188.01	0.224
43	4 a.m	0.1	5429-6018	250	12.992	142.74	142.35	149.09	0.281
44	12 p.m	0.1	2894-3261	250	9.8712	121.62	121.21	126.45	0.33
45	8 p.m	0.1	4516-4661	250	11.668	134.15	133.78	139.85	0.299

Table A.5-Results of Temperature Computer Simulations for LWD using Ritz method and TDA (P=7.8 kN)

#	Station, Time	h_p (m)	Average E_p (MPa) varies with h_p	E_s (MPa)	C 10^3 (kg/s)	K (MN/m)	K_{peak} (MN/m)	K_{aver} (MN/m)	w under the plate (mm)
1	4 a.m	0.2	5200-5992	75	329.56	98.465	106.85	101.96	0.073
2	12 p.m	0.2	2969-4496	75	235.88	82.245	87.74	85.39	0.0889
3	8 p.m	0.2	4456-4662	75	282.46	90.598	97.50	94.00	0.08
4	4 a.m	0.15	4991-5791	75	239.68	74.463	78.95	78.40	0.0988
5	12 p.m	0.15	3200-4730	75	193.69	66.253	69.58	69.57	0.1121
6	8 p.m	0.15	4445-4619	75	212.85	69.866	73.65	73.41	0.1059
7	4 a.m	0.1	5429-6018	75	127.77	53.741	55.56	56.11	0.1404
8	12 p.m	0.1	2894-3261	75	85.068	43.296	44.24	44.80	0.1763
9	8 p.m	0.1	4516-4661	75	109.43	49.519	50.95	51.52	0.1531
10	4 a.m	0.2	5200-5992	100	289.02	116.47	123.61	125.89	0.0631
11	12 p.m	0.2	2969-4496	100	206.42	96.949	101.43	103.61	0.0769
12	8 p.m	0.2	4456-4662	100	247.50	107.10	112.88	115.10	0.0691
13	4 a.m	0.15	4991-5791	100	222.83	89.363	93.08	95.87	0.0838
14	12 p.m	0.15	3200-4730	100	180.12	79.373	82.11	84.54	0.095
15	8 p.m	0.15	4445-4619	100	197.88	83.751	86.86	89.45	0.0898
16	4 a.m	0.1	5429-6018	100	121.96	65.161	66.78	68.78	0.1168
17	12 p.m	0.1	2894-3261	100	81.478	52.447	53.50	54.703	0.1458
18	8 p.m	0.1	4516-4661	100	104.65	60.033	61.42	63.06	0.127
19	4 a.m	0.2	5200-5992	150	257.84	148.19	152.64	165.48	0.0511
20	12 p.m	0.2	2969-4496	150	177.07	122.02	124.40	133.58	0.0627
21	8 p.m	0.2	4456-4662	150	217.27	135.78	139.04	150.13	0.0561
22	4 a.m	0.15	4991-5791	150	198.31	115.56	117.47	125.59	0.0664
23	12 p.m	0.15	3200-4730	150	159.45	102.20	103.45	110.09	0.0754
24	8 p.m	0.15	4445-4619	150	175.67	108.06	109.55	116.81	0.0712
25	4 a.m	0.1	5429-6018	150	112.69	85.569	86.09	91.14	0.0906
26	12 p.m	0.1	2894-3261	150	76.063	68.713	68.97	72.23	0.1131
27	8 p.m	0.1	4516-4661	150	97.070	78.783	79.19	83.48	0.0985
28	4 a.m	0.2	5200-5992	200	219.08	176.23	178.90	191.85	0.0436
29	12 p.m	0.2	2969-4496	200	148.08	143.55	144.98	154.01	0.0538
30	8 p.m	0.2	4456-4662	200	183.12	160.78	162.84	173.79	0.0479
31	4 a.m	0.15	4991-5791	200	176.27	138.66	139.78	148.29	0.0558
32	12 p.m	0.15	3200-4730	200	140.78	122.09	122.64	129.68	0.0636
33	8 p.m	0.15	4445-4619	200	155.71	129.35	130.22	137.78	0.0599
34	4 a.m	0.1	5429-6018	200	102.57	103.92	104.14	109.35	0.0749

35	12 p.m	0.1	2894-3261	200	69.303	83.201	83.07	86.74	0.0939
36	8 p.m	0.1	4516-4661	200	88.489	95.592	95.59	100.24	0.0816
37	4 a.m	0.2	5200-5992	250	193.73	200.99	202.60	214.10	0.0385
38	12 p.m	0.2	2969-4496	250	129.29	162.19	163.18	170.96	0.0478
39	8 p.m	0.2	4456-4662	250	161.72	182.74	183.96	193.69	0.0424
40	4 a.m	0.15	4991-5791	250	160.26	159.43	160.16	167.73	0.0487
41	12 p.m	0.15	3200-4730	250	127.16	139.81	140.29	146.38	0.0556
42	8 p.m	0.15	4445-4619	250	140.99	148.42	149.14	155.73	0.0523
43	4 a.m	0.1	5429-6018	250	95.499	120.80	121.12	125.58	0.0644
44	12 p.m	0.1	2894-3261	250	69.303	83.201	96.42	86.74	0.0809
45	8 p.m	0.1	4516-4661	250	82.402	111.03	111.27	115.15	0.0701

Table A.6-Results of Temperature Computer Simulations for IE using full system equations and TDA

#	Station, Time	Average E_p (MPa) varies with h_p	E_s (MPa)	h_p (m)	M (kg)	C 10^3 (kg/s)	K (MN/m)	K_{peak} (MN/m)	$K_{aver.}$ (MN/m)	h_p (m) under the plate (mm)
1	D,4 a.m	5200-5992	100	0.2	2.9597	135.96	33.711	40.87	38.9	.2447E-04
2	D,12 p.m	2969-4496	100	0.2	2.5937	130.69	31.664	37.94	35.9	.2636E-04
3	D,8 p.m	4456-4662	100	0.2	5.2370	130.45	31.538	37.76	35.7	.2648E-04
4	C, 4 a.m	4991-5791	100	0.15	4.0614	144.25	27.605	34.01	32.5	.2940E-04
5	C, 12	3200-4730	100	0.15	1.7885	142.49	27.052	33.18	31.7	.3014E-04
6	C, 8 p.m	4445-4619	100	0.15	3.6927	137.44	26.462	32.24	30.7	.3102E-04
7	B, 4 a.m	5429-6018	100	0.1	1.3269	132.71	23.893	29.30	28.1	.3413E-04
8	B, 12	2894-3261	100	0.1	3.0373	82.288	20.072	23.04	21.8	.4341E-04
9	B, 8 p.m	4516-4661	100	0.1	3.4703	107.45	22.343	26.57	25.3	.3764E-04
10	D,4 a.m	5200-5992	150	0.2	7.3224	118.56	39.792	45.77	43.4	.2185E-04
11	D,12 p.m	2969-4496	150	0.2	6.2841	112.20	37.314	42.43	40.1	.2357E-04
12	D,8 p.m	4456-4662	150	0.2	3.7507	111.81	37.162	42.21	40.0	.2369E-04
13	C, 4 a.m	4991-5791	150	0.15	5.2723	122.73	33.583	38.85	37.0	.2574E-04
14	C, 12	3200-4730	150	0.15	2.8756	120.38	32.891	37.88	36.0	.2640E-04
15	C, 8 p.m	4445-4619	150	0.15	4.6970	117.26	32.101	36.76	34.9	.2720E-04
16	B, 4 a.m	5429-6018	150	0.1	4.1949	119.99	30.010	34.49	33.0	.2899E-04
17	B, 12	2894-3261	150	0.1	3.7608	70.696	24.610	26.89	25.6	.3719E-04
18	B, 8 p.m	4516-4661	150	0.1	4.1026	97.187	27.776	31.19	29.7	.3206E-04
19	D,4 a.m	5200-5992	200	0.2	7.7411	105.15	45.013	50.03	47.5	.1999E-04
20	D,12 p.m	2969-4496	200	0.2	6.6520	97.557	42.071	46.25	43.9	.2162E-04
21	D,8 p.m	4456-4662	200	0.2	6.8249	97.122	41.890	46.02	43.7	.2173E-04
22	C, 4 a.m	4991-5791	200	0.15	4.0904	106.59	38.673	43.05	41.0	.2323E-04
23	C, 12	3200-4730	200	0.15	6.0742	104.03	37.824	41.93	40.0	.2385E-04
24	C, 8 p.m	4445-4619	200	0.15	5.5653	100.76	36.850	40.65	38.7	.2460E-04
25	B, 4 a.m	5429-6018	200	0.1	3.4788	103.98	35.355	39.06	37.4	.2560E-04
26	B, 12	2894-3261	200	0.1	4.2524	61.967	28.338	30.12	28.9	.3320E-04
27	B, 8 p.m	4516-4661	200	0.1	3.0949	87.202	32.409	35.19	33.7	.2842E-04

Table A.7 –Results of backcalculation of synthetic non-isothermal data for FWD using MODULUS-Mac

#	Asphalt thickness h_p (mm), station	Time	Average E_p varies with depth (MPa)	Real E_s (MPa)	Estim. E_s (min value) (MPa)	Estim. aver. E_s (MPa)	Estim. effective thick-ness h_{eff} (mm)	Equiv. asphalt thick-ness* (see below) h_a (mm)	Backcalculated E_p (MPa)
1	200, D	4 am	5562.9	75	72.2	72.6	826	220	5082
2		12 pm	3767.5	75	70.5	70.6	729	192	3416
3		8 pm	4516.3	75	71.4	71.7	777	206	4186
4	150, C	4 am	5299.4	75	68.7	69.2	621	162	4865
5		12 pm	4112.1	75	67.5	68.3	560	145	3504
6		8 pm	4453.1	75	68.2	68.8	587	153	4079
7	100, B	4 am	5878.4	75	65.7	65.9	442	114	5678
8		12 pm	3077.8	75	65.6	66.0	346	89	2716
9		8 pm	4588.3	75	65.7	66.0	404	104	4345
10	200, D	4 am	5562.9	100	91.9	92.2	769	221	5230
11		12 pm	3767.5	100	90.1	90.5	678	194	3511
12		8 pm	4516.3	100	91.3	91.5	723	208	4314
13	150, C	4 am	5299.4	100	88.7	89.8	570	162	4873
14		12 pm	4112.1	100	87.1	87.1	543	154	4128
15		8 pm	4453.1	100	87.8	87.8	565	160	4691
16	100, B	4 am	5878.4	100	86.2	86.7	406	114	5777
17		12 pm	3077.8	100	85.8	85.8	346	97	3542
18		8 pm	4588.3	100	86.3	86.9	370	104	4386
19	200, D	4 am	5562.9	150	133	133.3	681	221	5250
20		12 pm	3767.5	150	131	132.5	597	193	3482
21		8 pm	4516.3	150	132	133.0	638	207	4279
22	150, C	4 am	5299.4	150	130	130.0	524	169	5541
23		12 pm	4112.1	150	129	129.0	475	153	4085
24		8 pm	4453.1	150	130	130.0	496	160	4701
25	100, B	4 am	5878.4	150	128	129.3	339	109	4988
26		12 pm	3077.8	150	128	128.0	298	96	3370

27		8 pm	4588.3	150	127	127.0	343	110	5126
28	200, D	4 am	5562.9	200	175	176.5	623	222	5277
29		12 pm	3767.5	200	174	175.5	548	195	3577
30		8 pm	4516.3	200	175	176.0	585	208	4379
31	150, C	4 am	5299.4	200	173	173.0	478	170	5595
32		12 pm	4112.1	200	172	172.7	431	153	4093
33		8 pm	4453.1	200	173	173.3	452	160	4741
34	100, B	4 am	5878.4	200	171	171.0	334	118	6388
35		12 pm	3077.8	200	171	171.0	263	93	3103
36		8 pm	4588.3	200	171	171.0	306	108	4917
37	200, D	4 am	5562.9	250	219	220.5	580	222	5345
38		12 pm	3767.5	250	217	217.0	527	202	3980
39		8 pm	4516.3	250	219	220.5	543	208	4394
40	150, C	4 am	5299.4	250	216	216.7	447	170	5703
41		12 pm	4112.1	250	216	216.7	401	153	4141
42		8 pm	4453.1	250	217	217.7	422	161	4841
43	100, B	4 am	5878.4	250	215	215.0	310	118	6386
44		12 pm	3077.8	250	199	199.0	306	108	4717
45		8 pm	4588.3	250	215	215.0	283	108	4848

Table A.8- Results of backcalculation of synthetic non-isothermal data for LWD using MODULUS-Mac

# simulation	Asphalt thickness h_p (mm), station	Time	Average E_p varies with depth (MPa)	Real E_s (MPa)	Estim. E_s (min value) (MPa)	Estim. aver. E_s (MPa)	Estim. effective thick-ness h_{eff} (mm)	Equiv.asphalt thickness* (see below) h_a (mm)	Back-calculated E_p (MPa)
1	200, D	4 am	5562.9	75	80	81.0	706	194	3523
2		12 pm	3767.5	75	77.1	78.2	628	170	2382
3		8 pm	4516.3	75	79	80.0	662	181	2865
4	150, C	4 am	5299.4	75	75.7	76.2	538	145	3495
5		12 pm	4112.1	75	74	74.4	495	133	2662
6		8 pm	4453.1	75	74.7	75.2	515	138	3018
7	100, B	4 am	5878.4	75	71.6	71.7	387	103	4150
8		12 pm	3077.8	75	71	71.4	309	82	2098
9		8 pm	4588.3	75	71.4	71.5	356	94	3209
10	200, D	4 am	5562.9	100	102	102.8	653	195	3554
11		12 pm	3767.5	100	99.2	100.2	579	171	2410
12		8 pm	4516.3	100	100	101.4	618	183	2953
13	150, C	4 am	5299.4	100	96.9	97.6	504	148	3681
14		12 pm	4112.1	100	95.9	96.3	459	134	2739
15		8 pm	4453.1	100	96.8	97.3	475	139	3076
16	100, B	4 am	5878.4	100	93.7	93.8	357	104	4281
17		12 pm	3077.8	100	93.1	93.8	287	83	2197
18		8 pm	4588.3	100	93.4	93.7	329	95	3333
19	200, D	4 am	5562.9	150	146	147.8	580	195	3563
20		12 pm	3767.5	150	144	145.5	515	172	2457
21		8 pm	4516.3	150	145	147.2	544	182	2913
22	150, C	4 am	5299.4	150	143	143.8	438	146	3571
23		12 pm	4112.1	150	141	141.3	406	135	2800
24		8 pm	4453.1	150	142	143.5	414	137	2975
25	100, B	4 am	5878.4	150	138	139.3	308	101	4044
26		12 pm	3077.8	150	137	137.0	259	85	2384
27		8 pm	4588.3	150	138	139.3	284	93	3151

28	200, D	4 am	5562.9	200	193	195.2	530	195	3589
29		12 pm	3767.5	200	190	192.5	469	172	2448
30		8 pm	4516.3	200	192	194.3	498	183	2960
31	150, C	4 am	5299.4	200	191	192.0	397	146	3545
32		12 pm	4112.1	200	189	189.0	368	134	2789
33		8 pm	4453.1	200	189	190.0	382	140	3125
34	100, B	4 am	5878.4	200	184	184.0	289	105	4431
35		12 pm	3077.8	200	183	183.0	234	84	2332
36		8 pm	4588.3	200	184	184.0	267	97	3489
37	200, D	4 am	5562.9	250	240	243.3	493	195	3604
38		12 pm	3767.5	250	238	240.3	436	172	2460
39		8 pm	4516.3	250	239	242.3	462	182	2953
40	150, C	4 am	5299.4	250	237	237.7	376	148	3733
41		12 pm	4112.1	250	235	236.0	344	135	2831
42		8 pm	4453.1	250	238	238.3	353	139	3109
43	100, B	4 am	5878.4	250	231	231.0	268	105	4439
44		12 pm	3077.8	250	231	231.0	214	84	2276
45		8 pm	4588.3	250	231	231.0	247	97	3497

APPENDIX B

```
%%%%%%%%%%%%%%%%%%%%%%%%%%%%%%%%%%%%%%%%%%%%%%%%%%%%%%%%%%%%%%%%%%%%%%%%%%%%
% Matlab program to calculate the real and imaginary components of the
% Normalized Dynamic Impedance for a Mindlin plate theory, using
% typically encountered values of the parameters: mr = modulus ratio,
% k = angular freq./wave velocity, h = Thickness of plate
%%%%%%%%%%%%%%%%%%%%%%%%%%%%%%%%%%%%%%%%%%%%%%%%%%%%%%%%%%%%%%%%%%%%%%%%%%%%

clear

global k2 s1 s2 h damping

nstep=2000;

ksi = 0.005; % 0.5% damping
ES = [75, 100, 150, 200, 250];
EP = [1000, 2000, 3000, 4000, 5000, 6000];
www = [30, 60, 120, 200, 400];
hh = [0.05, 0.10, 0.15, 0.2, 0.30];
damping = 1 + 2 * ksi * i;
result = [0, 0, 0, 0, 0, 0];
n=0

for imr = 1:6
for ik = 1:5
for iw = 1:5
mr = EP(imr)/ES(ik);
k = www(iw)*sqrt(2/(ES(ik)*1000/3)); %density of 2.0,Poisson's ratio =
0.5

for ih = 1:5
h = hh(ih);

n = n + 1;
s1 = mr*h^3/3;
s2 = 2*h^2/5;
he = (mr)^(1/3)*h;
khe= k*he;
k2=k*k;
bound=2*k;
xmaxd = fminbnd('zdyna',0,bound);

DIstatic=quadgq('statDI',0,2*xmaxd,nstep )+quads
('statDI',2*xmaxd,2*nstep);
DIdynamic=quadgq('dynaDI',0,2*xmaxd,nstep )+quads
('dynaDI',2*xmaxd,2*nstep);

ratio = DIstatic/DIdynamic;
```

```
Real = real(ratio);
Imag = imag(ratio);
result = [result; mr, k, h, khe, Real,Imag];
end
end
end
end

khe = result( : ,4);
real = result( : ,5);
imag = result( : ,6);
figure
plot(khe,real,'.');
grid on
title('Real Part of Normalized Dynamic Impedance vs. k*he')
xlabel('k*he')
ylabel('Real')
figure
plot(khe,imag,'.');
title('lmaginary Part of Normalized Dynamic Impedance vs. k*he')
grid on
xlabel('k*he')
ylabel('lmaginary')
save OUTPUT result -ascii
```

```
%%% SUBROUTINE
%Matlab program which provides the integrand, in the equation of the
%Dynamic Impedance S(ω), to be integrated in the main program.

function y = dynaDI(m)
global k2 s1 s2 h damping nplate
kc = k2/damping;
A=1.0;
a=1/(1+0.4*m^2*h^2);
B = a*s1 * m ^ 4 - A * k2 * h;
C = (4 * m ^3) .* sqrt( m ^2 - kc);
if real(C) < 0
C = -1 * C;
end
F = ((2 * m ^2 - kc)^2 - C) ./ ( kc * m );
y = ( A .* m ) ./ (B - A .* F * damping );


%%% SUBROUTINE
%Matlab program which provides the integrand, in the equation of the
%static Dynamic Impedance S(0), to be integrated in the main program.

function y = statDI(m)
global k2 s1 s2 h damping nplate
A = 1.0;
a=1/(1+0.4*m^2*h^2);
y = A ./ (a*s1 * m ^ 3 + 2 * A);
```

```
%%% SUBROUTINE
%Matlab program which provides the inverse of the integrand, in the
%equation of the Dynamic Impedance S(ω), to be minimized in the main
%program.

function z = zdyna(m)
global k2 s1 s2 h damping
kc = k2/damping;
A=1.0;
a=1/(1+0.4*m^2*h^2);
B = a*s1 * m ^ 4 - A * k2 * h;
C = (4 * m ^3) .* sqrt( m ^2 - kc);
if real(C) < 0
C = -1 * C;
end
F = ((2 * m ^2 - kc)^2 - C) ./ ( kc * m );
y = ( A .* m ) ./ (B - A .* F * damping );
z = 1 ./ abs(real(y));


%%% SUBROUTINE
%Matlab program to perform integrations

function cnt = quadgq(funfcn,a,b,Nstep)
if nargin < 4, Nstep = 10; end
sum = 0;
del = (b-a)/Nstep;
dx = sqrt(0.15)*del;
x = a + 0.5 * del;
for i = 1:Nstep
x1 = x - dx;
x2 = x + dx;
sum = sum+5*feval(funfcn,x1 )+8*feval(funfcn,x)+5*feval(funfcn,x2);
x = x + del;
end
cnt = sum * del/18;
```

```
%%% SUBROUTINE
%Matlab program to perform integrations

function cnt = quads(funfcn,a,Nstep)
if nargin < 4, Nstep = 11; end
dl=0.1^15;
du =20;
sm = sqrt(dl*du);
rat = (du/dl)^(1/(2*Nstep));
h = sm*log(rat);
sum = feval(funfcn,sm+a);
rm = 1/rat; rp = rat;
for i = 1:Nstep
sum = sum + rp*feval(funfcn,a+sm*rp) + rm*feval(funfcn,a+sm*rm);
rp =rp*rat;
rm = rm/rat;
end;
cnt = h * sum;
```

```
%-------------------------------------------------------------------------
% Matlab program to perform Frequency Domain Analysis on LWD test data.
% It finds and plots the real and imaginary components of the dynamic
% impedance of the system and calculates M,C and K of a SDOF oscillator
% equivalent to a pavement-subgrade structure.
%-------------------------------------------------------------------------

clear

%-----------------------------------------
%  input data for time steps,loads and deflections
%-----------------------------------------

fid = fopen('B(1).txt','r');
[a] = fscanf(fid,'%g %g %g',[3 inf]);
a = a';
def(:,1) = a(:,2)*10^-6;
load(:,1) = a(:,3)*10^3;
n = size(a,1);
a = [];
fclose(fid);

p=load(:,1);
u=def(:,1);
dt=0.00025;
t2=(n-1)*dt;
t=0:dt:t2;
for m=n+1:1024
    p(m)=0;
    u(m)=0;
end
freq=(0:511)'/(0.00025*1024);
w1=2*pi*freq;
w2=w1.*w1;
P=fft(p,1024);
U=fft(u,1024);
DynImp=P./U;
R=real(DynImp);
I=imag(DynImp);
p1=max(p);
u1=max(u);
K=p1/u1; % calculates S(0)=K to normalize the dynamic impedance S(ω)
I1=I/K; % Normalized imaginary component of dynamic impedance
R1=R/K; % Normalized real component of dynamic impedance

figure
plot(w2(1:7)*10^-3,R1(1:7))
grid on
xlabel('w^2 x1000 (rad/s)^2')
ylabel('Real')
```

```
figure
plot(w1(1:7),I1(1:7))
grid on
% title('Imaginary Component of Dynamic Impedance vs. w')
xlabel('w (rad/s)')
ylabel('Imaginary')

M=-(R(7)-R(1))/(w2(7)-w2(1));
C=(I(7)-I(1))/(w1(7)-w1(1));
K=R(1);

save  A(7).dat M C K -ascii
save IA(7).dat I -ascii
save RA(7).dat R -ascii
save wA(7).dat w1 -ascii
```

```
%%%%%%%%%%%%%%%%%%%%%%%%%%%%%%%%%%%%%%%%%%%%%%%%%%%%%%%%%%%%%%%%%%%%%%%%%%%%
%%% Script to solve the 1D heat equation in soil with
%%% daily temperature forcing
%%%%%%%%%%%%%%%%%%%%%%%%%%%%%%%%%%%%%%%%%%%%%%%%%%%%%%%%%%%%%%%%%%%%%%%%%%%%
clc
clear

%%% Initialize variables

    dz = .01; %each depth step(in meters)
    Nz = 60; % Choose the number of depth steps (should go to 60 cm)
    Nt = 7200; % Choose the number of time steps
    dt = (5*24*60*60)/Nt; %Length of each time step in seconds (3.6*10^3
seconds, or 60 minutes)
    K1 = 0.4348*10^-6; %  K for asphalt-concrete layer in m^2/s
    K2 = 0.5324*10^-6; %  K for base (clay) layer in m^2/s
    C = 1;                  % Require a heat capacitance
    K(1:9,1)=K1/C;            %  Start at 1 cm below surface, therefore
    K(10,1)=(K1+K2)/2/C;      %  Interface at 10th node
    K(11:60,1)= K2/C;


T = 22.5*ones(Nz+1,Nt+1);             %Create temperature matrix with
Nz+1 rows, and Nt+1 columns
                                      % Initial guess is that T is fixed
                                        (22.5C) at the bottom.


time = [0:5/Nt:5];

T(1,:)=13*sin(6.02*(time-19))+28; %Set surface temperature


maxiter = 10;
for iter = 1:maxiter
    Tlast = T; %Save the last guess
    T(:,1) = Tlast(:,end); %Initialize the temp at t=0 to the last temp
    for i=2:Nt+1,
        depth_2D = (T(1:end-2,i-1)-2*T(2:end-1,i-1)+T(3:end,i-1))/dz^2;
        time_1D = K(1:end-1,1).*depth_2D;
        %time_1D = K*depth_2D;
        T(2:end-1,i) = time_1D*dt + T(2:end-1,i-1);


        T(end,i) = 22.5; % Enforce bottom BC

    end
    err(iter) = max(abs(T(:)-Tlast(:)));  %Find difference between last
                                           two solutions
    if err(iter)<1E-4
```

```
        break; % Stop if solutions very similar, we have convergence
    end
end
if iter==maxiter;
    warning('Convergence not reached')
end

stepslag=(4*60*60./dt)-1;
j=1;
for ii=1:stepslag:size(Tlast,2)
    Tfinal(:,j)=Tlast(:,ii);
    j=j+1;
end
E=exp(9.37196-0.03608145*(Tlast));  %calculates elastic modulus of
                                     asphalt-concrete layer using
                                     Ali and Lopez model (1996)

figure(1)
depth = [0:dz:Nz*dz];
time = [0:5/Nt:5];
contourf(time,-depth,T); title('Temperature variations (station B)')
xlabel('Time (days)'); ylabel('Depth (m)');
colorbar
%ylim([-.2 0])
axis([0  1  -.1  0])
%xlim([0 1])

figure(2)
depth = [0:dz:Nz*dz];
time = [0:5/Nt:5];
contourf(time,-depth,E); title('Elastic modulus variations (station B)')
xlabel('Time (days)'); ylabel('Depth (m)');
colorbar
%ylim([-.2 0])
axis([0  1  -.1  0])
```

```
%-------------------------------------------------------------------------
% Matlab program for Time-Domain Analysis (TDA) on an FWD and LWD
% simulated  data. It calculates M,C and K of a SDOF oscillator
% equivalent to  a pavement-subgrade structure.

%-------------------------------------------------------------------------


clear

%-------------------------------------------
%  input data for loads and timesteps
%-------------------------------------------

fid = fopen('test1.gg1','r');
[a] = fscanf(fid,'%g %g %g',[3 inf]);
a = a';
time(:,1) = a(:,1);
x(:,1) = a(:,2)*0.001;
p(:,1) = -40000*a(:,3); % load vector for FWD data
% p(:,1) = -7800*a(:,3);  % load vector for LWD data
n = size(a,1);
a = [];
fclose(fid);

dt=0.0002;
k =0;
for j=3:n-2
    k=k+1;
    B(k,3)=x(j);
    B(k,2)=(-x(j+2)+8*x(j+1)-8*x(j-1)+x(j-2))/(12*dt);
    B(k,1)=(-x(j+2)+16*x(j+1)-30*x(j)+16*x(j-1)-x(j-2))/(12*dt^2);
    f(k)=p(j);
end

C=B'*B;
D=B'*f';
A = C\D;
M=A(1)
C=A(2)
K=A(3)

save OUTPUT M C K -ascii
```

```
%-------------------------------------------------------------------------
% Matlab program to perform Frequency Domain Analysis (FDA) on FWD and
% LWD synthetic simulated data. It finds and plots the real and
% imaginary components of the dynamic impedance of the system and
% calculates M,C and K of a SDOF % oscillator equivalent to a pavement-
% subgrade structure.
%-------------------------------------------------------------------------

clear

%-------------------------------------------------
%  input data for time steps,loads and deflections
%-------------------------------------------------

fid = fopen('1.gg1','r');
[a] = fscanf(fid,'%g %g %g',[3 inf]);
a = a';
def(:,1) = a(:,2)*0.001;
load(:,1) = -40000*a(:,3); % load vector for FWD data
% load(:,1) = -7800*a(:,3);  % load vector for LWD data
n = size(a,1);
a = [];
fclose(fid);

p=load(:,1);
u=def(:,1);
dt=0.0002;
t2=(n-1)*dt;
t=0:dt:t2;
for m=n+1:1024
    p(m)=0;
    u(m)=0;
end
freq=(0:511)'/(0.0002*1024);
w1=2*pi*freq;
w2=w1.*w1;
P=fft(p,1024);
U=fft(u,1024);
DynImp=P./U;
R=real(DynImp);
I=imag(DynImp);

figure
plot(w2(1:7),R(1:7))
grid on
title('Real Component of Dynamic Impedance vs. w^2')
xlabel('w^2')
ylabel('Real')

figure
plot(w1(1:7),I(1:7))
```

```
grid on
title('Imaginary Component of Dynamic Impedance vs. w')
xlabel('w')
ylabel('Imaginary')

M=-(R(7)-R(1))/(w2(7)-w2(1));
C=(I(7)-I(1))/(w1(7)-w1(1));
K=R(1);

save 1FDA.dat M C K -ascii
save I1.dat I -ascii
save R1.dat R -ascii
save w1.dat w1 -ascii
```

```
%-------------------------------------------------------------------------
% Matlab program for finding plotting coefficients for LWD and FWD test
% data. It calculates m, n, p and α coefficients for condensation of
% Pi groups
% π1 = α·(π2)^m·(π3)^n·(π4)^p
%-------------------------------------------------------------------------

clear

%-----------------------------------------------------------------------
% input data for log10(π1)-x, log10(π2)-z, log10(π3)-y, log10(π4)-t
%-----------------------------------------------------------------------

fid = fopen('Im.txt','r');
[a] = fscanf(fid,'%g %g %g %g',[4 inf]);
a = a';
x(:,1) = a(:,1);
z(:,1) = a(:,2);
y(:,1) = a(:,3);
t(:,1) = a(:,4);
n = size(a,1);
a = [];
fclose(fid);

k =0;
for j=1:n
    k=k+1;
    B(k,4)=t(j);
    B(k,3)=y(j);
    B(k,2)=z(j);
    B(k,1)=1;
    f(k)=x(j);
end

C=B'*B;
D=B'*f';
A = C\D;
g=A(1)
m=A(2)
n=A(3)
p=A(4)
alfa=10^g
```

APPENDIX C

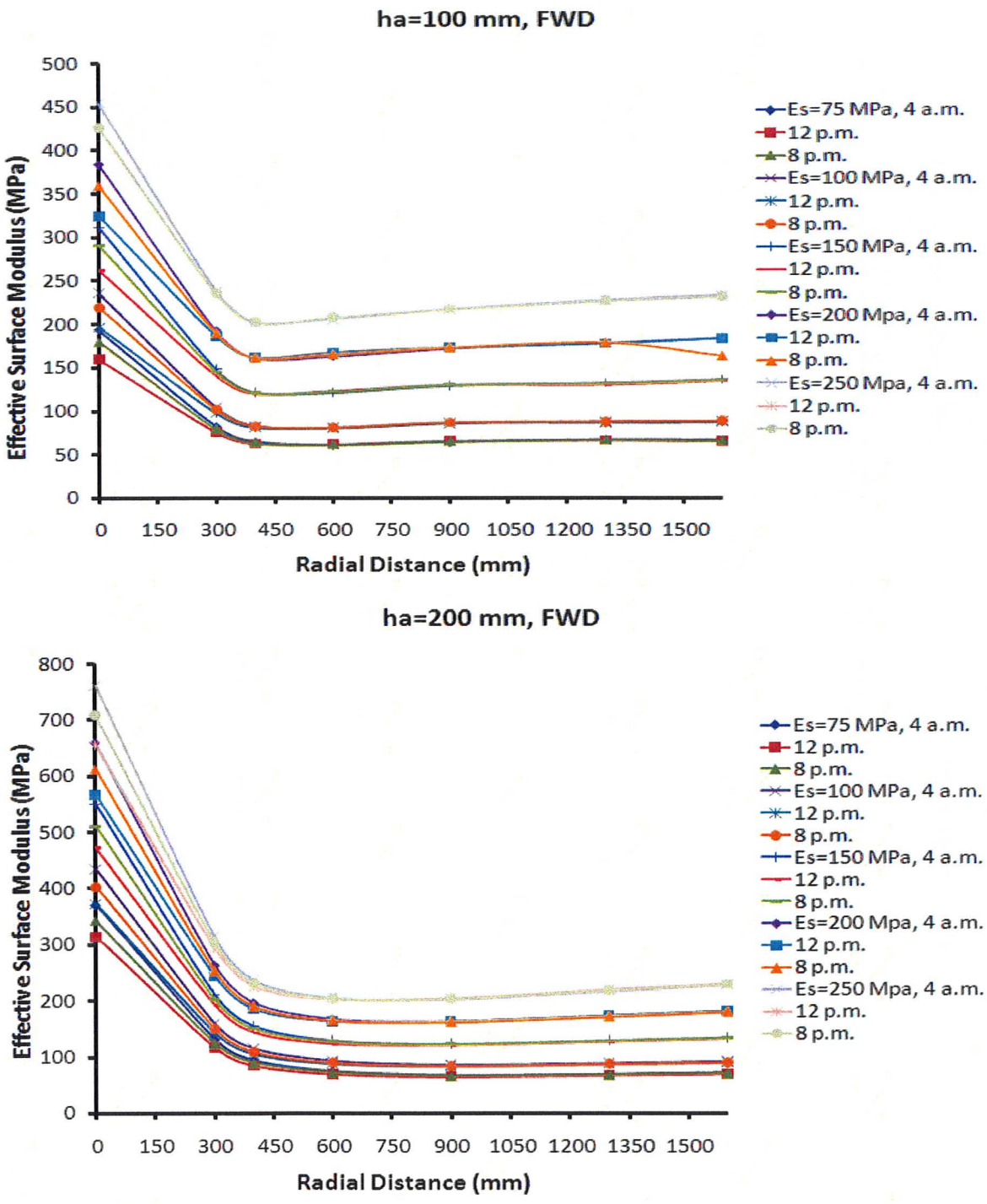

Figure C.1- Influence of subgrade modulus and temperature on effective surface modulus measured by FWD

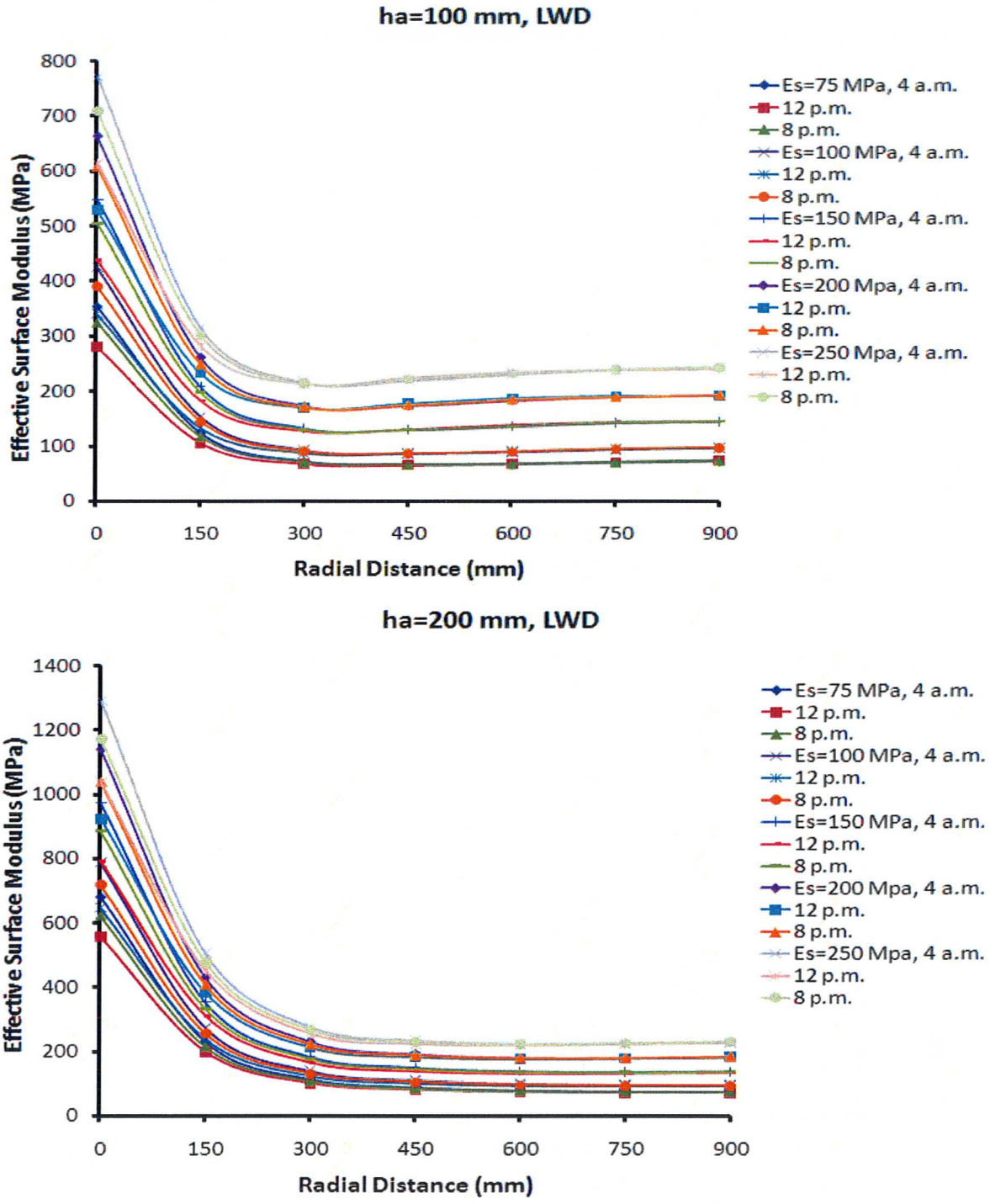

Figure C.2- Influence of subgrade modulus and temperature on effective surface modulus measured by LWD

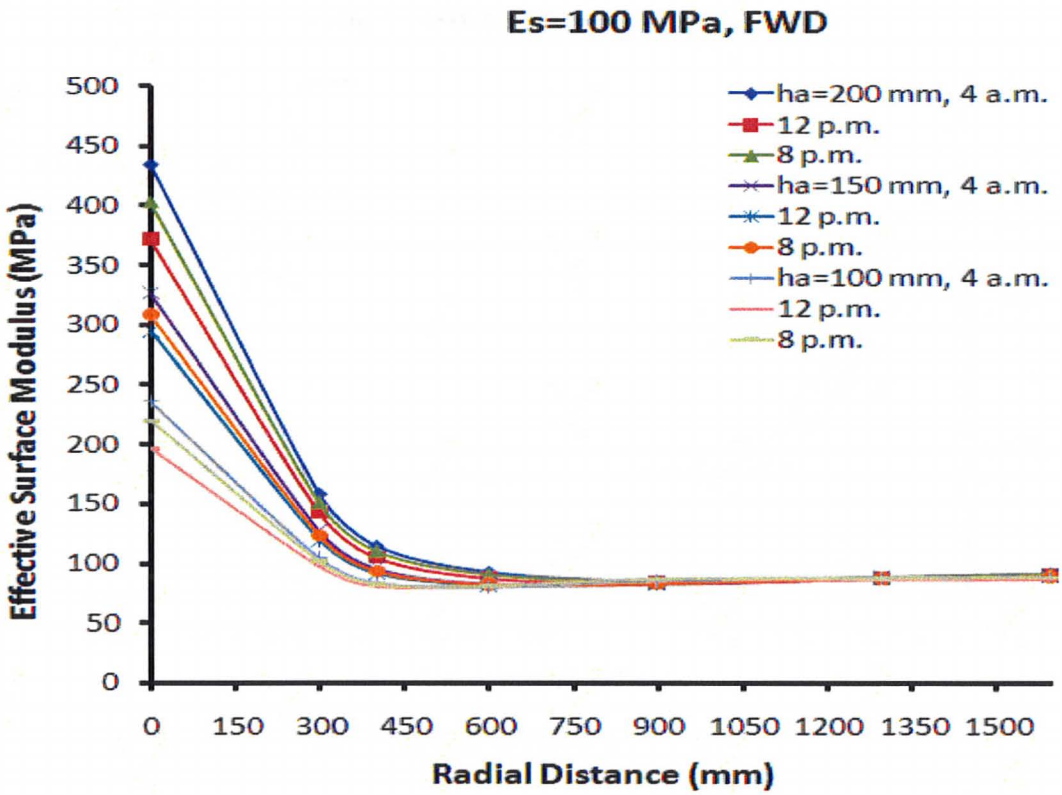
Es=100 MPa, FWD
Effective Surface Modulus (MPa)
Radial Distance (mm)
ha=200 mm, 4 a.m.
12 p.m.
8 p.m.
ha=150 mm, 4 a.m.
12 p.m.
8 p.m.
ha=100 mm, 4 a.m.
12 p.m.
8 p.m.
0
50
100
150
200
250
300
350
400
450
500
0
150
300
450
600
750
900
1050
1200
1350
1500

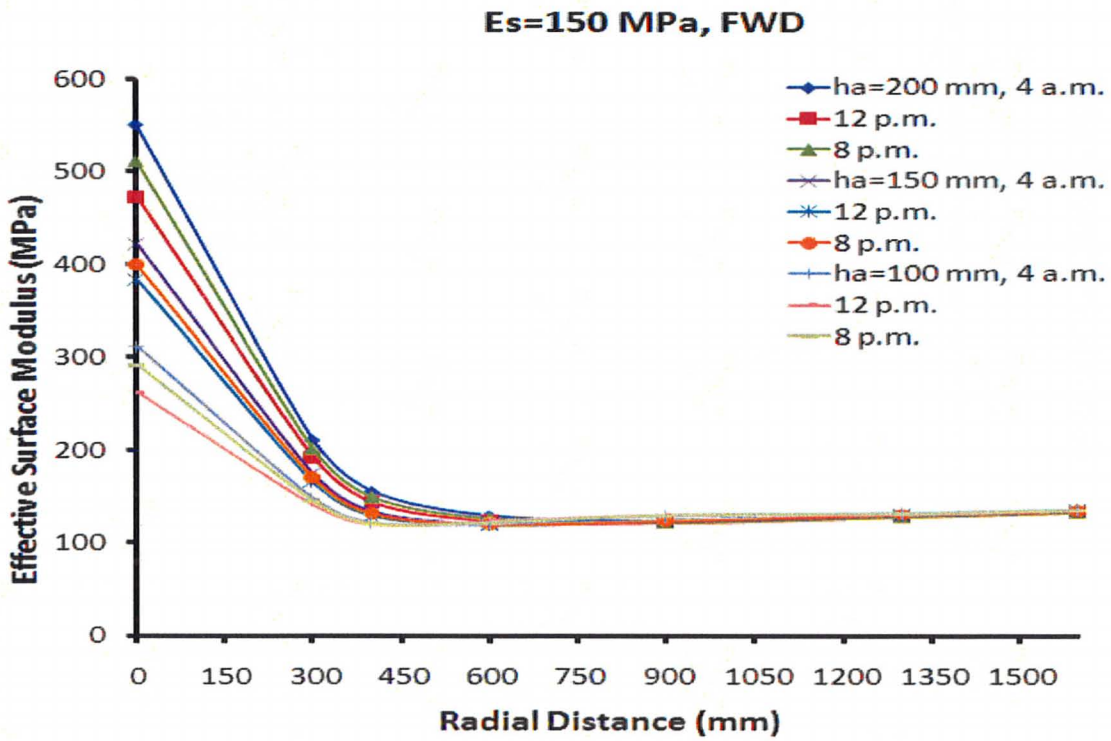
Es=150 MPa, FWD
Effective Surface Modulus (MPa)
Radial Distance (mm)
ha=200 mm, 4 a.m.
12 p.m.
8 p.m.
ha=150 mm, 4 a.m.
12 p.m.
8 p.m.
ha=100 mm, 4 a.m.
12 p.m.
8 p.m.
0
100
200
300
400
500
600
0
150
300
450
600
750
900
1050
1200
1350
1500

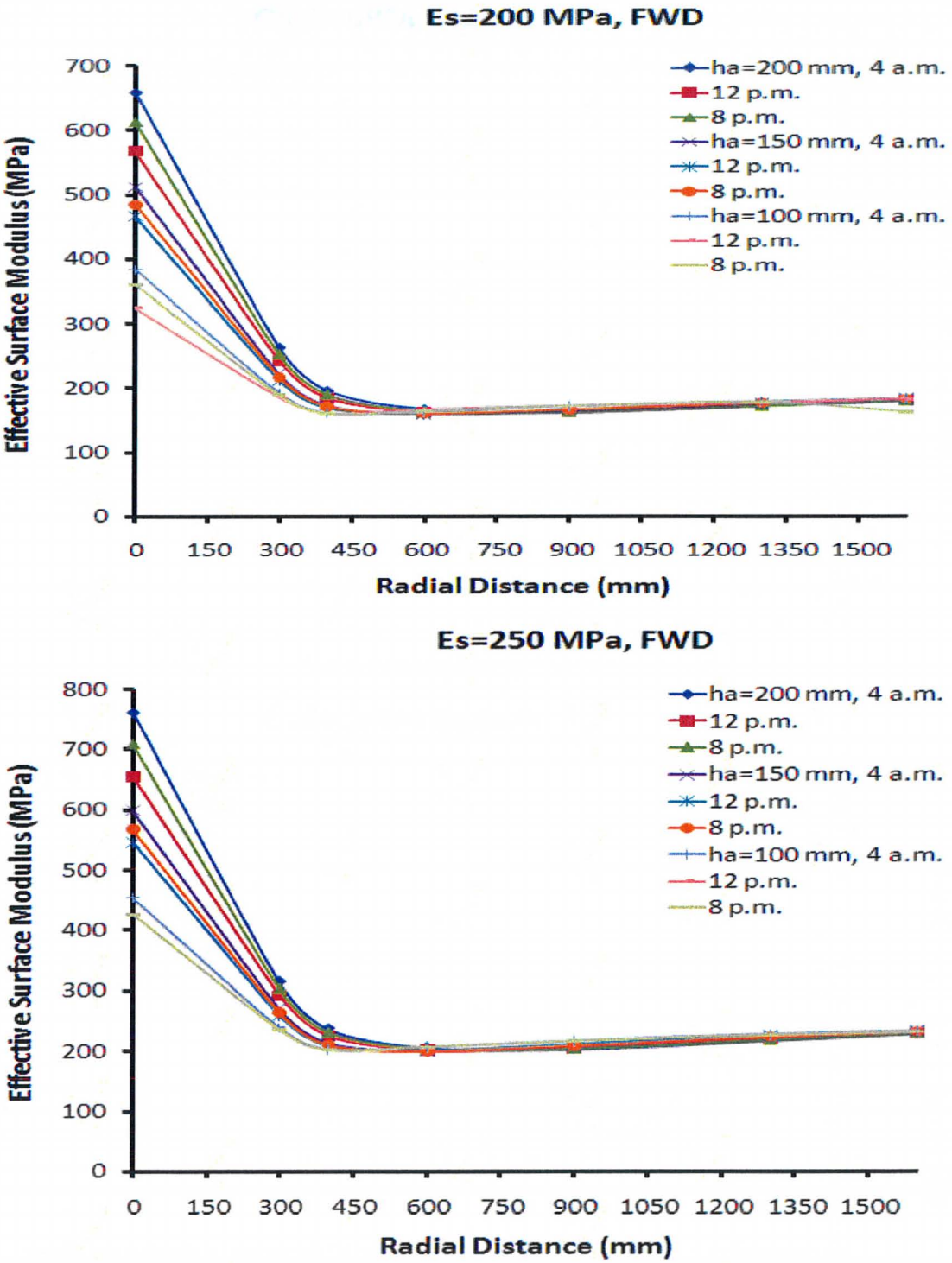

Figure C.3- Influence of pavement thickness and temperature on effective surface modulus for FWD

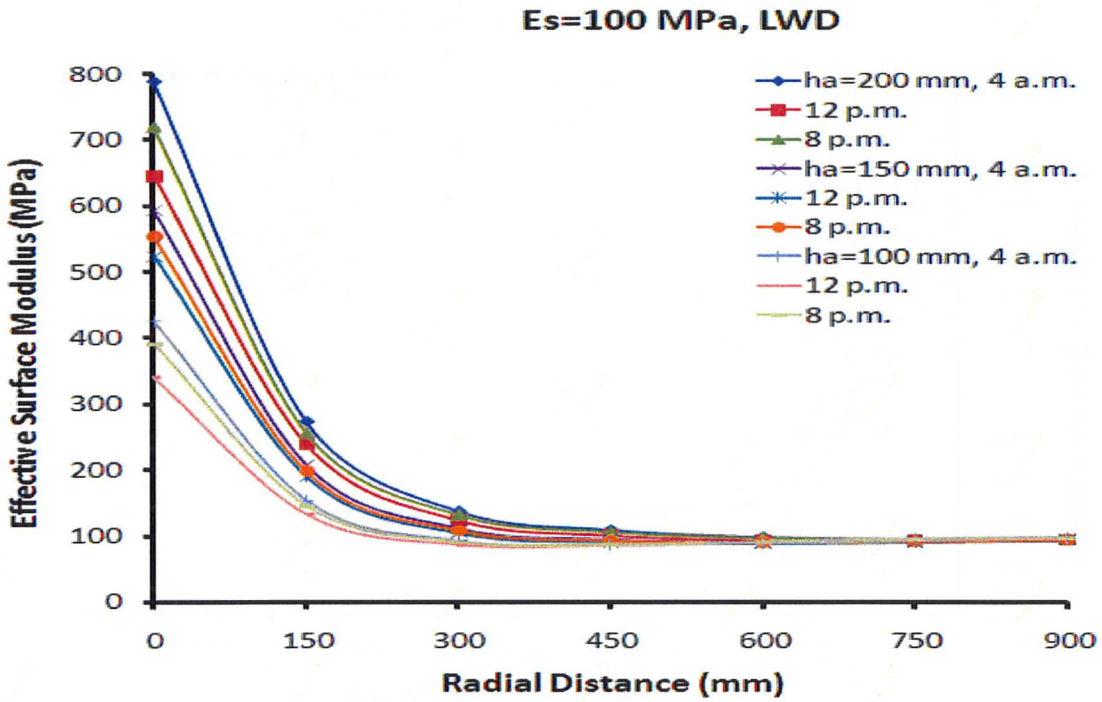
Es=100 MPa, LWD
Effective Surface Modulus (MPa)
800
700
600
500
400
300
200
100
0
0
150
300
450
600
750
900
Radial Distance (mm)
ha=200 mm, 4 a.m.
12 p.m.
8 p.m.
ha=150 mm, 4 a.m.
12 p.m.
8 p.m.
ha=100 mm, 4 a.m.
12 p.m.
8 p.m.

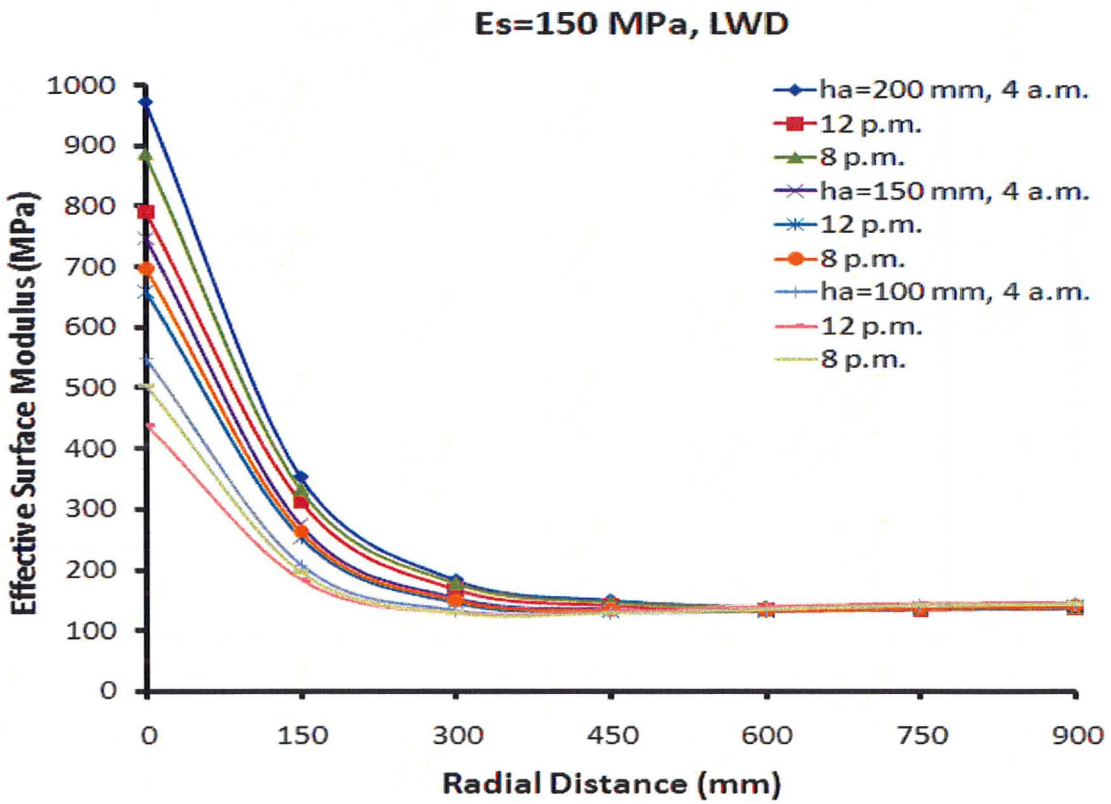
Es=150 MPa, LWD
Effective Surface Modulus (MPa)
1000
900
800
700
600
500
400
300
200
100
0
0
150
300
450
600
750
900
Radial Distance (mm)
ha=200 mm, 4 a.m.
12 p.m.
8 p.m.
ha=150 mm, 4 a.m.
12 p.m.
8 p.m.
ha=100 mm, 4 a.m.
12 p.m.
8 p.m.

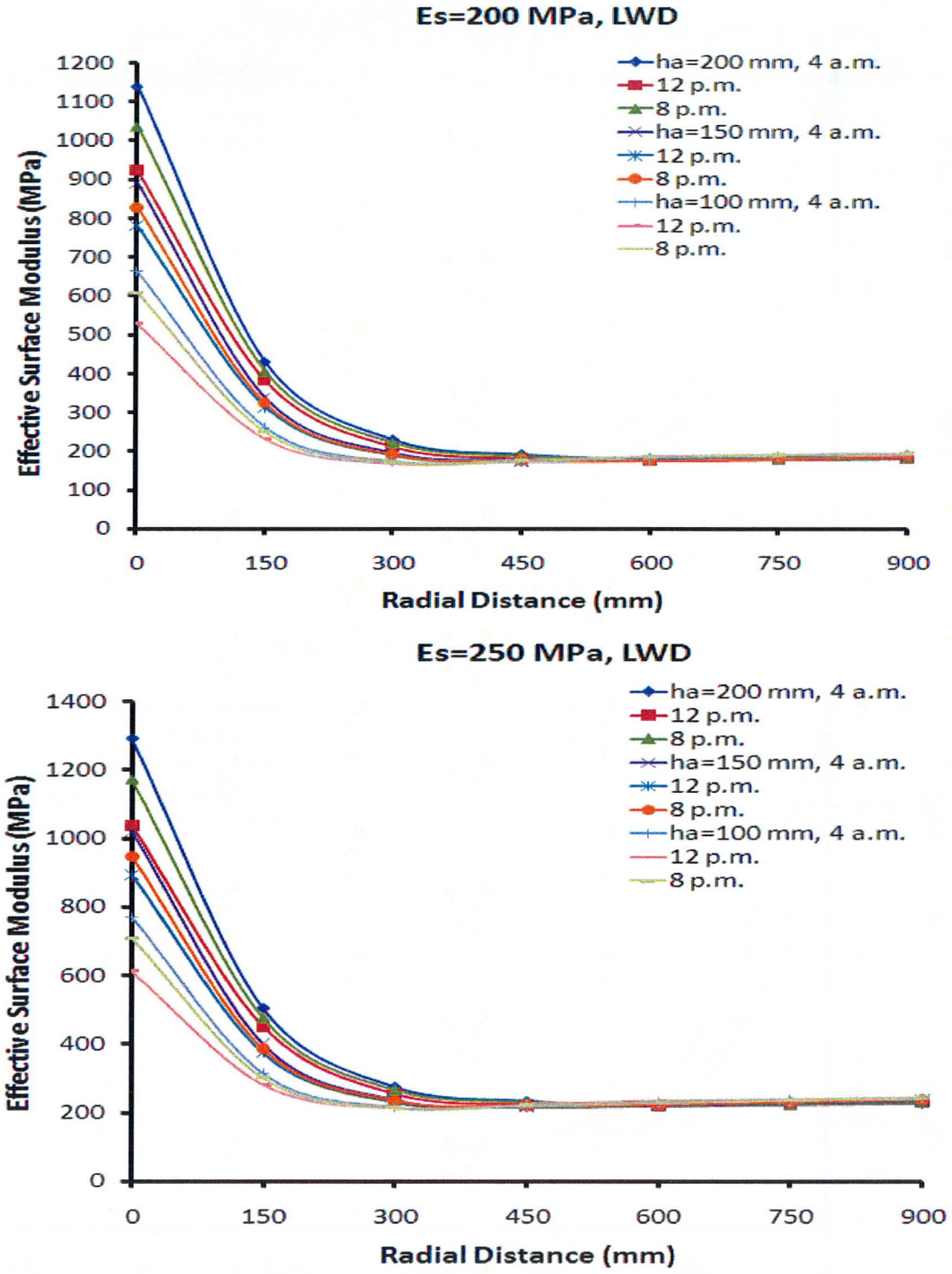

Figure C.4- Influence of pavement thickness and temperature on effective surface modulus for LWD

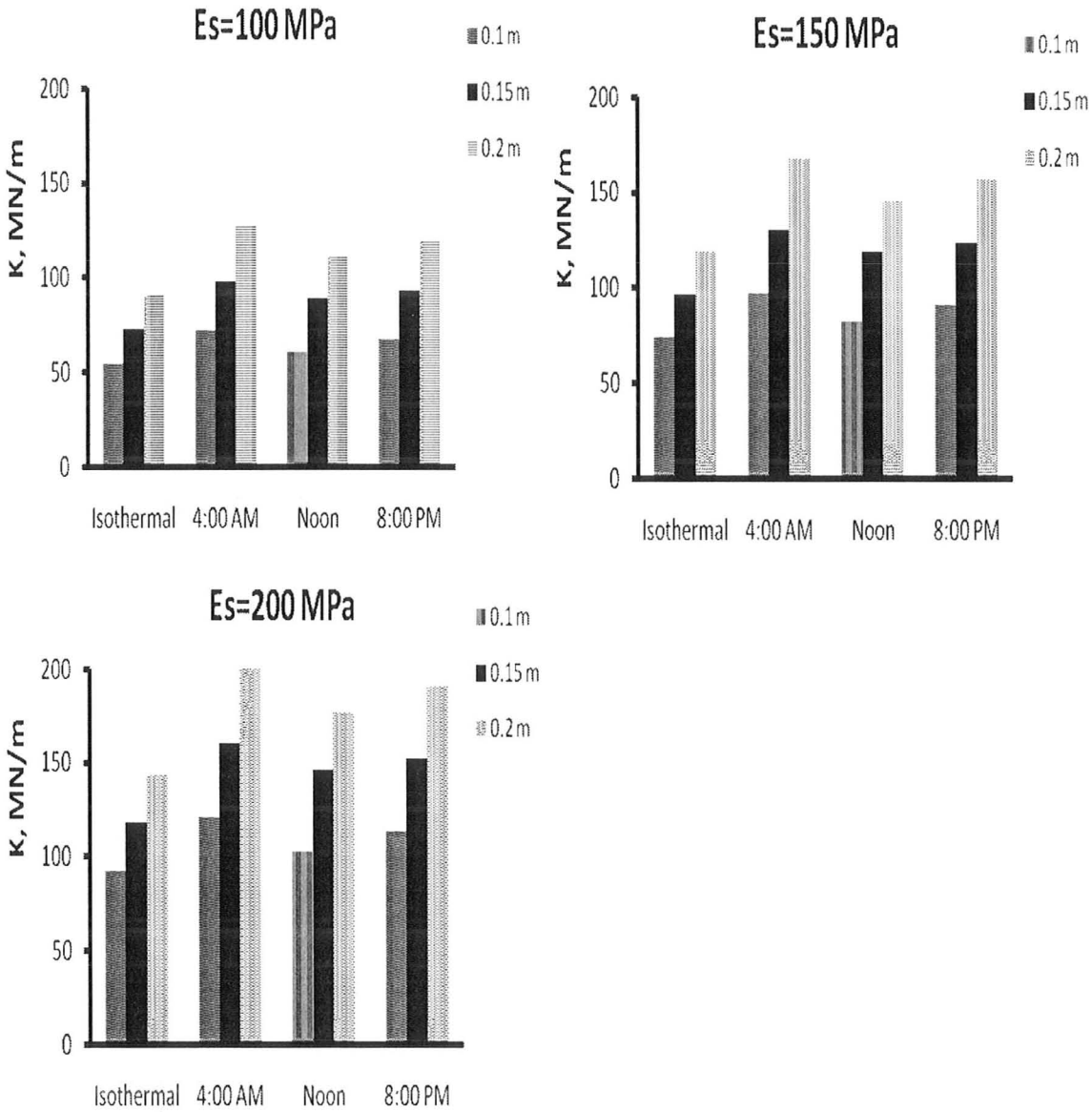

Figure C.5- Stiffness Coefficients for FWD corresponding to E_s = 100;150;200 MPa.

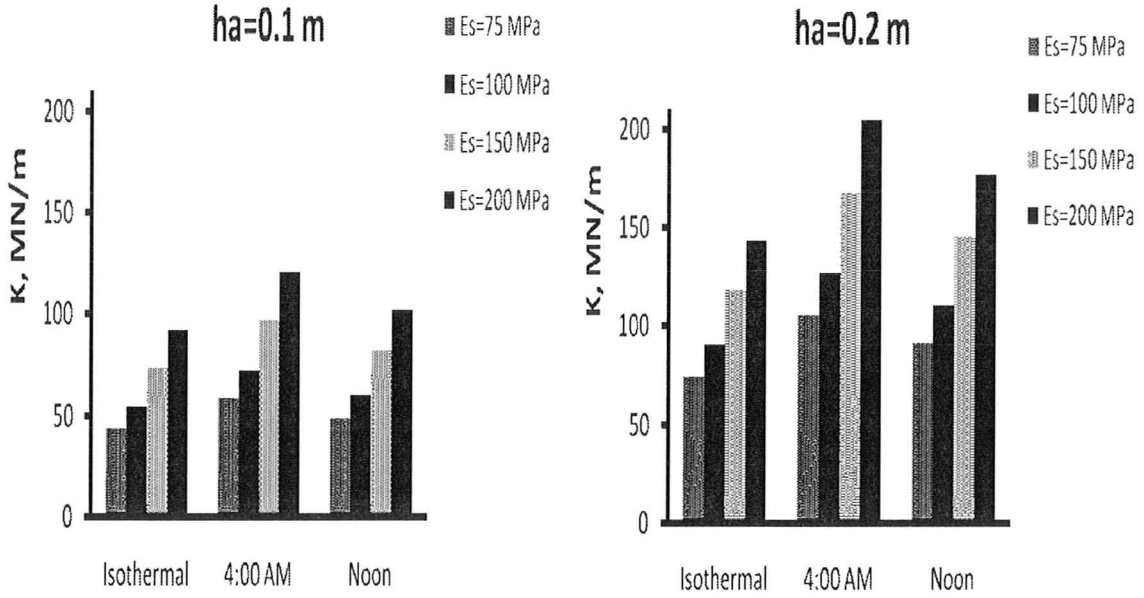

Figure C.6- Stiffness Coefficients for FWD corresponding to h_a= 0.1; 0.2 m.

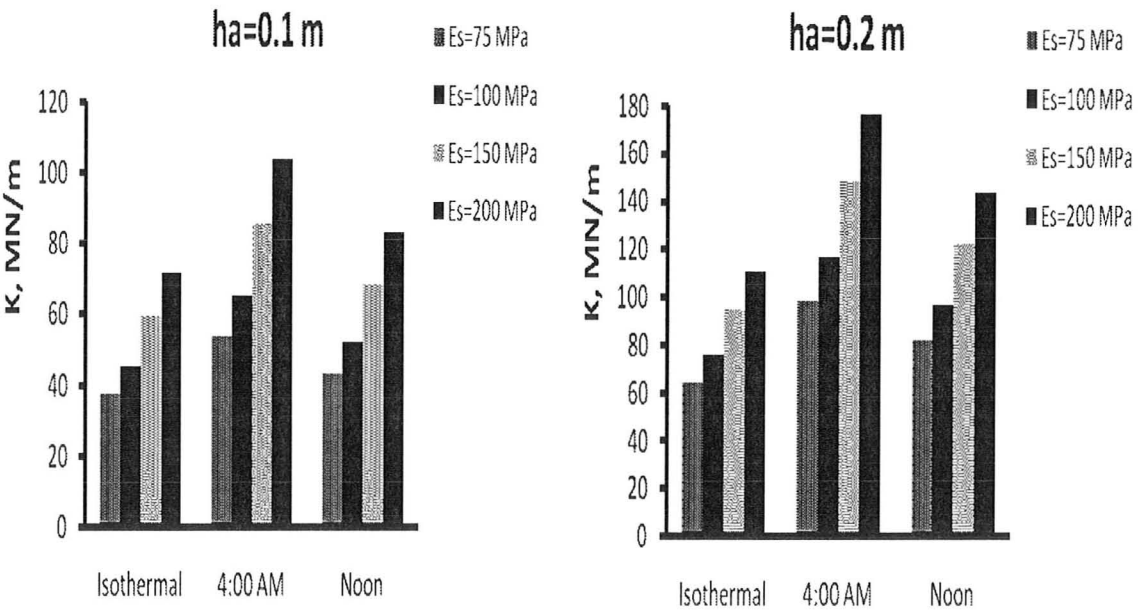

Figure C.7- Stiffness Coefficients for LWD corresponding to h_a=0.1; 0.2 m.

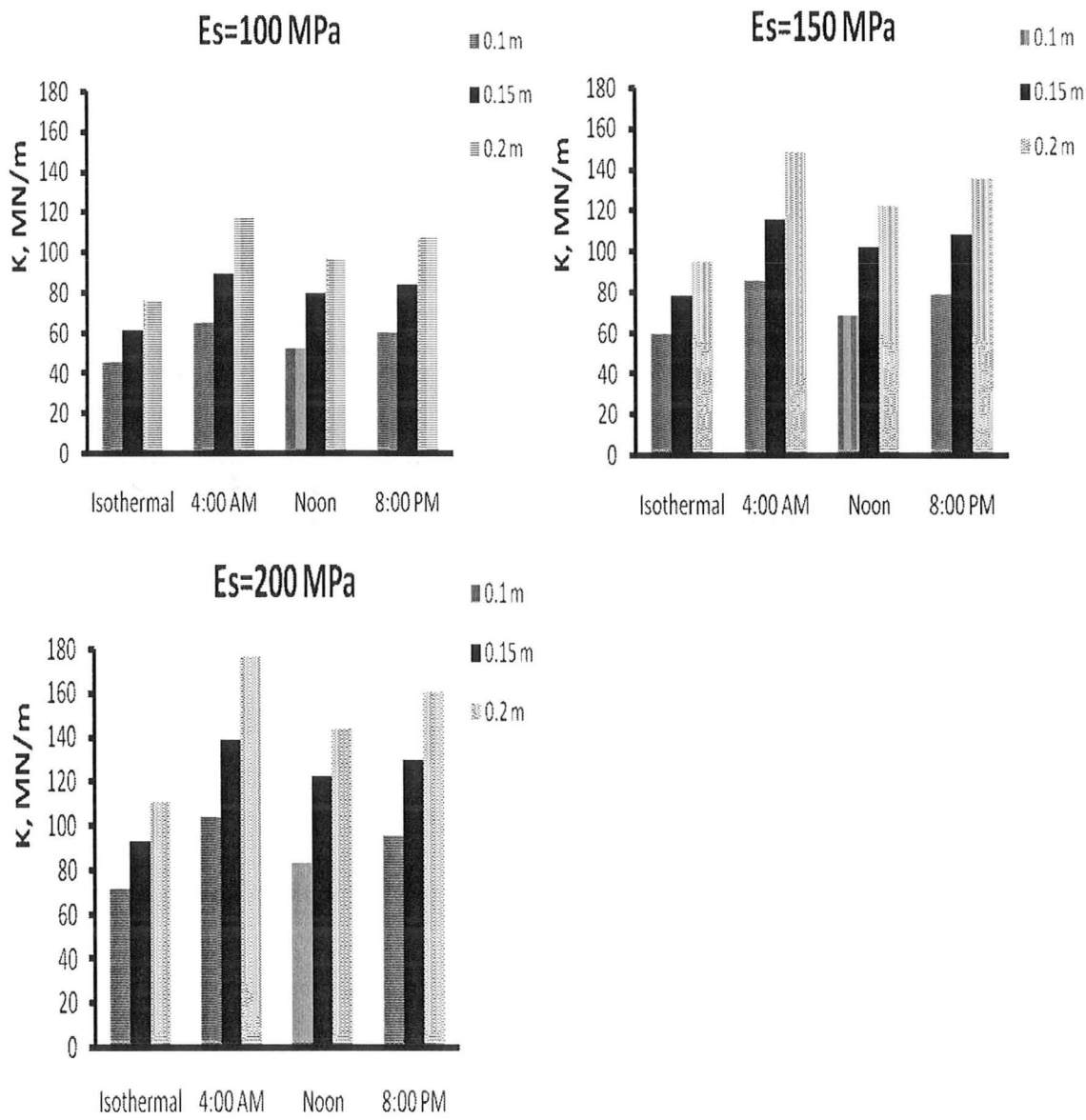

Figure C.8- Stiffness Coefficients for LWD corresponding to E_s = 100;150;200 MPa.

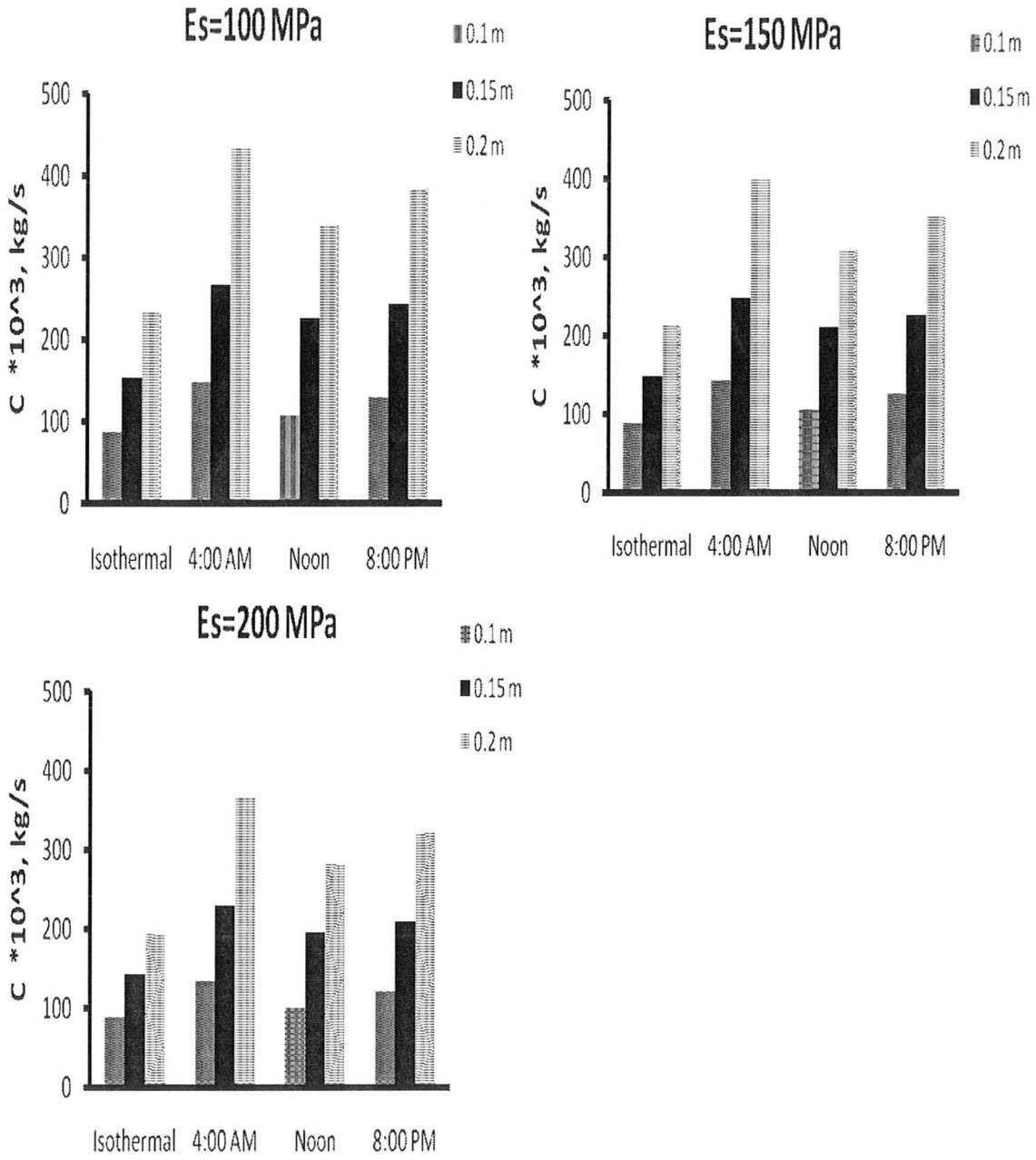

Figure C.9- Damping Coefficients for FWD corresponding to E_s = 100;150;200 MPa.

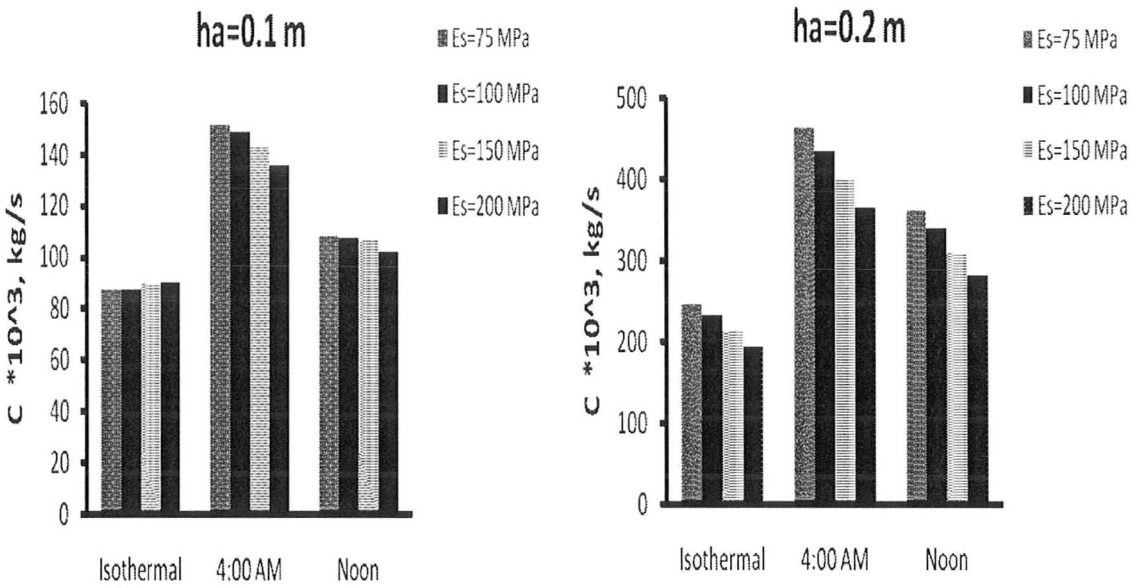

Figure C.10- Damping Coefficients for FWD corresponding to $ha = 0.1$; 0.2 m.

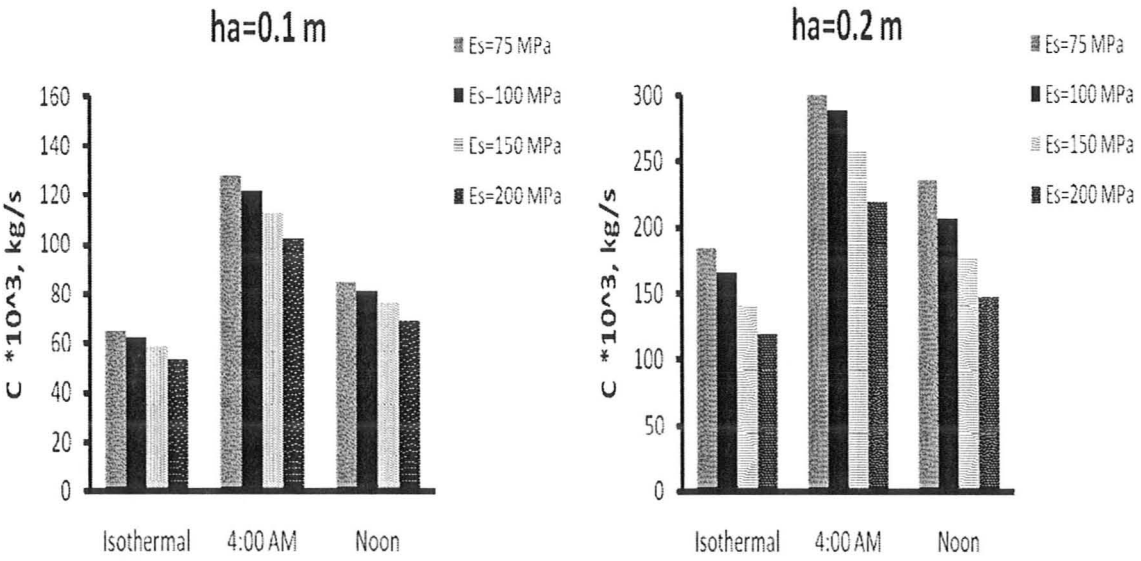

Figure C.11- Damping Coefficients for LWD corresponding to $h_a = 0.1$; 0.2 m

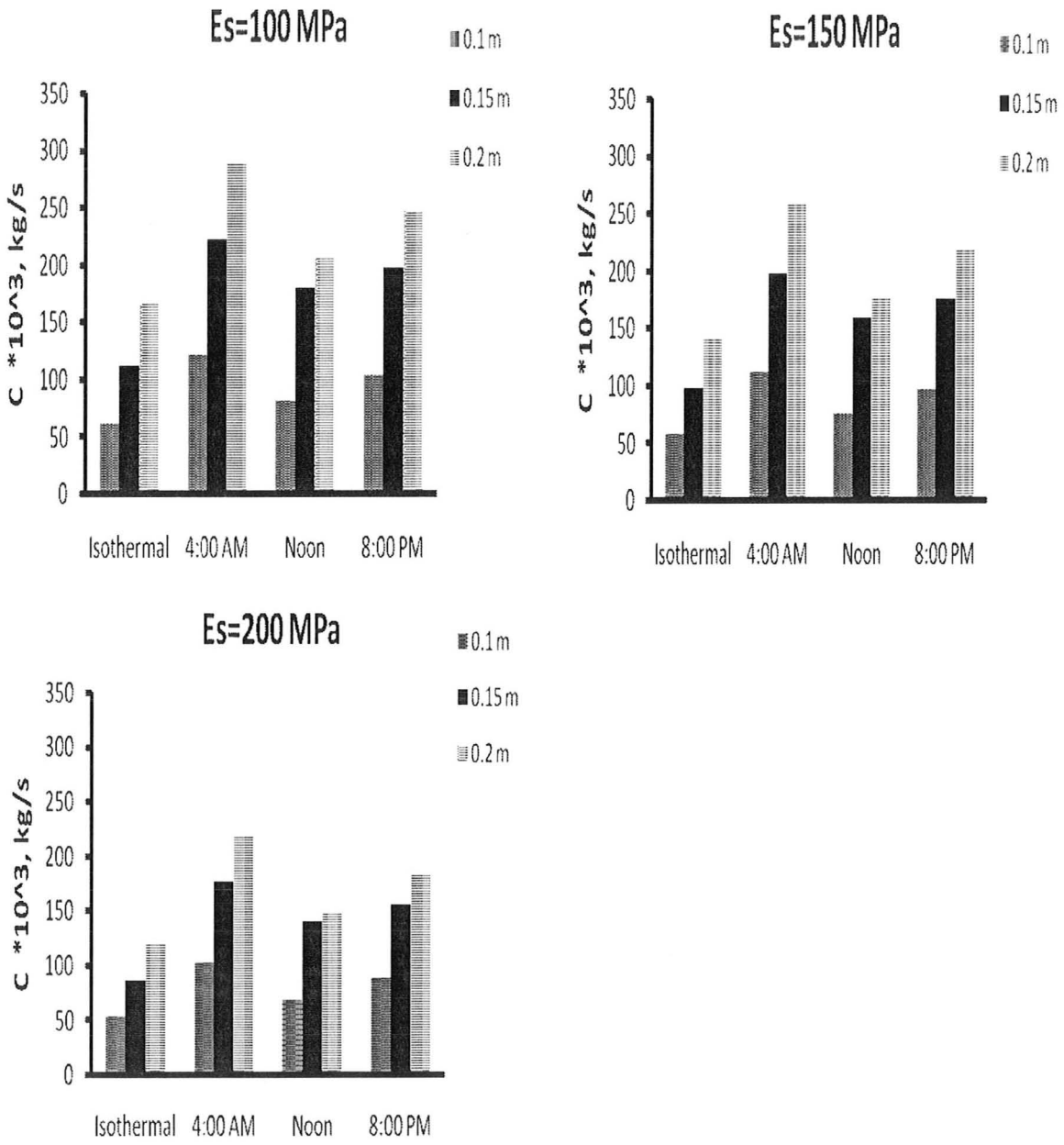

Figure C.12- Damping Coefficients for LWD corresponding to E_s = 100;150;200 MPa.

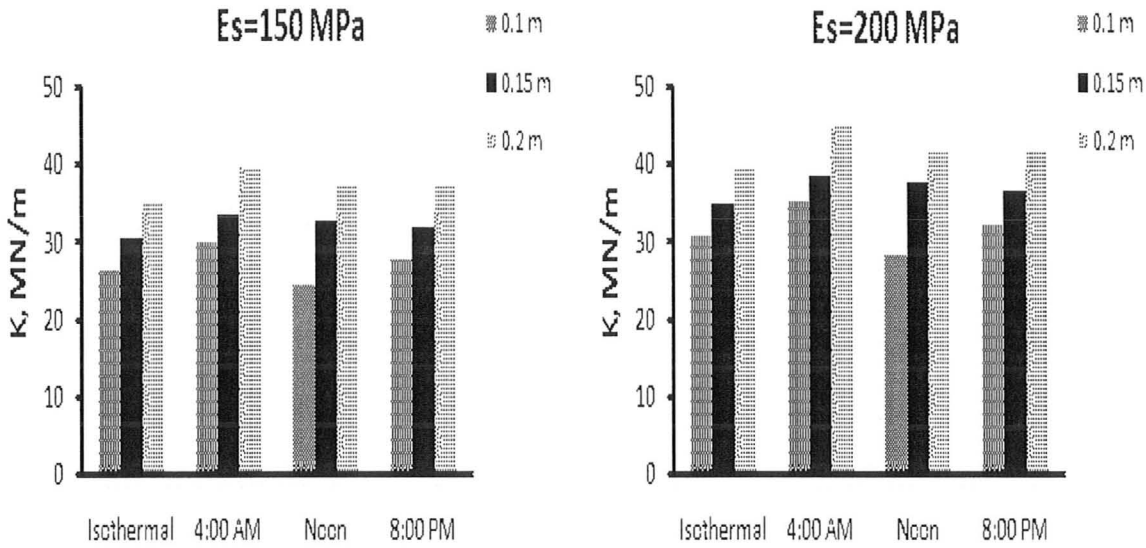

Figure C.13- Stiffness Coefficients for IE corresponding to E_s = 150;200 MPa.

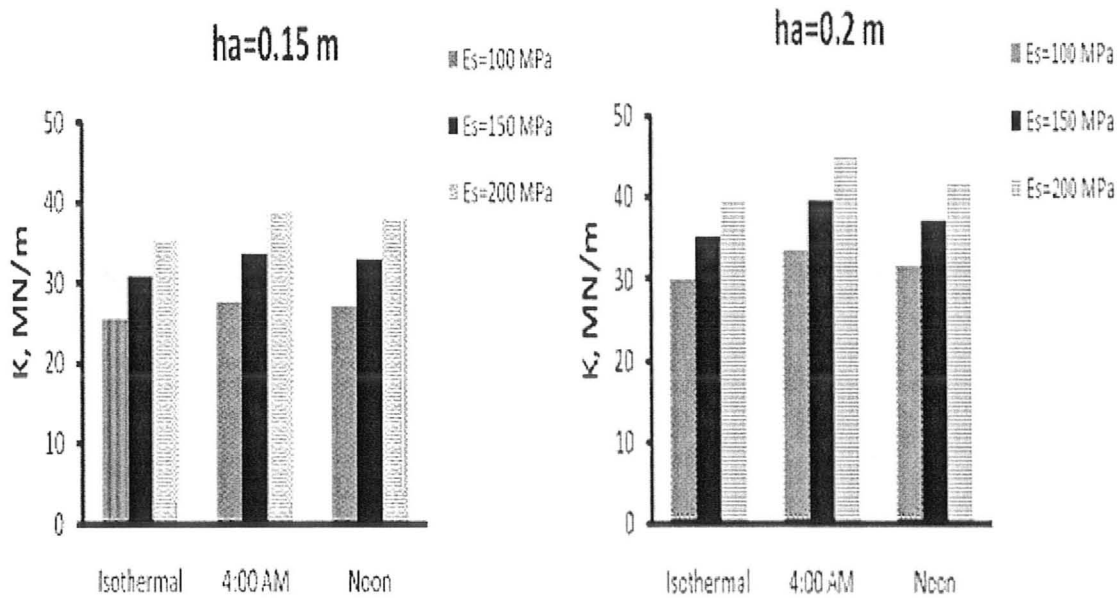

Figure C.14- Stiffness Coefficients for IE corresponding to h_a = 0.15; 0.20 m.

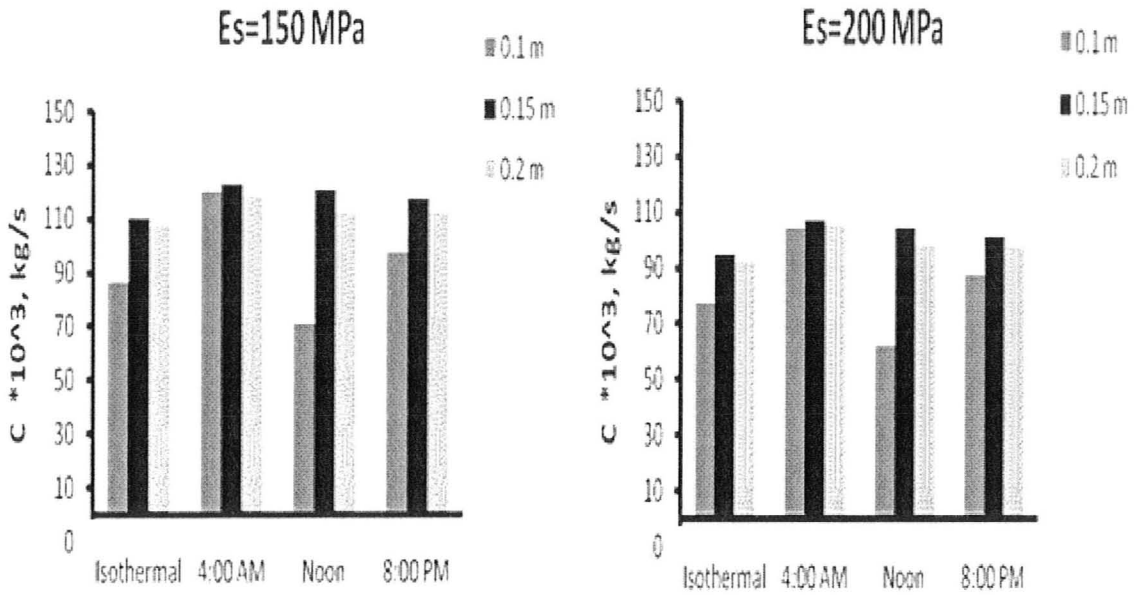

Figure C.15- Damping Coefficients for IE corresponding to E_s = 150;200 MPa.

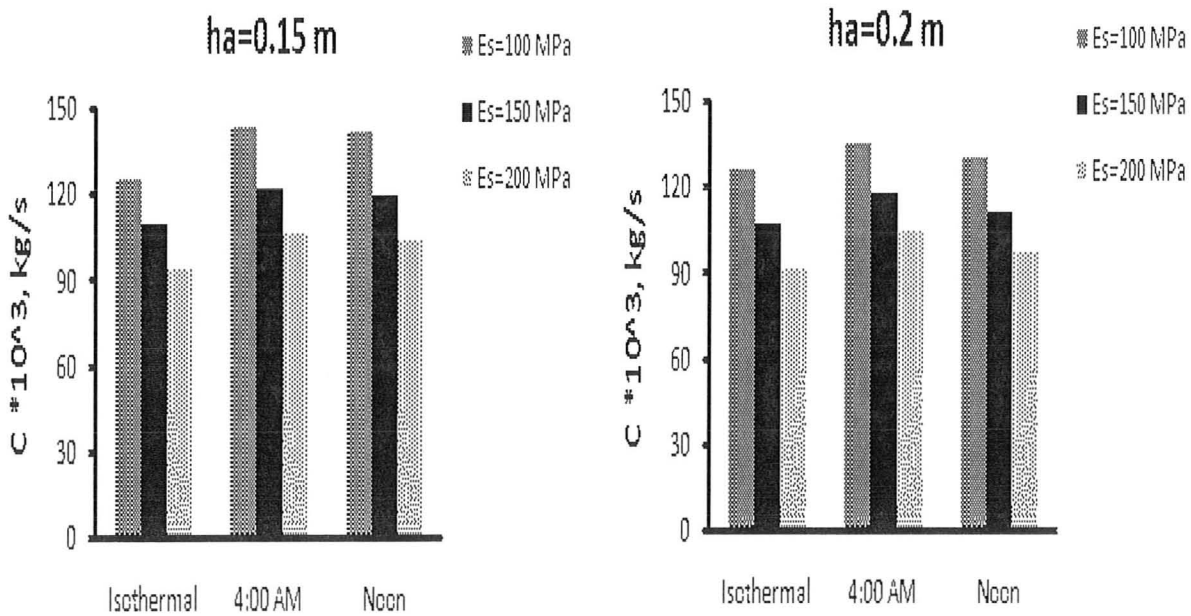

Figure C.16- Damping Coefficients for IE corresponding to h_a = 0.15;0.20 m.

REFERENCES

Abraham O., Léonard C., Côte P., Piwakowski B. *Time Frequency Analysis of Impact-Echo Signals: Numerical Modeling and Experimental Validation.* ACI Materials Journal, V.97, No. 6, pp.645-657, November-December, 200.

Abu-Halimeh I. *Surface Colour Effects on the Thermal Behaviour and Mechanical Properties of Hot Mix Asphalt.* M.A.Sc. thesis. McMaster University, April, 2007.

Ali H. and Lopez A. *Statistical Analysis of Temperature and Moisture Effects on Pavement Structural Properties Based on Seasonal Monitoring Data.* Transportation Research Records 1540, pp. 48-55, Transportation Research Council: Washington, DC, 1996.

Ali H.A. and Parker N.A. *Using Time Series to Incorporate Seasonal Variations in Pavement Design.* Transportation Research Records 1539, pp. 33-43, Transportation Research Council: Washington, DC, 1996.

Alkasawneh W., Pan E., Han F., Zhu R. and Green R. *Effect of Temperature Variation on Pavement Responses Using 3D Multilayered Elastic Analysis.* International Journal of Pavement Engineering, Vol. 8, No.3, September 2007, pp. 203-212, 2007.

Anderson P.D. *Non-Destructive Dynamic Deflection Testing and Pavement Layer Analysis - A Cost Effective Approach to Pavement Rehabilitation.* Proceedings of the 32-nd annual conference of CTAA, Montreal, Canada, pp.74-91, 1987.

Barber, E.S. *Calculation of Maximum Pavement Temperatures From Weather Reports.* Highway Research Board Bulletin, 168: pp. 1-8. 1957

Båth M. and Berkhout A.J. *Handbook of Geophysical Exploration, Vol. 17: Mathematical aspects of seismology.* Geophysical Press, pp. 329-365. 1984

Bayo E.P., Wilson E.L. *Use of Ritz Vectors in Wave Propagation and Foundation Response*. Earthquake Engineering and structural Dynamics, Vol. 12, pp. 499-505, 1984.

Bayomy F., and Salem H., *Monitoring and Modeling Subgrade Soil Moisture for Pavement Design and Rehabilitation in Idaho. Phase III: Data Collection and Analysis National Institute for Advanced Transportation Technology*, Prepared for Smith R. (Idaho Transportation Department). NIATT Project No. KLK 459, ITD Project No. SPR-0010(27) 124. University of Idaho. FINAL REPORT, July 2004. Revised and re-submitted May, 2005.

Berg, R. L. *Energy Balance on a Paved Surface.* Technical Report Number 26, sub-Project 42. US Army Cold Regions Research and Engineering Laboratory. Hanover, N.H. 03755. 1974.

Bosscher, P. J., Bahia H. U., Thomas S., Russell J. S. *Relationship between Pavement temperature and Weather Data.* Transportation Research Record. 1609. 1998.

British Geological Survey. Georeports. *Ground Source Heat Pump (Basic)* pp.1-18, February 2007.

Buckingham E.. *On physically similar systems; illustrations of the use of dimensional equations.* Phys.Rev., 4: pp. 345-76, 1914.

Burmister D.M. *The Theory of Stresses and Displacements in Layered Systems and Applications to the Design of Airport Runways*. Highway Research Record, Vol. 23, Highway Research Board, Washington, D.C., 1943.

Buttlar W.G., Paulino G.H. and Song S.H. *Application of Graded Finite Elements for Asphalt Pavements*. Journal of Engineering Mechanics. ASCE, pp. 240-249, March, 2006.

Cam E., Orhan S.and Luy M. *An analysis of cracked beam structure using impact echo method.* NDT&E International Vol. 38, pp. 368–373, 2005.

Carino N.J. *The Impact-Echo Method: An Overview*. Reprinted from the Proceedings of the 2001 Structures Congress&Exposition, May 21-23, 2001, Washington, DC., American Society of Civil Engineers, Reston, Virginia, Peter C. Chang, Editor, 18p., 2001.

Celaya M. and Nazarian S. *Seismic Testing to Determine Quality of Hot-Mix Asphalt.* Transportation Research Record: Journal of the Transportation Research Board, No. 1946, Transportation Research Board of the National Academies, Washington, DC, pp.113-122, 2006.

Celaya M. and Nazarian S. *Stripping Detection in Asphalt Pavements with Seismic Methods*. Transportation Research record: Journal of the Transportation Research Board, No. 2005, pp. 64-74, 2007.

Chang D.-W., Kang Y.V., Roesset J.M. and Stokoe II K.H. *Effect of Depth to Bedrock on Deflection Basins Obtained with Dynaflect and FWD Tests.* Transportation Research Record No. 1355, pp. 8-16, 1992.

Chapra S.C., Canale R.P. *Numerical Methods for Engineers*. McGraw-Hill, NY, 1988.

Chatti K., Haider S.W., Lee H.S., Ji Y., and Salama H. *Evaluation of Non-linear and Dynamic Effects on Asphalt Pavement Response under FWD Loading.* International Journal of Pavement, 2 (1-2), pp.88-99, 2003.

Chatti K., Ji Y. and Harichandran R. *Dynamic Time Domain Backcalculation of Layer Moduli, Damping, and Thickness in Flexible Pavements.* Transportation Research Record, No.1869, pp.106-116, 2004.

Chen D.-H., Bilyeu J., Lin H.-H. and Murphy M. *Temperature Correction on Falling Weight Deflectometer Measurements*. Transportation Research Record No. 1716, pp. 30-39, 2000.

Cheng C., Sansalone M. *The impact-echo response of concrete plates containing delaminations: numerical, experimental and field studies*. Materials and Structures, V. 26, pp. 274-285, 1993.

Cho M.R., Lee H.S., Kim H.H. and Kim K.B. *Finite Element Analysis of the Impact-Echo Testing at a Concrete Slab with Complex Boundary Conditions.* KSCE Journal of Civil Engineering, Vol. 9, No. 2, pp. 113-117. March, 2005.

Chou, Y.J. and Lytton R.L. *Accuracy and Consistency of Backcalculated Pavement Layer Moduli*. Transportation Research Board, Record 1293, National Research Council, Washington, DC, pp. 72-85, January, 1991.

Chowdhury I., Dasgupta S.P. *Computation of Rayleigh Damping Coefficients for Large Systems.* Petrofac International Limited, Sharjah, U.A.E., Indian Institute of Technology, Kharagpur, India.

Christison, J. T., Anderson K. O. *The Response of Asphalt Pavements to Low Temperature Climatic Environments.* Proceedings of the 3rd International Conference on the Structural Design of Asphalt Pavements. September 1972.

Clough R.W. and Penzien J. *Dynamics of Structures*. McGraw-Hill,NY,1975.

Dai S. and Van Deusen D. *Field Study of In Situ Subgrade Soil Response Under Flexible Pavements.* Transportation Research Record 1639: pp.23-35, 1998.

Davies T.G. and Mamlouk M.S. *Theoretical Response of Multilayer Pavement Systems to Dynamic Nondestructive Testing.* Transportation Research Record No. 1022, pp.1-7, 1985.

Deen, R.C., Southgate H.F. *Temperature Distributions in Asphaltic Concrete Pavements.*

Transportation Research Record, 549: pp. 39-46, 1975.

Dym C.L. and Shames I.H. *Solid Mechanics: A Variational Approach.* McGraw-Hill, Inc, 1973.

Emery J. *Full-Depth Asphalt Pavements.* Draft, for comments.

Fernando E.G. *Temperature Correction of Backcalculated AC Modulus.* Project Summary report 0-1863-S. Project 0-1863: Evaluate the Use of FWD Data in Determining Seasonal Variations in Pavement Structural Strength. Texas Transportation Institute, The Texas A&M University System, pp. 1-4, 2003.

Fleming P.R. *Field Measurement of Stiffness Modulus For Pavement Foundations.* Transportation Research Board 1755, Submitted to the 2001 Annual Meeting of the Transportation Research Board For Presentation and Publication. Washington, D.C, 2001.

Fleming P.R., Frost M.W., Lambert J.P. *Review of the Lightweight Deflectometer (LWD) for Routine In Situ Assessment of Pavement Material Stiffness*. Transportation Research Record: Journal of the Transportation Research Board, No. 2004, Transportation Research Board of the National Academies, Washington, D.C., pp. 80–87, 2007.

Germar F.J. *The Impact Echo Method: A Review*. Research report, University of the Philippines, March 2000.

Gibson A., Popovics J. Lamv *Wave Basis for Impact-Echo Method Analysis. Journal of Engineering Mechanics.* ASCE. pp. 438-443, April, 2005.

Goel A. and Das A. *Nondestructive Testing of Asphalt Pavements for Structural Condition Evaluations: a State of the Art*. Nondestructive Testing and Evaluation, Vol. 23, No. 2, pp. 121-140, June, 2008.

Goldsmith,W. *Impact: The Theory and Physical Behavior of Colliding Solids*, Edward Arnold Press, Ltd., pp. 24-50.1965.

Guidelines for Review and Evaluation of Backcalculation Results. Publication No. FHWA-HRT-05-152 Final Report. February 2006.

Guzina B.B. and Osburn R.H. *An Effective Tool for Enhancing the Static Backcalculation of Pavement Moduli.* Submitted to Committee A2B05 for possible presentation and publication at 81st Annual Meeting of Transportation Research Board, Washington, D.C., January 13-17, 2002.

Guzina B.B. and Osburn R.H. *Effective Tool for Enhancing Elastostatic Pavement Diagnosis.* Transportation Research Record No.1806, pp.30-37, 2002.

Haigh S.K., Ghosh B., Madabhusni S.P.G. *Importance of time step discretisation for nonlinear dynamic finite element analysis*. Canadian Geotechnical Journal, Vol. 42, pp. 957-963, 2005.

Herb W., Marasteanu M. and Stefan H.G. *Simulation and Characterization of Asphalt Pavement Temperatures*. Project Report No. 480, prepared for the Minnesota Department of Transportation (MNDOT), University of Minnesota, pp. 1-42, September, 2006.

Heukelom, W., and Foster, C.R. *Dynamic testing of pavements.* ASCE Journal of the Structural Division, Vol. 86(1): pp. 1-28, 1960.

Highter, W.H., Wall D.J., *Thermal Properties of Some Asphaltic Concrete Mixes.* Transportation Research Record, 968: pp. 38-45, 1984.

Hoffman O, Guzina B.B. and Drescher A.. *Enhancements and Verification Tests For Portable Deflectometers*, Final Report 2003-10. Minnesota Department of Transportation, St-Paul, MN, 2003.

Hoffman O, Guzina B.B. and Drescher A.. *Stiffness Estimates Using Portable Deflectometers.* Transportation Research Records No. 1869, pp. 59-66, Transportation Research Council: Washington, DC, 2004 .

Hogg A.H.A. *Equilibrium of a Thin Plate on an Elastic Foundation of Finite Depth.* Philosophical Magazine, Vol. 3(242), pp.265-276, 1944.

Horak E. *Benchmarking the structural condition of flexible pavements with deflection bowl parameters*. Journal of the South African Institution of Civil Engineering, Vol. 50, No.2, pp.2-9, Paper 652, 2008.

Horak E., Khumalo T. *Deflection bowl parameters correlation of a light and standard falling weight deflectometer*. Southern African Road Federation (SARF) combined international Conference with The International Road federation (IRF), September, Durban, South Africa, 2006.

Horak E., Emery S. *Falling Weight Deflectometer Bowl Parameters as analysis tool for pavement structural evaluations*. 22nd Australian Road research Board (ARRB) International Conference. October 2006, Brisbane, Australia, 2006.

Horak E. , Maina J., Guiamba D. , Hartman A.. *Correlation study with the Light Weight Deflectometer in South Africa*. Proceedings on the 27-th Southern African Transport Conference (SATC 2008). 7-11 July 2008, Pretoria, South Africa, 2008.

Huang, Y.H. *Pavement analysis and design*. Prentice Hall, Englewood Cliffs, N.J., 1993.

Inge, E.H., Jr., Kim. Y.R. *Prediction of Effective Asphalt Layer Temperature.* Transportation Research Record, 1473: pp. 93-100, 1995.

Irwin L.H. *Backcalculation: An Overview and Perspective.* Cornell University, Ithaca, NY, USA, pp. 1-22, 2002.

Janoo V. and Berg R. *Layer Moduli Determination During Freeze-thaw Periods*. Transportation Research Records 1377, pp. 26-35, Transportation Research Council: Washington, DC, 1991 .

Ji Y., Wang F., Luan M. and Guo Z. *A Simplified Method for Dynamic Response of Flexible Pavement and Applications in Time Domain Backcalculation.* The Journal of American Science, 2(2), pp. 70-81, 2006.

Joo K.-J., Wilson E.L. and Leger P. *Ritz Vectors and Generation Criteria for Mode Superposition Analysis.* Earthquake Engineering and structural Dynamics, Vol. 18, pp. 149-167, 1989.

Jose M. Roesset. *Nondestructive Dynamic Testing of Soils and Pavements*. Tamkang Journal of Science and Engineering, vol.1, No.2, pp. 61-81, 1998.

Jung F.W. and Phang W.A. *Elastic Layer Analysis Related to Performance in Flexible Pavement Design.* Report RR-191, Research and Development Division, Ministry of Transportation and Communication, Ontario, Canada, 1975.

Jung F.W. *Interpretation of Deflection Basin for Real-world Materials in Flexible Pavements.* The Research and Development Branch Ontario Ministry of Transportation, February, 1990.

Jung F.W. *Deflection Basin Testing, Interpretation and Overlay Design with the Falling Weight Deflectometer.* The Research and Development Branch Ontario Ministry of Transportation, March, 1993.

Kamiura M., Sekine E., Abe N. and Meruyama T. *Stiffness Evaluation of the Subgrade and Granular Aggregate Using the Portable FWD.* Proc., 5th International Conference on Unbound Aggregate in Roads, Nottingham, United Kingdom, 2000.

Kim D.-S. and Kim H.-W. *Non-Destructive Testing of Civil Infrastructures using Stress Wave Propagation*. Key Engineering Materials, Vols. 270-273, pp. 1616-1621, 2004. online at http://www.scientific.net

Lamb H. *On the Propagation of tremors over the surface of an elastic solid.* Philosophycal Transactions of the Royal Society, Vol. 203, pp. 1-42. 1904.

Lee M.A. *Resilient Modulus and Dynamic Poisson's Ratio of Asphaltic Concrete Mixes*. M.Eng. Thesis, McMaster University, December, 1976.

Lin D.-F., Liau C.-C., Lin J-D. *Factors Affecting Portable Falling Weight Deflectometer Measurements.* Journal of Geotechnical and Geoenvironmental Engineering. ASCE. pp. 804-808, June, 2006.

Lin Y., Sansalone M., Carino N.J. *Finite Element Studies of the Impact-Echo Response of Plates Containing This Layers and Voids*. Journal of Nondestructive Evaluation, Vol.9, No.1, pp.27-47, 1990.

Livneh M. *Uncertainty Associated with Pre-Defined Correlative Expressions of Various In-Situ Test Outputs*. Transportation Research Institute, Technion-Israel Institute of Technology. Presented for the 2007 FAA Worldwide Airport technology Transfer Conference, Atlantic City, New Jersey, USA. April, 2007.

Livneh, M, Goldberg Y. *Quality Assessment During Road Formation and Foundation Construction: Use of Falling-Weight Deflectometer And Light Drop Weight*; Transportation Research Record 1755, Submitted to the 2001 Annual Meeting of the Transportation Research Board For Presentation and publication, pp 69-77, 2001.

Luca J. and Mrawira D. *New Measurement of Thermal Properties of Superpave Asphalt Concrete*. Journal of Materials in Civil Engineering. ASCE. pp.72-79, January/February, 2005.

Lukanen, E.O., Han C., and Skok, E. L. Jr. *Probabilistic Method of Asphalt Binder Selection Based on Pavement Temperature*. Transportation Research Record, 1609: pp. 12-20, 1998.

Lukanen E.O., Stubstad R. and Briggs R. *Temperature Predictions and Adjustment Factors for Asphalt Pavement,* Federal Highway Administration Report FHWA-RD-98-085,U.S. Department of Transportation, 2000.

Lysmer J. and Kuhlemeyer R.L. *Finite Element Model for Infinite Media*. Journal of the Engineering Mechanic Division. ASCE, pp. 859-877, 1969.

Lytton, R.L. *Backcalculation of Pavement Layer Properties. Nondestructive Testing of Pavements and Backcalculation of Moduli*, ASTM STP 1026, A.J. Bush III and G.Y.Baladi, Eds., American Society for Testing and Materials, Philadelphia, pp. 7-38, 1989.

Magnuson A.H., Lytton R.L., and Briggs R.C. *Comparison of Computer Predictions and Field Data Imposed by Nondestructive Tests.* Transportation Research Record No. 1293, pp. 61-71, 1991.

Medina R., Garrido M. *Improving impact-echo method by using cross-spectral density.* Journal of Sound and Vibration, No.304, pp. 769-778, 2007.

MEPDG, National Research Council, *Guide for Mechanistic-Empirical Design (MEPDG)*. National Cooperative Highway Research Program (NCHPR). 2004.

Mindlin, R.D. *Influence of Rotatory Inertia and Shear on Flexural Motions of Isotropic, Elastic Plates*. Journal of Applied Mechanics, American Society of Mechanical Engineers, Vol.18, 1951, pp.31-38.

Mohseni, A. *LTPP Seasonal Asphalt Concrete (AC) Pavement Temperature Models.* FHWA-RD-97-103: 71pp, 1998.

Mooney M.A. and Miller P.K. *Analysis of Lightweight Deflectometer Test Based on In Situ Stress and Strain Response.* Journal of Geotechnical and Geoenvironmental Engineering. Pp. 199-208. January, 2009.

Mrawira D. and Luca J. *Effect of aggregate type, gradation, and compaction level on thermal properties of hot-mix asphalts*. Canadian Journal of Civil Engineering. No. 33. pp.1410-1417, 2006.

Nazzal M.D., Abu-Farsakh M.Y., Alshibli K.and Mohammad L. *Evaluating the Light Falling Weight Deflectometer Device for In Situ Measurement of Elastic Modulus of Pavement Layers.* Transportation Research Record 2016, pp.13-22, 2007.

Newmark, N. M., *A Method of Computation for Structural Dynamics*, ASCE Journal of the Engineering Mechanics Division, Vol. 85 No. EM3, July, 1959.

Nofziger D.L. and Wu J. *Soil Temperature Changes with Time and Depth: Theory*, (http://soilphysics.okstate.edu/software/SoilTemperature/document.pdf). Department of Plant and Soil Sciences, Oklahoma State University, Stillwater,. pp. 1-8. October, 2003.

Nondestructive Thickness of Distressed Concrete Pavement Using Impact-Echo. SPS-2, Interstate 10, Maricopa County, Arizona. FHWA MCL Project # 0207. Summary report. December, 2002.

Noss, P.M. *The Relationship Between Meteorological Factors and Pavement Temperature.* Symposium on Frost Action on Roads Conference Paper: pp. 77-87, 1973.

Odemark N. *Investigations as to the Elastic Properties of Soils Design of Pavements According to the Theory of Elasticity*. Staten Vaeginstitut, Stockholm, Sweden, 1949.

Ongel A., Harvey J. *Analysis of 30 Years of Pavement Temperatures using the Enhanced Integrated Climate Model (EICM)*. Draft report prepared for the California Department of Transportation. Pavement Research Center Institute of Transportation Studies University of California, Berkeley, University of California, Davis. August, 2004.

Park H.M., Kim R. and Park S. *Temperature Correction of Multiload-Level Falling Weight Deflectometer Deflections.* Transportation Research Record No. 1806, pp. 3-8. 2002.

Parvini M. *Pavement Deflection Analysis Using Stochastic Finite Element Method.* Ph.D. thesis. McMaster University, October, 1997.

Parvini M., Stolle D.F.E. *Application of Stochastic Finite-Element Method to Deflection Analysis of Pavement Structures*. Transportation Research Record 1540, Transportation Research Board, pp.65-71, 1996.

Parvini M., Stolle D.F.E. *Interpretation of pavement deflection measurement data using an elastodynamic stochastic approach* . Canadian Journal of Civil Engineering Vol. 25, 1998, no 1, pp. 151-160, 1998.

Peiravian F. *Interpretation of In-Situ Pavement Properties Using FWD Testing Technique.* A thesis submitted to the School of Graduate Studies in Partial Fulfillment of the Requirements for the Degree of Master of Engineering, McMaster University, Canada, August, 1994.

Pellinen T. *Evaluation of Surface (Top-Down) Longitudinal Wheel Path Cracking in Indiana*. Proposal for Research study. Joint Transportation Research Program, Project No. C-16-31P File No.2-11-16. Purdue University, May, 2002.

Popovics J.S. *Effects of Poisson's Ratio on Impact-Echo Test Analysis*. Journal of Engineering Mechanics, pp.843-851, August, 1997.

Powell A. *Finite Difference Solution of the Heat Equation* (http://www.core.org.cn/NR/rdonlyres/Nuclear-Engineering/22-00JIntroduction-to-Modeling-and-SimulationSpring2002/55114EA2-9B81-4FD8-90D5-5F64F21D23D0/0/lecture_16.pdf) 22.091. March 13–15, 2002

Rada, G.R., Richter, C.A, Stephanos, P.J. *Layer Moduli from Deflection Measurements.* Software Selection and Development of SHRP's Procedure for Flexible Pavements, Beltsville, MD. 1991

Rahimzadeh B, Jones M and Thom N. *Performance Testing of Unbound Materials Within the Pavement Foundation*, 6th International Symposium on Pavement Unbound-UNBAR6, Nottingham, 6-8 July,2004.

Ramirez R.W. *The FFT, Fundamentals and Concepts.* Prentice Hall, Inc., Englewood Cliffs, NJ, 1985.

Recktenwald G.W. *Finite-Difference Approximations to the Heat Equation* (http://web.cecs.pdx.edu/~gerry/class/ME448/codes/FDheat.pdf) January 21, 2004.

Richart F.E., Hall J.R. Jr. and Woods R.D. *Vibrations of Soils and Foundations.* Prentice Hall, Englewood Cliffs, NJ, 1970.

Roesset J.M. *Nondestructive Dynamic Testing of Soils and Pavements.* Tamkang Journal of Science and Engineering, vol.1, No. 2, pp. 61-81, 1998.

Roesset J.M. and Shao K. *Dynamic Interpretation of Dynaflect and Falling Weight Deflectometer Tests.* Transportation Research Record, vol. 1022, TRB, pp.7-16, 1985.

Ross M. *Modeling Methods for Silent Boundaries in Infinite Media.* ASEN 5519-006: Fluid-Structure Interaction. Aerospace Engineering Sciences- University of Colorado at Boulder, February 26, 2004.

Rumney, T.N., Jimenez. R.A. *Pavement Temperatures in the Southwest.* Highway Research Record, 361: pp. 1-19, 1971.

Ryden N. and Mooney M.A. *Analysis of Surface Waves from the Light Weight Deflectometer.* Soil Dynamics and earthquake Engineering, Vol. 29, pp.1134-1142, 2009.

Schubert F., *Impact-Echo Signature Analysis (IESA) – A New Evaluation Procedure for Impact- Echo Data based on Spectrograms*. Fraunhofer-IZFP, Dresden Branch, Germany, ECNDT 2006 - Fr.1.4.1., pp. 1-15.

Scrivner F.H., Michalak C.H. and Moore W.M. *Calculation of the Elastic Moduli of a Two-Layer Pavement System from Measured Surface Deflection*. Highway Research Record No.431, Highway Research Board, Washington, DC,1973.

Scrivner F., Peohl R., Moore W. and Phillips M. *Detecting Seasonal Changes in Load-Carrying Capabilities of Flexible Pavements*. NCHRP Report 76, Transportation Research Council: Washington, DC ,1969.

Sebaaly B., Davis T.G. and Mamlouk M.S. *Dynamics of Falling Weight Deflectometer*. Journal of Transportation Engineering, ASCE, 111 (6), pp. 618-632, 1985.

Sedran G. *Dynamics of pavement-subgrade interaction via Ritz vectors*. McMaster University, Hamilton, Canada. July, 1994.

Shao L., Park S.W. and Kim Y.R. *Simplified Procedure for Prediction of Asphalt Pavement Subsurface Temperatures Based on Heat Transfer Theories.* Transportation Research Record. Vol. 1568 , pp.114-123, 1997.

Siddharthan R., Norris G.M. and Epps J.A. *Use of FWD Data for Pavement Material Characterization and Performance*. Journal of Transportation Engineering, ASCE, 117 (6), pp. 660-678, 1991.

Solaimanian, M., Bolzan P. *Analysis of the Integrated Model of Climatic Effects on Pavements.* SHRP-A-637: 158pp. 1993.

Spall, M. *Developing A Thermal Model For Asphaltic Concrete.* MS Thesis. Clarkson College of Technology. Department of Mechanical and Industrial Engineering. 1982

Steinert B., Humphrey D.N. and Kestler M.A. *Portable Falling Weight Deflectometers for Testing Seasonal Variations in Asphalt Surfaced Roads*. TRB 2006 Annual Meeting CD-rom. 2006.

Steven B., Alabaster D. and de Pont J. *Elastic Nonlinear Finite Element Analysis of a Flexible Pavement Subjected to Varying Falling Weight Deflectometer Loads.* Transportation Research Record No.2016, pp.31-38, 2007.

Stolle D.F.E. *A Direct Integration Algorithm and the Consequence of Numerical Stability*. Journal of Sound and Vibration, Vol. 180 (3), pp. 513-518, 1995.

Stolle D.F.E. *Comparison of Simplified Elastostatic and Elastodynamic Models for Falling Weight Deflectometer Data Interpretation.* Transportation Research Record 1540, Transportation Research Board, pp.72-75, 1996.

Stolle D.F.E. *Pavement Displacement Sensitivity to Layer Moduli*. Canadian Geotechnical Journal, No. 39, pp.1-5, 2002.

Stolle D.F.E. and Guo P. *A Practical Approach to Falling-Weight Deflectometer (FWD) data reduction*. Canadian Geotechnical Journal, No. 42, pp.641-645, 2005.

Stolle D.F.E., Guo P., Heska D., Baker G., *Influence of Backcalculation Strategy on Prediction of Subgrade Modulus*. Transportation Research Board, 2101 Constitution Ave., N. W., Washington, D.C. 20418, July 22, 2004.

Stolle, D.F.E. and Hein, D. *Parameter Estimates of Pavement Structure Layers and Uniqueness of the Solution*. Nondestructive Testing of Pavements and Backcalculation of Moduli, ASTM STP 1026, A.J. Bush III and G.Y.Baladi, Eds., American Society for Testing and Materials, Philadelphia, pp. 313-322, 1989.

Stolle, D.F.E., Peiravian, F. *Falling Weight Deflectometer data interpretation using dynamic impedance*. Canadian Journal of Civil Engineering. Volume 23, Number 1, February 1996.

Stolle, D.F.E., Jung F.W. *Simplified, Rational Approach to falling Weight Deflectometer Data Interpretation*. Transportation Research Record 1355, pp.82-89, 1992.

Straub, A.L., Schenck H.N. Jr., Przybycien F.E. *Bituminous Pavement Temperature Related to Climate.* Highway Research Record, 256: pp.53-77, 1968.

Stubstad R., Jiang Y. J. and Lukanen E. *Forwardcalculation of Pavement Moduli with Load-Deflection Data.* Transportation Research Record, No.2005, pp.104-111, 2007.

Tayabji S.D., Lukanen Erland O. *Nondestructive testing of pavements and backcalculation of moduli* : Third volume. West Conshohocken, PA: ASTM, 1999.

Turkiyyah G. *Feasibility of Backcalculation Procedures Based on Dynamic FWD Response Data*. Project Report, University of Washington. June, 2005.

Ullidtz, P., J.T. Harvey, M. Riemer, and J.A. Prozzi, *Layer Moduli during HVS Testing: Comparing Laboratory Results with Backcalculations from FWD and MDD Deflections*. Proceedings of the First International Conference on Accelerated Pavement Testing, Reno, NV, October 1999.

Ullidtz P. *Pavement Analysis*. Institute of Roads, Transport and Town Planning, The Technical University of Denmark, Lyngby, Denmark, 1987.

U.S. Department of Transportation. Federal Highways Administration. *LTPP Temperature Prediction and Correction Guide: The BELLS Equations*. http://www.tfhrc.gov/pavement/ltpp/fwdcd/tempred.htm

Uzan J. *Dynamic Linear Back Calculation of Pavement Material Parameters*. ASCE Journal of Transportation Engineering, Vol. 120, No. 1, pp. 109-126, 1994.

Uzan J., Lytton R.L. *Experiment Design Approach to Nondestructive Testing of Pavements*. Journal of Transportation Engineering, ASCE, 115(5), pp. 505-520, 1989.

Uzan J., Lytton R.L. and Germann F.P. *General Procedure for Backcalculating Layer Moduli*. STP 1026, American Society for Testing and Materials, pp. 217-228, 1989.

Uzan J., Scullion T., Michalek C.H., Paredes M. and Lytton R.L. *A Microcomputer Based Procedure for Backcalculating Layer Moduli from FWD Data*. Research Report 1123-1, Tezas Transportation Institute, 1988.

Vignaux G.A. *Dimensional Analysis in Data Modelling*. Published in C R Smith, G J Erickson and P O Neudorfer(eds), Maximum Entropy and Bayesian Methods, Seattle, 1991, Kluwer Academic Publishers, pp. 1-9, 1992.

Voller, V.R., Newcomb D.E., et al. *A Computer Tool for Predicting the Cooling of Asphalt Pavements*. 9th International Conference on Cold Regions Engineering,: pp. 27-30, September 1998.

Wilson E.L., Yuan M.W. and Dickens J.M. *Dynamic Analysis by Direct Superposition of Ritz Vectors. Earthquake Engineering and Structural Dynamics*, Vol. 10, pp. 813-821, 1982.

Wiseman G. and Greenstein J. *Comparison of Methods of Determining Pavement Parameters from Deflection Bowl Measurements*. Proceedings of the 7th Asian Regional Conference on Soil Mechanics and Foundation Engineering, pp. 158-165, 1983.

Westover T. M. and Guzina B. B. *Engineering Framework for Self-Consistent Analysis of Falling Weight Deflectometer Data*. Transportation Research Record No.2005, pp.55-63, 2007.

Williamson, R.H. *Effects of Environment on Pavement Temperatures.* International Conference on Structural Design Proceedings: pp. 144-158, 1972.

Wilson, A.H. *The Distribution of Temperatures in Experimental Pavements at Alconbury By-pass.* TRRL Lab Report 719: 30pp. 1976.

Wilson, E. L. *Dynamic Response by Step-By-Step Matrix Analysis.* Proceedings, Symposium On The Use of Computers in Civil Engineering, Labortorio Nacional de Engenharia Civil, Lisbon, Portugal, October 1-5, 1962.

Wilson E.L., Yuan M.W. and Dickens J.M. *Dynamic analysis by direct superposition of Ritz vectors.* Earthquake Engineering and Structural Dynamics, Vol. 10, pp. 813-821, 1982.

Wiseman G., and Greenstein J. *Comparison of Methods of Determining Pavement Parameters from Deflection Bowl Measurements.* Proc., 7th Asian Regional Conference on Soil Mechanics and Foundation Engineering, 1983.

Wolf J.P. *Soil-Structure Interaction Analysis in Time Domain.* Prentice-Hall, Inc., Englewood Cliffs, NJ, 1988.

Wolfe, R. K., Heath G. L., Colony D. C. *The University of Toledo Time-Temperature Model Laboratory and Field Validation.* Report to The Ohio Department of Transportation. 1987.

Xu B., Ranjithan R. and Kim Y. R. *New Relationships Between Falling Weight Deflectometer Deflections and asphalt Pavement Layer Condition Indicators.* Transportation Research Record No.1806, pp.48-56, 2002.

Yavuzturk C. and Ksaibati K. *Assessment of Temperature Fluctuations in asphalt Pavements Due to Thermal Environmental Conditions Using a Two-Dimensional, Transient Finite-Difference Approach.* Report on Analysis. Department of Civil and Architectural Engineering University of Wyoming. October 2002.

Yavuzturk C., Ksaibati K. and Chiasson A.D. *Assessment of Temperature Fluctuations in asphalt Pavements Due to Thermal Environmental Conditions Using a Two-Dimensional, Transient Finite-Difference Approach.* Journal of Materials in Civil Engineering. ASCE, pp. 465-475, July/August, 2005.

Yin H., Solaimanian M., Kumar T., Stoffels S. *The effect of loading time on flexible pavement dynamic response : a finite element analysis.* Mechanics of Time-Dependent Materials, Volume 11, Numbers 3-4 / December, 2007, pp.265-288, 2008.

Zanko L.M. and Hopstock D.M. *Minnesota Taconite as a Microwave-Absorbing Road Aggregate Material for Deicing and Pothole Patching Applications*. Final Report. Minnesota Department of Transportation Research Services Section. 2004.

Zeng M. and Shields D.H. *Nonlinear thermal expansion and contraction of asphalt concrete*. Canadian Journal of Civil Engineering. No. 26. pp. 26-34, 1999.